PHOTOACOUSTIC TRACE GAS SENSING; APPLICATION TO FRUIT AND INSECTS

PHOTOACOUSTIC TRACE GAS SENSING; APPLICATION TO FRUIT AND INSECTS

EEN WETENSCHAPPELIJKE PROEVE OP HET GEBIED VAN
DE NATUURWETENSCHAPPEN, WISKUNDE EN INFORMATICA

PROEFSCHRIFT

TER VERKRIJGING VAN DE GRAAD VAN DOCTOR
AAN DE KATHOLIEKE UNIVERSITEIT NIJMEGEN,
VOLGENS BESLUIT VAN HET COLLEGE VAN DECANEN
IN HET OPENBAAR TE VERDEDIGEN
OP DONDERDAG 20 SEPTEMBER 2001,
DES NAMIDDAGS OM 3:30 UUR PRECIES

DOOR

Stefan Timotheüs Persijn

GEBOREN OP 4 JUNI 1973
TE ZEVENAAR

PROMOTOR : PROF. DR. D.H. PARKER

CO-PROMOTOR DR. F.J.M. HARREN

MANUSCRIPTCOMMISSIE : PROF. DR. M.W. SIGRIST
SWISS FEDERAL INSTITUTE OF TECHNOLOGY ZURICH

PROF. DR. D.D. BICANIC
WAGENINGEN UNIVERSITEIT

DR. N. DAM

Kupersembahkan untuk Ayik

Voorwoord

Alle betrokkenen wil ik graag bedanken voor hun bijdrage aan mijn onderzoek en het proefschrift. Het waren vier hele leuke jaren mede dankzij de vele borrels, het zeilen, dagjes uit etcetera. In het bijzonder wil ik de volgende mensen bedanken:

- Mijn co-promotor Frans Harren die mij tijdens de promotie op een hele goede manier heeft begeleid. Het zou goed zijn als ik wat vaker naar zijn ideeën luisterde.

- Dave Parker, mijn promotor en kapitein van onze afdeling.

- De (ex-)fotoakoestici: de af en toe fijnzinnige Luc-Jan, onder zijn leiding gaat de Large Scale Facility een zonnige toekomst tegemoet; Sacco, dankzij de door hem ontworpen laser mocht ik de zee op; Jos, die Steppie in het begin uitstekend op weg heeft geholpen; Edi, goede collega die met veel doorzettingsvermogen een prima draaiende machine heeft gemaakt; Simona en Iuliaatje, voor mijn verbeterde begrip van vrouwen; Tim, eigenzinnig wereldreiziger; Jan-Matthijs, vertrok met minder haren en tanden dan dat hij kwam; Brenda, de enige fotoakoestische vrouw met wie ik nooit ruzie heb gehad; koning Ri(s)k, in zijn eigen ogen ook een begenadigd voetballer (verder zie boven); Jörg Reuss; Li from far away China en OPO Maarten.

- Mijn kamergenoten Bernard, Ralph en Sergio. Iedereen die dit illustere drietal kent, weet hoe zwaar ik het heb gehad. Kreten zoals 'ik ga je pletten', 'lekker veertje', 'moie maisjes' en 'ieck spreek ahl sonder accent' moest ik dagelijks vele malen aanhoren. De keuze tussen kijken naar of Bernard of het Duitse elftal was ook niet altijd makkelijk. Maar desondanks had ik dit boeiende gezelsschap niet willen missen.

- Rob=ert??, Michiel, Rogier, Ivan, Giel, Rudy, Martina, Dmitri, Marcela, Floris, Hans, Eugène, Hans, Leo, Nico, Graalburchters en Rijnhuizers.

- Chris en Peter voor de elektronische ondersteuning, Henry voor het onmisbare computer werk en Leander voor de mechanische hulp.

- Cor voor zijn eenvoudige en efficiënte ontwerpen. Samen werden we door de loods gebracht (=zeeziek, voor de landrotten onder ons). Zo'n oceaan blijkt toch net even anders te zijn dan een heel groot meer. Marc Staal hield ons in leven door droog brood en beschuit aan te dragen.

- Rob Veltman, alias 'De Perenman'. De metingen vielen niet altijd mee omdat vaak of laser of peer 'het' niet deed.

- De onmisbare secretaresses Magda, Ine en Erna.

- Ferry Derksen voor de 'zelf'-service, Teun Diels, Japie Nieboer en Piet Homberg voor het ontwerp en bijna gereed maken van 'mijn laser' en Gerben Wulterkens voor de tekeningen.

- De mensen van de glasblazerij voor de ware kunstwerken die, vaak vliegensvlug, uit jullie atelier kwamen.

- Mitrayana, Rofandi dan Rohadi, mereka tinggal dan bekerja setengah tahun di Belanda yang dingin. Saya selalu suka masakkan mereka.

- Dr. Joko Wasono and Dr. Suparmo who organised a great photoacoustic symposium with delicious Indonesian snacks, Rus Fitrihadi (voor de mooie brommerritten door Yogya), and the students Fajri and Herbert who played badminton so much better than I did at 35 °C.

- Paul Kestler who taught me everything about insects, and in addition he explained me, using biological grounds, the poor performance of the German soccer team.

- Stefan Hetz and Annabel Wobschall who combined their hard working on the amazing desert ant with short sleeps (in the university!) and good wine.

- Dane, die alles met een aanstekelijk enthousiasme doet.

- Ineke Wijkamp met wie ik tripsen en ander klein gespuis uitroeide.

- Gespuis van een hele andere orde; de onvermoeibare vrijdagmiddag annex zomeravond voetballers, mijn huisgenoten en long-time vriend Roben.

- Terima kasih atas sambutan hangat keluarga Supardi.

- Mijn familie, van klein tot groot en van de dikke tot de dunne, die ik de komende tijd zal moet missen.

- Ayik, for your continuous support and unsurpassed humor.

Stefan Persijn

Contents

Chapter 1

General introduction

Outline

The work described in this thesis is concerned with the interplay between Physics and Biology. The Physics is confined in the photoacoustic technique applied to study trace emission of gases by, and here comes the Biology into play, fruits and insects. In particular, the following three topics have been studied:

- The CO laser based spectrometer was further improved resulting in a fast instrument which is capable of measuring a wide range of biologically interesting gases at a (sub) ppb level. Absorption coefficients of various trace gases were determined and applied in a multicomponent analysis.

- Modern storage technology often implies the use of low O_2 levels to reduce respiration of the crop. Emission of fermentative metabolites by avocado has been monitored under such low O_2 conditions. The fast response of the photoacoustic detector enabled one to gain better insights into the dynamics of the fermentation process under (post-)anaerobic and (post-) hypoxic conditions.

- Respiration and water loss were also investigated for a variety of insects; ranging from the large Attacus pupae (5 g) to the tiny thrips (50 μg), the latter are so far the smallest insects of which the water loss has ever been measured. A SF_6 wash-out technique was used to estimate the tracheal volume of insects.

1.1 On the importance of sensitive trace gas detection

In the 18th century Lavoisier and Laplace analyzed the breath from a guinea pig and demonstrated the expiration of CO_2 and consumption of O_2 [12]. Over the last few decades people have realized that many more molecules are found in the exhaled air. Animals but also plants and humans were shown to produce ethylene, methane, nitric oxide, methanol, ethanol, and hundreds of other molecules [9, 10, 11]. Monitoring the emission of such molecules could provide insight into internal processes, although usually complementary measurements are needed to obtain a complete description of these processes. To study

the emission of these molecules requires highly sensitive detectors due to the normally very low release rates.

One of the applications of trace gas analysis is that to fruit storage. Storage of horticultural commodities extends the season of availability allowing a more diverse diet. Modern storage of crops started some eight decades ago with the pioneering research of Kidd and West, who applied modified ambient conditions, i.e., elevated CO_2 and lowered O_2 levels to reduce respiration and hence extend the storage period of the crop [7, 17]. Storage life times of certain crops have been drastically improved; for instance, some apple cultivars can be stored for a whole year without a substantial loss in firmness. At very low O_2 levels, the fruit start to ferment (i.e., breakdown of sugar to ethanol and a series of other, normally minor, compounds) [15]. It has been hypothesized that under optimum storage conditions respiration is suppressed as much as possible without the occurrence of fermentation since the latter can lead to off-flavors and disorders [14]. However, even for a single cultivar these conditions are not fixed but depend for instance on climate and orchard, in addition they can also change during the storage period. To test if there is ongoing fermentation in the fruit, the volatiles formed during fermentation can be measured. In a so-called dynamically controlled system, these products are monitored on a regular basis and decisions are made whether or not storage conditions should be adjusted. In other words, the crop itself signals what are its optimum storage conditions [16].

Monitoring the emission of trace gases in insects can not only provide insight in internal processes but even behaviour can be calibrated after correlating gas emission data with the visual observations. For example, in cockroaches, grooming or stress leads to an altered emission pattern as compared to their normal respiration pattern during resting [6]. However, care must be taken when interpreting such emission data without simultaneous visible observations or other complementary measurements. To make this clear, ants continue after decapitation (i.e., cutting off the ants' head) their normal respiration period for many hours [8]. Trace gas emissions do not only reflect the ongoing processes inside the sample, but provide information how plants and animals communicate with each other. For example, plants being attacked by caterpillars can start to emit gases that attract predators like parasitic wasps [2, 18].

Although not investigated in this thesis, it is worthwhile to mention another highly interesting application of trace gas analysis. After Pauling et al. reported that exhaled human air contains as much as several hundred identified volatile organic compounds (VOCs) there has been a search for VOCs that could serve as marker of disease [11]. Progress in this field has been slow, mainly due to a lack of sensitive gas detectors [12]. However, new trace gas detectors have recently been developed while older techniques have been refined and, at present, a number of these detectors among which proton transfer mass spectrometry [9] and laser-based photoacoustics [5] is suited for (on-line) breath analysis. Measuring a combination of VOCs allowed one to distinguish between patients with and without lung cancer [13] while Harren and co-workers use ethylene as an early biomarker for damage of the human skin due to ultraviolet radiation [5].

It is important to stress that, unlike many other analytical techniques, trace gas detection is a non-invasive technique. Therefore trace gas detection can open new ways to

study and diagnose plants, animals, and humans without imposing stress on them.

1.2   The photoacoustic technique; from light absorption to sound generation

Insight into the dynamics of biological processes can be obtained by using fast and highly sensitive trace gas detectors. In the research reported in this thesis, detectors operating on the principle of the photoacoustic effect have been used (see Fig 1.1).
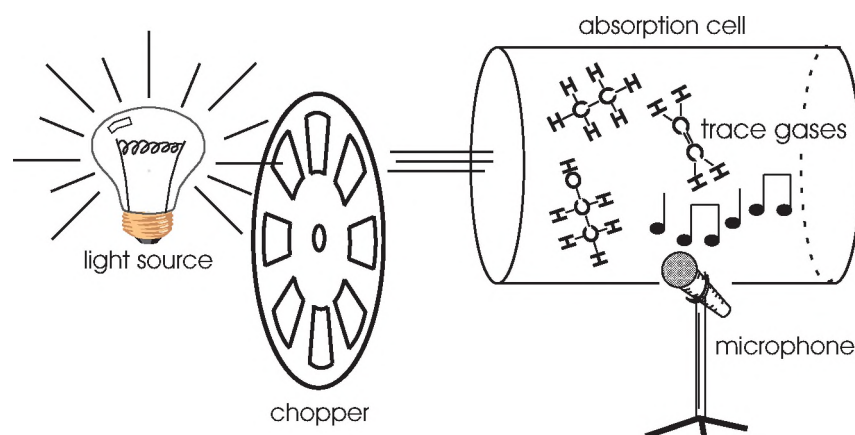
Figure 1.1: *Schematic view of the photoacoustic technique: A chopper modulates a light beam incident on a gas sample. If the emission wavelength coincides with an absorption of the sample, sound will be produced and its amplitude is recorded by a microphone. The amplitude of the recorded signal is proportional to the concentration of absorbing molecules.*

A gaseous sample is confined within an absorption cell, the shape resembles that of an organ pipe. When the sample is exposed to infrared radiation, some fraction of the light will be absorbed if the frequency of the radiation matches a ro-vibrational transition of the trace gas molecules under study. By collisions with other molecules the vibrational energy is converted to translational energy causing the temperature of the gas to increase. On-off switching of the light source (chopper) produces an alternating temperature and hence pressure in the gas sample. Such an alternating pressure (acoustical wave) can be transformed into electrical signals by means of a microphone. The amplitude of the electrical signal thus produced is a measure for the concentration of absorbing molecules. Note that the generated sound can even be heard by the human ear in case a strong radiation source is used in combination with a high concentration of strongly absorbing molecules. However, when detecting low trace gas concentrations the generated sound is very feeble (typically induced pressure changes are on the order of 10^{-4} Pa). Therefore,

sensitive lock-in techniques are required to amplify the signal and suppress parasitic signals generated by the surrounding.

The most appropriate wavelength region for sensitive trace gas analysis is that between 2.5 and 25 μm (the so-called fingerprint region), since it includes fundamental ro-vibrational bands of molecules [1]. The PA signal is proportional to the light intensity and hence powerful light sources are required to detect low gas concentrations while frequency tunability is necessary to obtain selectivity. Excluding the recently developed OPO's and quantum cascade lasers, there has been a general lack of intense and continuously tunable light sources in the mid-infrared. Line-tunable gas lasers represent a good alternative due to their yet unparalleled high output power, frequency stability, and simple operation. For this thesis powerful CO and CO_2 lasers have been used as radiation source in a photoacoustic (PA) spectrometer. A CO_2 laser based PA spectrometer can detect minute amounts of ethylene (plant hormone) and the tracer gas SF_6 [4, 3]. The CO laser can operate in two wavelength regions (2.8-4.1 and 5.1-8.0 μm); where many molecules of biological interest including aldehydes, ketones, and alcohols show strong absorptions. The CO laser is a suitable radiation source for multi-component analysis due to its wide emission range.

1.3   Outline of the thesis

Chapter 2 gives a description of the photoacoustic detector that is used in Chapters 4 and 5. With this set-up, various trace gases of biological relevance are measured and their absorption coefficients determined. For H_2O and CO_2 the obtained absorption coefficients are compared with literature data. The absorption coefficients were used in a multi-component analysis of Conference pears kept under anaerobic conditions.

In Chapter 3 a novel photoacoustic detector based on a modified design of the CO laser is presented. The laser can operate both in the $\Delta v=1$ and $\Delta v=2$ mode (5.1-8.0 and 2.8-4.1 μm, respectively) on about 400 laser lines. A newly designed grating holder allows easy switching between the two modes. A number of applications are described, indicating the versatility of this detector.

Chapter 4 describes trace gas emission from avocado fruit during anaerobic and post-anaerobic conditions. Simultaneous recordings of CO_2, ethanol, acetaldehyde, and ethylene are shown. Next to the post-anaerobic effect also the post-hypoxic effect is investigated.

Chapter 5 deals with water loss recordings from the tiny thrips (weight 50 μg), a serious worldwide pest. The H_2O loss of a single thrips could be recorded. As a potential insecticide the effect of elevated CO_2 levels was tested.

An estimate of the tracheal volume of insects (pupae from *Attacus atlas* and adult American cockroaches *Periplaneta americana*) is obtained using a novel SF_6 wash-out technique (Chapter 6). The respiration pattern of the insect is recorded in detail from both CO_2 and SF_6 release. Furthermore, length changes of *Attacus atlas* pupae are monitored using an infrared reflection sensor. The high sensitivity of the detector for SF_6 (5 ppt) opens new ways for studying respiration in even smallest insect species.

References

[1] S. Bernegger, M.W. Sigrist, CO-Laser photoacoustic spectroscopy of gases and vapours for trace gas analysis. Infrared Phys. **30** 375-429 (1990)

[2] M. Dicke, P. Van Baarlen, R. Wessels, H. Dijkman. Herbivory induces systemic production of plant volatiles that attract herbivore predators: extraction of endogenous elicitor. J. Chem. Ecol. **19** 581-599 (1993)

[3] T.T. Groot, G. Cotti, D.H. Parker, H.A.J. Meijer, F.J.M. Harren, Monitoring gas transport in rice using SF_6 as tracer gas detected by laser photoacoustics. In: Photoacoustic and Photothermal Phenomena, (ed. F. Scudieri and M. Bertolotti) AIP Conference Proceedings 463 (Woodbury, New York, 673-675 (1998)

[4] F. Harren, J. Reuss, E.J. Woltering, D.D. Bicanic, Photoacoustic measurements of agriculturally interesting gases; detection of C_2H_4 below the ppb level. Appl. Spectrosc. **44** 1360-1368 (1990)

[5] F.J.M. Harren, R. Berkelmans, K. Kuiper, S. te Lintel Hekkert, P. Scheepers, R. Dekhuijzen, P. Hollander, D.H. Parker. On-line laser photoacoustic detection of ethene in exhaled air as biomarker of ultraviolet radiation damage of the human skin. Appl. Phys. Lett. **74** 1761-1763 (1999)

[6] P. Kestler, Cyclic CO_2 release as a physiological stress indicator in insects. Comp. Biochem. Physiol. **100** 207-211 (1991)

[7] F. Kidd, C. West, A relation between the concentration of oxygen and carbon dioxide in the atmosphere, rate of respiration, and length of storage of apples. Food invest. Board Rep. London for 1925 41-42 (1927)

[8] J.R.B. Lighton, T. Fukushi, R. Wehner, Ventilation in Cataglyphis bicolor: regulation of CO_2 release from the thoracic and abdominal spiracles. J. Insect Physiol. **39** 687-699 (1993)

[9] W. Lindinger, A. Hansel, A. Jordan, On-line monitoring of volatile organic compounds at pptv level by means of proton-transfer-reaction mass spectrometry (PTR-MS). Medical applications, food control and environmental research. Int. J. Mass Spectrom. Ion Proc. **173** 191-241 (1998)

[10] J.P. Mattheis, D.A. Buchanan, J.K. Fellman, Volatile compound production by Bisbee Delicious apples after sequential atmosphere storage. J. Agric. Food. Chem. **43** 194-199 (1995)

[11] L. Pauling, A.B Robinson, R. Teranishi, P. Cari, Quantitive analysis of urine vapor and breath by gas-liquid partition chromatography. Proc. Nat. Acad. Sci. USA **68** 2374-2376 (1971)

[12] M. Phillips, Breath tests in medicine. Sci. Am. **267** 74-79 (1992)

[13] M. Phillips, K. Gleeson J.M.B. Hughes, J. Greenberg, R.N. Cataneo, L. Baker, W.P. McVay, Volatile organic compounds in breath as markers of lung cancer: a cross-sectional study. Lancet **353** 1930-1933 (1999)

[14] D.G. Richardson, M. Kosittrakun, Off-flavor development of apples, pears, berries and plums under anaerobiosis and partial reversal in air. In: 'Fruit flavors: Biogenesis, characterization and authentication.' R.L. Rouseff, M.L. Leahy (eds), American Chemical Society, Washington, DC, 211-225 (1995)

[15] F.B. Salisbury, C.W. Ross, Respiration. In: 'Plant Physiology', 4th ed., Wadsworth Publishing Company, Belmont, California, 266-288 (1992)

[16] S.P. Schouten, Dynamic control of the oxygen content during CA storage of fruits and vegetables. CAPPT'95 Ostend, Belgium. 131-136 (1995)

[17] R.M. Smock, Controlled atmosphere storage of fruits. Hort. Rev. **1** 301-336 (1979)

[18] T.C.J. Turlings, J.H. Loughrin, P.J. McCall, U.S.R. Rose, W.J. Lewis, J.H. Tumlinson. How caterpillar-damaged plants protect themselves by attracting parasitic wasps. Proc. Natl. Acad. Sci. USA **92** 4169-4174 (1995)

Chapter 2

CO laser absorption coefficients for gases of biological relevance: H_2O, CO_2, ethanol, acetaldehyde, and ethylene.

Abstract

The pressure broadened spectra of gaseous water, carbon dioxide, ethylene, ethanol, and acetaldehyde were recorded using a photoacoustic spectrometer based on a liquid nitrogen-cooled CO laser. From this, absorption coefficients were determined and the results obtained for CO_2 and H_2O were compared with data from the Hitran database. Finally, the measured spectra were used in a multicomponent analysis of trace gases released by pears (*Pyrus communis*, cultivar Conference).

S.T. Persijn[1], R.H. Veltman[2], J. Oomens[1,*], F.J.M. Harren[1], D.H. Parker[1]
[1] Life Science Trace Gas Exchange Facility, University of Nijmegen, Toernooiveld 1, 6525 ED Nijmegen, the Netherlands
[2] Agro-Technological Research Institute, Bornsesteeg 59, 6700 AA Wageningen, the Netherlands
*Current address: FOM-Institute for Plasma Physics, Edisonbaan 14, Postbus 1207, 3430 BE Nieuwegein, the Netherlands

2.1 Introduction

Studies of trace amounts of volatile compounds released by biological samples may provide better insight into physiological processes occurring inside the tissue. Gas chromatography (GC), sometimes in combination with mass spectrometry, is widely used for this purpose. For some applications, however, GC has drawbacks such as limited sensitivity and a low time resolution. Preconcentration of gases emitted from the biological tissue, needed to overcome the limited sensitivity, lowers the time resolution and may also disturb the processes within the sample. Infrared laser-based photoacoustic (PA) detection, owing to its higher sensitivity, is an alternative for such applications, especially when dealing with small molecules [8].

The PA effect, discovered and described by Bell in 1880 [2], basically involves the conversion of light into acoustic waves. The intensity of the generated sound is proportional to the concentration of absorbing trace molecules. Kerr and Atwood performed the first trace gas analysis using laser PA detection in 1968 [13]. From that date, PA detection has proven a very sensitive method with applications in different fields. One example of trace gas analysis is the CO_2 laser-based PA detection of ethylene released by a single Orchid flower; an impressive detection limit of 20 ppt (20 parts in 10^{12} volume) was achieved [11].

The PA signal is proportional to the intensity of the incident laser beam and, therefore, high power sources, such as CO_2 lasers (λ = 9-11 μm, intracavity power up to 100 Watt) or CO lasers (λ = 5-8 μm, intracavity power up to 30 Watt), are required for sensitive trace gas detection [16]. Here we focus on the use of a CO laser; owing to its wide tuning range this laser is better suited for multicomponent analysis than the CO_2 laser [3]. Absorption of water vapor in the wavelength region of the CO laser causes interferences in particular when the analyte gas is present in relatively small amounts. In order to obtain reliable measurements, the concentration of water vapor in the incoming flow must be reduced; e.g., by leading the gas flow through a chemical scrubber or over a cold surface.

To conduct multicomponent analysis, absorption coefficients of the gases under investigation need to be accurately known. Biological trace gas experiments are normally performed in a mixture of O_2 (between 0 and 21%) and N_2 as carrier gas; therefore the measurement of the absorption coefficients was carried out in air and N_2 with, typically, a few hundred ppm of the species diluted in the carrier gas. When using this approach, one encounters several complications. Firstly, oxygen has its first vibrational level at 1554 cm^{-1}. Trace gases with a near resonant vibrational level can transfer their vibrational energy to slowly relaxing oxygen, forming a buffer of vibrational energy and leading to a lower in-phase PA signal [5]. Secondly, pressure shifting and pressure broadening coefficients for water vapor absorption lines in air and nitrogen are different [26, 29, 10].

This contribution is concerned with measurement of absorption coefficients for H_2O, CO_2, ethylene (C_2H_4), ethanol (C_2H_5OH) and acetaldehyde (CH_3CHO) at CO laser frequencies. As such the information obtained can be regarded as contribution to the currently available bulk of data mainly because:

- With exception of water and nitric oxide, only a very limited number of publications deal with measurement of absorption coefficients in the CO wavelength region;

- Most of the data were obtained with CO lasers operating at relatively high temperatures causing only lines with a high rotational quantum number J to lase [3]. Operation at these lines is difficult, or even impossible with a liquid nitrogen cooled CO laser where mainly low J-lines are accessible [9, 25, 17];

- Published absorption spectra are usually obtained at a total sample pressure below 1 bar [9], whereas in practice measurements are commonly carried out at atmospheric pressures; pressure broadening can lead to significantly different results.

The absorption coefficients determined here were used in a multicomponent analysis of C_2H_4, CH_3CH_2OH, and CH_3CHO released by pears (*Pyrus communis*, cultivar Conference) under anaerobic conditions. Under aerobic conditions, the fruit obtaines its energy by respiration, i.e., the stepwise oxidation of sugars to form H_2O and CO_2 as end products. In order to prolong the storage period of harvested products, respiration is commonly reduced by exposure to elevated CO_2 and reduced O_2 levels and temperature [23]. Currently, 40-50% of the Dutch pear harvest is stored under such Controlled Atmosphere (CA) conditions. The production of ethylene, a gaseous plant hormone that stimulates fruit ripening, also decreases at low O_2 levels [1]. At very low O_2 levels, however, an alternative metabolic process – alcoholic fermentation – takes place to provide the energy required by the fruit. During the fermentation process ethanol and its precursor acetaldehyde are being formed, which can be monitored by means of the CO laser based PA detector. Monitoring the emission of acetaldehyde, which is about 15 times more volatile than ethanol under ambient conditions [30], yields information on the dynamics of alcoholic fermentation.

2.2   Experimental

Figure 2.1 shows the experimental set-up (dimensions 3.5 x 0.5 x 0.6 meter); which was thoroughly described elsewhere [6]. Here we restrict ourselves only to the most important features of the apparatus and new developments.

2.2.1   PA cells

Three longitudinally resonant PA cells were mounted sequentially inside the laser cavity to enable three samples to be analyzed simultaneously [5, 4]. A very sensitive condenser microphone (1 V/Pa, Bruel & Kjaer 4179) is mounted in one of the cells; however the large membrane of this microphone influences strongly the resonance frequency of this cell. Less sensitive electret microphones (22 mV/Pa, Knowless EK 3024) with a much smaller membrane are used in the other two cells. To match the resonance frequency for all three PA cells, the resonator length of the cell containing the sensitive microphone (total length 138 mm) was 8 mm shorter than that of the two other cells. With the cell filled with 1 atmosphere nitrogen the resonance frequency is about 1130 Hz. A temperature control unit keeps the temperature of each PA cell slightly above ambient, compensating for any additional differences in resonance frequency. Buffer volumes suppress the PA signal generated by absorption of laser radiation at Brewster windows. For optimal suppression, the length
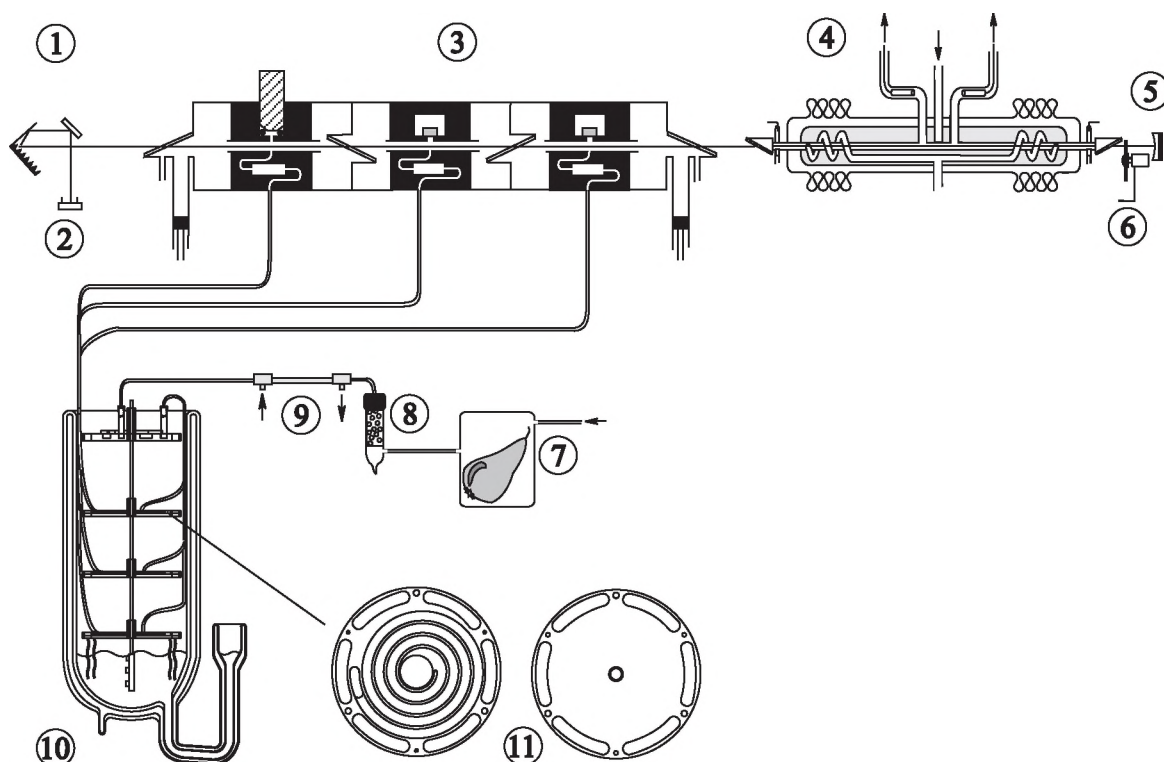
Figure 2.1: *CO laser-based photoacoustic spectrometer.*
1, grating; 2, pyroelectric detector; 3, triple photoacoustic cell; 4, liquid nitrogen cooled CO laser; 5, 100% reflecting mirror; 6, chopper; 7, sample in cuvette; 8, KOH scrubber; 9, Nafion gas sample dryer; 10, cold trap; 11, detail showing cold trap plates

of the buffers is half the resonator length. Two acoustical notch filters inserted into the gas inlet suppress acoustical noise from the surrounding laboratory. This results in a low background signal in the PA cell and a high sensitivity of approximately $2 \cdot 10^3$ Pa·cm/W. The output signal of each microphone is fed into a lock-in amplifier with an integration time of typically 0.3 s. The phase of the PA signal is a measure for the vibrational-translational (V-T) relaxation time of the sample in a gas mixture; this relaxation time must be much shorter than the inverse of the modulation frequency (typically 0.9 ms) to avoid substantial phase lag between laser beam modulation and PA signal.

2.2.2 CO laser

The CO laser used here is similar to the design proposed by Urban's group at the University of Bonn [27]. Biologically important gases such as ethanol and ethylene absorb strongly around 7 μm, and therefore a CO laser operating at a low temperature is preferred for our experiments. This was achieved by using a 1.3 m long laser tube provided

with a cooling jacket (a liquid nitrogen bath). However, the rotational temperature in a discharge is almost 100 K higher [20], (as derived from the J-dependency of the laser intensity), thereby decreasing the gain. The CO laser can be tuned over about 250 laser lines, yielding a single line emission between 5 and 7.9 μm, by tilting the grating with a stepper motor (Oriel 18512). Multiple line emission occurs only where different vibrational bands overlap, giving rise to less reliable measurements. The laser power is measured with a pyroelectric detector at the zero-order reflection of the grating. The intracavity laser power was then calculated by multiplying the signal from the pyroelectric detector by a frequency-dependent correction factor. This latter was derived by comparing the intensities of light coupled out at zeroth-order and at the outcoupling mirror with known frequency dependent transmission charecteristics [6].

2.2.3 Cold trap

Water absorbs strongly over almost the entire wavelength region of the CO laser and is always present in relatively large amounts. Many water scrubbers are commercially available; however, most of them to some extent also trap the analyte gas under study. The Nafion gas sample dryer (Perma Pure Inc., Model MD-050), operated in combination with a cold trap in the multicomponent experiments, removes water very efficiently. However, care should be exercised because ethanol, one of the detected trace gases, shows a tendency for sticking to the Nafion membrane (see Appendix 2.8).

The newly designed three-level cold trap reduces the effect of spectral interference and increases the selectivity by trapping water and possibly other interfering volatiles. The cold trap consists of a Duran$^{\text{TM}}$ Dewar and four sets of double plates made of aluminium and stainless steel (see Figure 2.1). Copper wires connected to the lowest level trap are immersed in liquid nitrogen at the bottom of the Dewar flask. Additional copper wires, interconnecting different levels of the trap, reduce the temperature of other levels. The incoming gas flow is first led to the upper level containing nine banana shaped holes enclosing the tubes with a relatively large inner diameter. This level is kept at a temperature of about -10 °C to freeze out major part of water vapor thus preventing early obstruction of thin tubes at lower levels. Each of the outlet tubes at the upper level is connected to one of the three lower stages. The upper plate of each stage encloses thin tubes with an inner diameter of 0.1 mm in a long coil-shaped hole milled in the plate for optimal heat exchange (see detail in Figure 2.1). The plates are temperature controlled by a sensor and heater mounted on these plates. For the moderate flows (up to 5 l/h) used in the experiments, the gas mixture in the tubes is at nearly the same temperature as the plates themselves. The temperatures of the lower, middle and upper levels, usually set to -170, -120, and -65 °C, are stable within 0.5, 0.2, and 0.2 °C, respectively, as measured locally by the temperature sensors. The cold trap is automatically refilled approximately every 2 h. Filling from below by a funnel prevents large temperature fluctuations at upper traps by the incoming liquid nitrogen.

The lowest level trap can be used for detection of, e.g., ethylene and ethane, separating them from other gases such as water, ethanol, and acetaldehyde. Many other gases have vapor pressures below the ppb level at this temperature thus allowing a precise concentra-

tion measurement. The -120 °C level trap is used for measurements of acetaldehyde and CO_2, while the -65 °C trap must be utilized in series of ethanol measurements. Therefore, ethanol concentration measurements generally possess a rather high uncertainty due to a large interference with other gases at such relatively high temperature (especially water, with a vapor pressure of around 5 ppm at -65 °C).

2.3 Multicomponent analysis

The PA trace gas detector is fully computer controlled and capable of measuring several gases quasi-simultaneously, i.e., within a time span of several minutes. The PA signal on a single laser line is the sum of the contributions of each constituent gas (that absorbs at this laser line) and a background signal, which is mainly due to heating of windows and absorption of laser radiation by the resonator wall. To calculate the concentrations of n absorbing trace gases, it is necessary to record the amplitude of the PA signal (in case of fast relaxing gas mixtures phase information can be omitted) on N laser lines, with N $\geq$ n+1. The PA signal S_i on line i (in V) is given by

$$S_i = F \cdot P_i \cdot [b_i + \sum_{j=1}^{n} C_j \alpha_{ij}] \qquad (2.1)$$

where F is the cell constant (in cmV/W); C_j is the partial pressure of gas j (in atm); α_{ij} is the absorption coefficient of gas j on line i (in $atm^{-1} \cdot cm^{-1}$); b_i is the background signal on line i (in cm^{-1}); and P_i is the intracavity laser power (in W). In the ideal case, there is a unique solution to this set of linear equations. In practice, however, there do exist sources of errors such as acoustical noise (important for very low PA signals), absorption of remaining trace gases not taken into account in the calculation, errors in the absorption coefficients and possibly strongly varying concentrations during a measurement cycle. If not all constituents in the gas mixture are known a complete spectrum must be recorded, revealing all absorbing constituents.

In fact, the PA signal is a vector quantity containing phase and amplitude information. However, since nearly all experiments were performed in rapidly relaxing gas mixtures (low O_2 and high H_2O vapor), the phase of the signal was fairly constant (and thus contained little information). Therefore, the applied algorithm to calculate the concentration of each compound [6, 18] based on equation 2.1 is adequate for our purposes. In general, an overdetermined (N > n+1) set of equations is preferred to reduce the error in calculated concentrations. However, for rapidly varying concentrations, the measuring time per cycle should be as short as possible. In this case, it is better to reduce the number of laser lines since it takes up to 1 minute to sample the PA signal on each laser line and move the grating with the stepper motor to the next laser line.

2.4 Determination of absorption coefficients

2.4.1 Experimental conditions

The PA spectra of H_2O, CO_2, ethanol, acetaldehyde, and ethylene gases and the background PA signal were recorded by scanning the laser over all emission lines at a PA cell temperature of 298-300 K and a pressure slightly above atmospheric. Each spectrum was recorded several times (typically five), and average values for absorption coefficients (with their standard deviations) were determined at each laser line.

The absorption coefficients of H_2O were determined first; the strong ν_2 bending mode of H_2O is centred at 1595 cm^{-1}. Water contributes significantly to the PA signal due to this strong absorption, even if the coldest level of the trap is being operated. This is partly due to a slow release of the highly polar water molecules that have formed molecular layers on the resonator walls and tubing. The relative H_2O absorption coefficients were determined by flowing the carrier gas through the cold trap set at a relatively high temperature, providing a water concentration of about 1000 ppm. However, this approach resulted in reduced intracavity laser power levels at frequencies corresponding to strong water absorption. Therefore, measurements at a lower water concentration of about 10 ppm were used for those laser lines. A constant background signal was consistently subtracted from the measured data. Absolute values for the absorption coefficients were obtained by scaling the data to the values obtained from the Hitran 1996 database [12] using a least squares fit on 160 data points (R = 0.995).

CO_2 possesses a medium absorption (3 ν_2 band) at 1932 cm^{-1} and a weaker absorption band around 1400 cm^{-1}. The highest CO_2 absorption coefficient is approximately 1000 times smaller than that of the other gases and therefore a much higher concentration was used. A mixture of 1.56% CO_2 in the carrier gas was produced on-line using electronic mass flow controllers (Brooks 5850, Veenendaal, the Netherlands). Scaling our values to the absorption coefficients from the Hitran 1996 database (where available) using a least-squares fit on 36 data points (R = 0.992) yielded absolute values.

Ethanol shows a strongly absorbing in-plane OH-bending mode around 1400 cm^{-1} and a weaker absorption around 1900 cm^{-1}. Acetaldehyde possesses a very strong absorption band due to the ν_4 C=O stretching mode centred at 1774 cm^{-1} and exhibits in addition few weaker absorptions between 1400 and 1500 cm^{-1} [28]. Relative absorption coefficients for ethanol and acetaldehyde were determined by applying a constant flow of carrier gas (air or nitrogen) through a small glass container containing a smaller bottle with the liquid sample. A number of small needles in the cap of the inner bottle act as diffusion channels to control the concentration of the sample. The measurement was initiated when the concentration (typically a few hundred ppm) in the flow was constant. Since ethanol absorbs very weakly between 1600 and 1800 cm^{-1}, a higher ethanol concentration was used in this wavelength region to obtain reliable absorption coefficients here, too.

Ethylene possesses a strong absorption band due to the ν_{12} scissor mode centred at 1444 cm^{-1} and in addition a slightly weaker absorption near 1889 cm^{-1} due to the $\nu_7 + \nu_8$ combination band [15]. The absorption coefficients for ethylene were determined by mixing gaseous ethylene with the carrier gas to a concentration of a few hundred ppm

using electronic mass flow controllers.

A scan over all 223 laser lines (only 202 laser lines are included in Table 2.2) takes about one hour. During the first few hours, the water concentration decreases rapidly, which is associated with cells becoming drier owing to the cold trap. For this reason, the first two or three scans were always rejected. The relative absorption coefficients were corrected by subtracting both the background signal and the contribution of water vapor from the PA spectra.

In order to obtain absolute values for absorption coefficients of selected trace gases, the PA cell response was first calibrated using a mixture containing a known concentration of CO_2 in nitrogen and by scaling the data to the CO_2 absorption coefficients from the Hitran 1996 database. The H_2O and CO_2 absorption coefficients were calculated from the database by taking into account homogeneous pressure broadening using a Lorentzian lineshape function. Subsequently, at specific laser lines the PA signal generated by a certified gas mixture of ethanol (Scott Specialty Gases, $50.9 \pm 5\%$ ppm in nitrogen) and ethylene (Praxair, 1.04 ppm in nitrogen) was recorded. The calibrated PA cell response allows a direct determination of absolute absorption coefficients because the concentration of trace gases is known. Absolute absorption coefficients for acetaldehyde were determined in a similar manner, however instead of a certified mixture, an injection of a known amount of vapor into a nitrogen flow was used to obtain an absolute calibration.

2.4.2 Experimental results

The absorption coefficients for H_2O, CO_2, ethanol, acetaldehyde and ethylene gases are tabulated in Table 2.2 including the standard deviation (see appendix). The calculated absorption coefficients of H_2O and CO_2 from the Hitran 1996 database are also shown in Table 2.2.

The H_2O measurements are in reasonable agreement with the Hitran data except for a region below 1400 cm^{-1} and for the case of overlapping vibrational CO bands (see Table 2.2 and Figure 2.2). After rejection of low-power laser lines and those showing multiple-line emission (leaving 168 laser lines), 67% of the measured absorption coefficients are within 20% of the values as calculated from the Hitran database. Below 1400 cm^{-1} deviations are partly due to the relatively low laser output power and a systematic error in the laser power. This error in the laser power is due to inaccuracy in the frequency-dependent ratio of the zero-order reflection of the grating and the intracavity laser power, which itself is difficult to determine precisely in the low-power region. In the case of overlapping vibrational CO bands, the CO laser can operate on two laser lines. Hence, the PA signal is the sum of individual PA signals on each laser line (the ratio of these two signals depends actually on the operating conditions of the CO laser). As an example, a discrepancy is observed when comparing measured H_2O absorption coefficients on v14j13 * (1732.85254 cm^{-1}) and v15j6 (1733.28711 cm^{-1}) and the calculated values in Table 2.2. Figure 2.2 shows clearly in case of overlapping vibrational bands that calculated and experimentally obtained values can deviate substantially.

---

*v=15 → 14, j=12 → 13
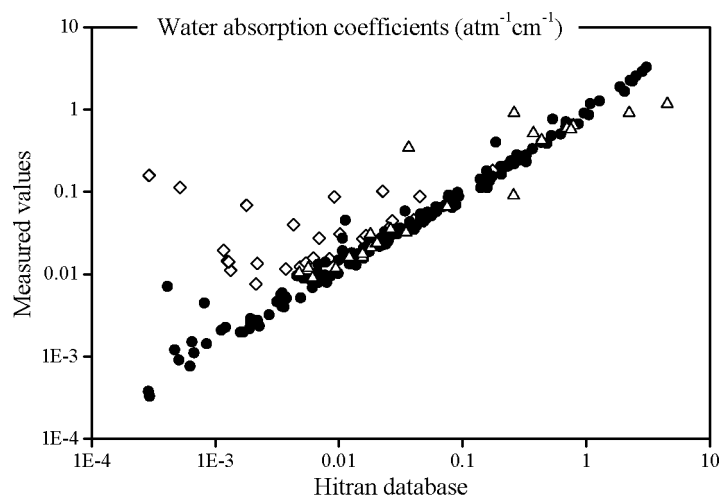
Figure 2.2: *Measured absorption coefficients for water vapor plotted against the values obtained from the Hitran database. (•) laser lines between 1400 and 2000 cm^{-1}; (△) nearly coinciding laser lines between 1400 and 2000 cm^{-1} in case of overlapping vibrational bands; and (◇) laser lines between 1300 and 1400 cm^{-1}.*

Figure 2.3 shows the CO_2 absorption coefficients and data from the Hitran database between 1845 and 1975 cm^{-1}. Between 1425 and 1810 cm^{-1} no data are available in the Hitran database. The CO_2 absorption is very weak outside this wavelength region except for the small absorption around 1400 cm^{-1}. Measured CO_2 absorption coefficients in the region between 1845 and 1975 cm^{-1} are in reasonable agreement with those from the Hitran database; 68% of the 39 measured absorption coefficients are within 20% of the values calculated from the Hitran database. On many laser lines, the PA signal generated by CO_2 is even smaller than the background signal, precluding a reliable determination of the absorption coefficient at these laser lines. Due to weak absorption by CO_2, a high concentration had to be used requiring the cold trap to be operated at a relatively high temperature. As this approach has resulted in a relatively high concentration of water in the flowing sample, no better agreement was expected. Improvement is anticipated if a chemical scrubber (such as P_2O_5) is used, that reduces the water concentration to a few ppm (while allowing simultaneously for high CO_2 concentration).

To our knowledge, in this spectral range literature data for ethanol, acetaldehyde, and ethylene (see Figures 2.4, 2.5, and 2.6) are lacking, and hence no comparison of the absorption coefficients obtained here could be made. In the analysis of the data, three important error sources are readily recognized. First, subtraction of the PA signal generated by water vapor introduces errors, in particular for trace molecules exhibiting weak absorption on a laser line at which absorption of water vapor is high. Similarly, trace gases requiring a relatively high operation temperature of the cold trap give rise to stronger interference. Examples of the latter are ethanol and CO_2 absorption coefficients, which show larger standard deviations. Second, in the case of overlapping vibrational CO bands,
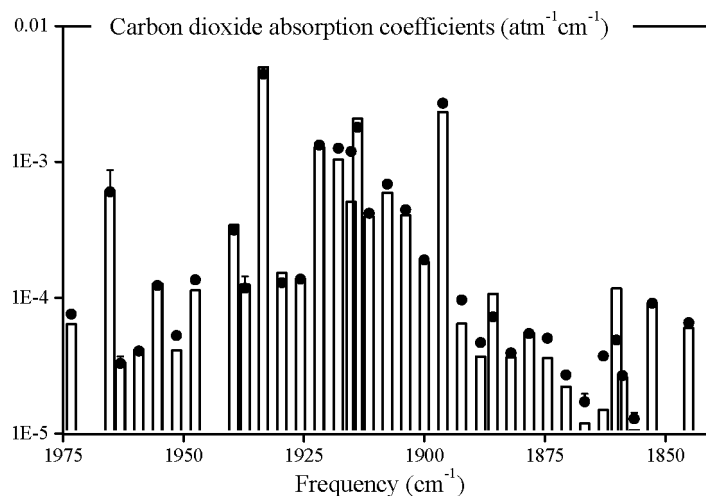
Figure 2.3: *Comparison between the PA spectrum (●) and the calculated Hitran infrared spectrum (⊓) for CO_2 gas between 1845 and 1975 cm^{-1}. Error bars refer to one standard deviation of the data. Missing error implies that the latter is smaller than the symbol size.*

the laser may show multiple-line emission, with the resulting PA signal being the sum of PA signals obtained at each laser line (see Figure 2.2). Finally, in case of weak absorptions the background signal becomes important, because the magnitude of the PA signal generated by the trace molecules becomes comparable to the background signal. In the presence of such relatively large background signals, the values of the absorption coefficients show a large uncertainty.

As compared to situations where nitrogen is used as carrier gas, the results for trace gas mixtures in air were similar. A phase lag (up to 45 °) occurred in samples with a low water content (water accelerates vibrational relaxation) indicating that relaxation properties of the gas mixture have changed. Facing a similar problem working with CO_2–N_2 gas mixtures using a CO_2 laser-based PA detector, Moeckli et al. applied a different algorithm taking into account phase information and vibrational relaxation times of the gas mixture [19]. The same algorithm can be applied here for gas mixtures containing O_2, although this approach would require accurate knowledge of the appropriate relaxation times.

2.5 Monitoring the emission of trace gases released by Conference pears

The PA detector was used to study emission of trace gases emitted by Conference pears exposed to a flow of pure nitrogen; low emission rates of volatiles require the use of such a detection scheme. Prior to the experiment, the pears were kept in large containers under normal storage conditions (2% O_2 and 0% CO_2) for nine months.
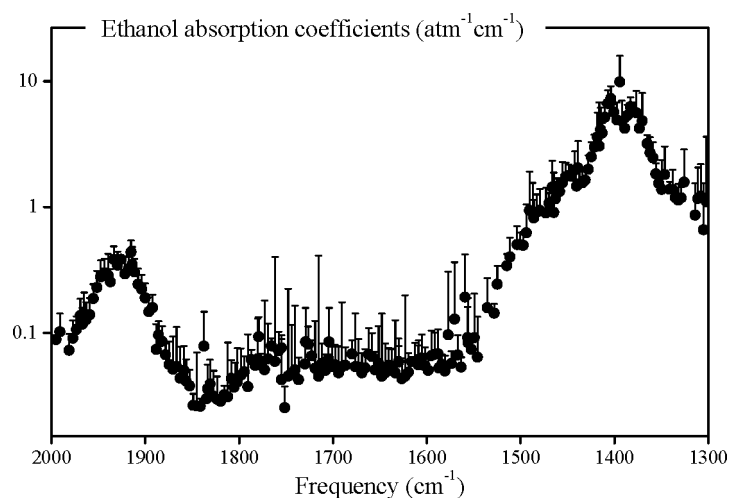
Figure 2.4: *The PA spectrum of ethanol; error bars refer to one standard deviation of the data. Missing error implies that the latter is smaller than the symbol size.*
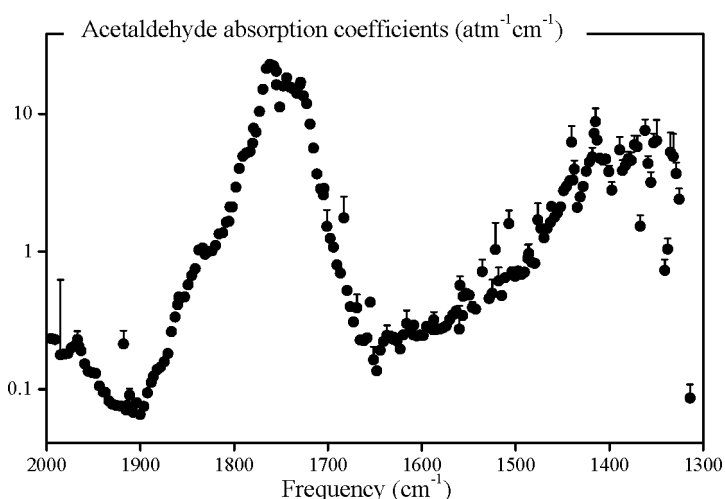
Figure 2.5: *The PA spectrum of acetaldehyde; error bars refer to one standard deviation of the data. Missing error implies that the latter is smaller than the symbol size.*

Ethylene, H_2O, ethanol, and acetaldehyde were analyzed (interference of other gases is expected to be small) by tuning the laser to six emission lines, marked by an asterisk (*) in Table 2.2. This selection of laser lines is based on factors such as laser power, absorption strength, and interferences. The latter can be quantitatively described in terms of cross-sensitivities as proposed by Meyer and Sigrist [18]. Cross sensitivities Q_{ij} were computed for four laser lines at which absorptions are maximal (see Table 2.1). Most off-diagonal elements in Table 2.1 are relatively small, indicating a low degree of mutual interference.
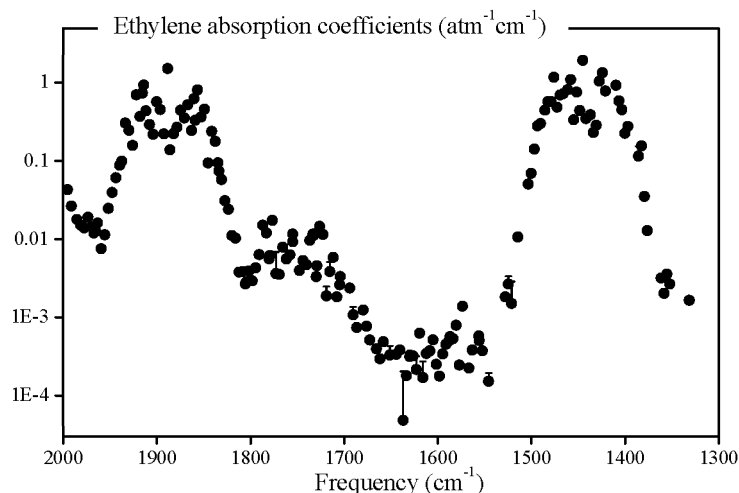
Figure 2.6: *The PA spectrum of ethylene; error bars refer to one standard deviation of the data. Missing error implies that the latter is smaller than the symbol size.*

The interference of ethylene and ethanol (Q_{21}) and that of acetaldehyde with all other trace gases (see last column) form an exception.

Table 2.1: *Cross sensitivities for four laser lines used in the multicomponent analysis of trace gases released by Conference pears.*

		Q_{ij}			
laser line	i↓ j→	C_2H_5OH	C_2H_4	H_2O	CH_3CHO
v28j8	C_2H_5OH	1	0.083	0.002	0.67
v26j11	C_2H_4	0.94	1	0.009	1.6
v19j11	H_2O	0.13	0.0005	1	0.75
v13j11	CH_3CHO	0.0038	0.00038	0.0001	1

A KOH scrubber was capable of removing CO_2 from the flow. To avoid early obstruction of the cold trap, sample flow was dried by means of a Nafion gas sample dryer (see Figure 2.1). A fraction of the flow was led to the cold trap level kept at -70 °C (for ethanol measurements), while the remaining part was directed to the -120 °C level to detect acetaldehyde and ethylene.

A typical result obtained for a single pear (weight of 175 g) is shown in Figure 2.7. At t= 0 h, the pear was placed in a cuvette at 0 °C exposed to a nitrogen flow. The ethylene production rate shows a high peak at the start of the measurement; this is ascribed to diffusion of ethylene from the pear. Ethylene is not produced under anaerobic conditions, because O_2 is required for the ethylene biosynthesis [1]. The production rate of acetaldehyde shows a two-hour delay; after that it increases during the next 8 hours. Such

a pattern of acetaldehyde production during the onset of fermentation is typical and has been previously observed for tomato [6] and bell pepper [21]. After reaching a maximum, the production rate declines slightly for almost 12 hours at a rate of 0.80 ± 0.02 nl/h^2.
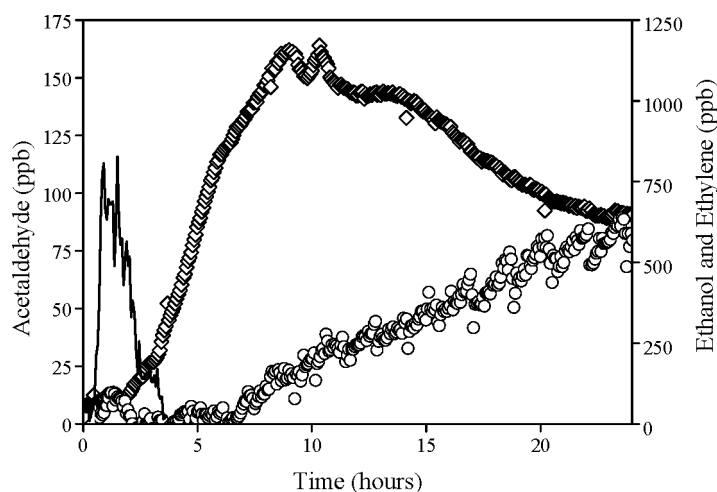
Figure 2.7: *Emission of acetaldehyde ($\Diamond$), ethanol (o), and ethylene (-) from a single pear (weight 175 g) under anaerobic conditions. The emission of ethylene is shown only for the first three hours.*

Initially an artificial peak is observed in the ethanol production rate. This is due to ethylene interference as both ethanol and ethylene exhibit strongest absorption in the very same wavelength regions (see Table 2.1 and Figures 2.4 and 2.6). After placing the pear in the cuvette the ethanol production rate shows a delay of approximately 5 hours. Subsequently, the ethanol release increases linearly with time (at a rate of 8.5 ± 0.2 nl/h^2) during the entire experiment. One reason for the observed delay in the onset of fermentation is a depletion of internal O_2 [21]. Furthermore, at a flow rate of 4 l/h it takes more than 1 h for the O_2 concentration within the cuvette to drop below 0.5%. It is known that at this O_2 level, the ratio of CO_2 release to O_2 uptake is around 2 indicating that respiration and fermentation rates are comparable [24]. The acetaldehyde and ethanol production rates are extremely low above this O_2 concentration, whereas they increase steeply below this concentration [23]. In similar experiments a cuvette was flushed with a nitrogen flow of 5 l/m for 1 min, reducing the onset of fermentation from 2 to 1 h. Measurements of internal O_2 are planned to determine the time period needed to establish anoxia within the pear after switching to anaerobic conditions [21].

2.6 Conclusions

The absorption coefficients of water vapor, carbon dioxide, ethylene, ethanol, and acetaldehyde at CO laser frequencies have been determined using a CO laser-based PA spectrometer. Measured relative absorption coefficients for CO_2 and H_2O agree reasonably well with data in the Hitran database. For laser lines showing multiple emission or having an intracavity power below about 0.3 Watt, agreement is less favourable. Comparison of calculated and measured H_2O absorption coefficients shows the presence of a systematic error in the long wavelength region. Most likely this result is caused by the inaccurate determination of the frequency dependent ratio of the zero order reflection and the intracavity laser power. However, with the present data it will be possible to correct this ratio on the basis of the observed and calculated H_2O absorption coefficients.

Measured spectra were used in a simultaneous multicomponent analysis of trace gases released by Conference pears. A three-level cold trap made it possible to detect four trace gases at ppb concentration levels (and sub-ppb acetaldehyde). PA detectors based on liquid nitrogen-cooled CO lasers are relatively large and therefore not appropriate for field measurements (e.g., a fruit storage room). Recently, small high power solid-state light sources have been developed and applied in PA experiments; e.g., Paldus and co-workers used a continuous wave (cw) quantum-cascade laser detecting ammonia and water vapor [22] while Kühnemann et. al. measured ethane, methane, and ethylene using a cw optical parametric oscillator [14]. Fehér and co-workers used a near-infrared laser diode attaining a sensitivity of 8 ppb for ammonia [7]. In the near future, detection limits of these systems may become comparable to those of gas laser-based PA detectors, making them perfectly suited for field measurements.

2.7 Acknowledgements

References

[1] F.B. Abeles, P.W. Morgan, M.E. Salveit Jr., In: 'Ethylene in Plant Biology', (Academic Press, London, 1992) 2nd ed., Chap. 3, p. 42-43

[2] A.G. Bell, On the production and reproduction of sound by light. Am. J. of Sciences, Third Series, **20** 305-324 (1880)

[3] S. Bernegger, M.W. Sigrist, CO-Laser photoacoustic spectroscopy of gases and vapours for trace gas analysis. Infrared Phys. **30** 375-429 (1990)

[4] F.G.C. Bijnen, J. Reuss, F.J.M. Harren, Geometrical optimization of a longitudinal resonant photoacoustic cell for sensitive and fast trace gas detection. Rev. Sci. Instru-

ments **67** 2914-2923 (1996).

[5] F.G.C. Bijnen, F.J.M. Harren, J.H.P. Hackstein, J. Reuss, Intracavity CO laser photoacoustic trace gas detection: cyclic CH_4, H_2O and CO_2 emission by cockroaches and scarab beetles. Appl. Opt. **35** 5357-5368 (1996)

[6] F.G.C. Bijnen, H. Zuckermann, F.J.M. Harren, J. Reuss, Multi-component trace gas analysis by three photoacoustic cells intracavity in a CO-laser; observation of anaerobic and post anaerobic emission of acetaldehyde and ethanol in cherry tomatoes. Appl. Opt. **37** 3345-3350 (1998)

[7] M. Fehér, Y. Jiang, J.P. Maier, A. Miklós, Optoacoustic trace gas monitoring with near-infrared diode-lasers. Appl. Opt. **33** 1655-1658 (1994)

[8] F.J.M. Harren, J. Reuss, Photoacoustic spectroscopy. In: 'Encyclopedia of applied physics', G.L. Trigg (ed.), VCH Wennheim, Vol. 19, pp. 413-435 (1997)

[9] A. Gerasimchuk, S. Kornilov, I. Ostrejkovskij, E. Protsenko, S. Tymper, Selective optothermal detection of NO_2 and H_2O with a frequecy-tuned CO wave-guide laser. Appl. Phys. B **55** 503-508 (1992)

[10] T. Giesen, R. Schieder, G. Winnewisser, K.M.T. Yamada, Precise measurements of pressure broadening and shift for several H_2O lines in the ν_2 band by argon, nitrogen, oxygen, and air. J. Mol. Spectrosc. **153** 406-418 (1992)

[11] F. Harren, J. Reuss, E.J. Woltering, D.D. Bicanic, Photoacoustic measurement of agriculturally interesting gases and detection of C_2H_4 below the ppb level. Appl. Spectrosc. **44** 1360-1368 (1990)

[12] Hitran Atmospheric Workstation for Windows, 1996 Ontar Corporation

[13] E.L. Kerr, J.G. Atwood, The laser illuminated absorptivity spectrophone: a method for measurement of weak absorptivity in gases at laser wavelengths. Appl. Opt. **7** 915-921 (1968)

[14] F. Kühnemann, K. Schneider, A Hecker, A.A.E. Martis, W. Urban, S. Schiller S, J. Mlynek, Photoacoustic trace-gas detection using a cw single-frequency parametric oscillator, Appl. Phys. B **66** 741-745 (1998)

[15] D. van Lerberghe, A. Fayt, High resolution study of the $\nu_7 + \nu_8$ band of ethylene (C_2H_4) at 1889 cm^{-1}. Mol. Phys. **31** 1875-1886 (1976)

[16] S. te Lintel Hekkert, M.J. Staal, R.H.M. Nabben, H. Zuckermann, S. Persijn, L.J. Stal, L.A.C.J. Voesenek, F.J.M. Harren, J. Reuss, D.H. Parker, Laser photoacoustic trace gas detection, an extremely sensitive technique applied in biological research. Instr. Sci. Technol. **26** 157-175 (1998)

[17] R.T. Menzies, M.S. Shumate, Optoacoustic measurements of water vapor absorption at selected CO laser wavelengths in the 5-μm region. Appl. Opt. **15** 2025-2027 (1976)

[18] P.L. Meyer, M.W. Sigrist, Atmospheric-pollution monitoring using CO_2-laser photoacoustic-spectroscopy and other techniques. Rev. Sci. Instrum. **61** 1779-1807 (1990)

[19] M.A. Moeckli, C. Hilbes, M.W. Sigrist, Photoacoustic multicomponent gas analysis using a Levenberg-Marquardt fitting algorithm. Appl. Phys. B **67** 449-458 (1998)

[20] G. Nelke, "Sealed-off"-CO-Lasertätigkeit nahe der unteren Grenztemperatur. MSc Thesis, Institut für Angewandte Physik der Universität Bonn (1992)

[21] J. Oomens, H. Zuckermann, S.T. Persijn, D.H. Parker, F.J.M. Harren, CO-laser-based photoacoustic trace-gas detection: applications in postharvest physiology. Appl. Phys. B **67** 459-466 (1998)

[22] B.A. Paldus, T.G. Spence, R.N. Zare, J. Oomens, F.J.M. Harren, D.H. Parker, C. Gmachl, F. Cappasso, D.L. Sivco, J.N. Baillargeon, A.L. Hutchinson, A.Y. Cho, Photoacoustic spectroscopy using quantum-cascade lasers. Opt. Lett. **24** 178-180 (1999)

[23] H.W. Peppelenbos, The use of gas exchange characteristics to optimize CA storage and MA packaging of fruits and vegetables. Ph.D. Thesis, Landbouw Universiteit Wageningen (1996)

[24] H.W. Peppelenbos, Press communication.

[25] W. Schnell, G. Fischer, Spectrophone measurements of isotopes of water vapor and nitric oxide and of phosgene at selected wavelengths in the CO and CO_2 laser region. Opt. Lett. **2** 67-69 (1978)

[26] G.D.T. Tejwani, Improved calculated linewidth for H_2O broadened by N_2. J. Quant. Spectrosc. Radiat. Transfer **40** 605-612 (1988)

[27] W. Urban, Infrared lasers for spectroscopy. In: 'Frontiers of laser spectroscopy of gases', A.C.P. Alves, J.M. Brown, M. Hollas, (Kluwer Academic Publishers, NATO-ASI Series, 1988) p. 9-42

[28] K.B. Wiberg, Y. Thiel, L. Goodman, J. Leszczynski, Acetaldehyde -harmonic frequencies, force-fields, and infrared intensities. J. Phys. Chem **99** 13850-13864 (1995)

[29] K.M.T. Yamada, M. Harter, T. Giesen, Survey study of air-broadened water-vapor lines in the ν_2 band by high-resolution FTIR spectroscopy. J. Mol. Spectrosc. **157** 84-94 (1993)

[30] H. Zuckermann, F.J.M. Harren, J. Reuss, D.H. Parker, Dynamics of acetaldehyde production during anoxia and post-anoxia in Red Bell pepper studied by photoacoustic techniques. Plant Physiol. **113** 925-932 (1997)

2.8   Appendix: Side effects of scrubbers

A gas mixture which is passed over a sample contains already a number of infrared absorbing gases like H_2O, CH_4, N_2O, and CO_2. Furthermore, the sample can release, in addition to the trace gas(es) of interest, a whole variety of other infrared absorbing trace gases. To achieve the most reliable detection of the trace gas of interest, spectral interference by these other compounds must be reduced by choosing the appropriate laser lines. However, in most cases some interference remains and lowering the concentration of interfering compounds can be the only solution. We apply (a combination of) four techniques to reduce the concentration of interfering compounds:

- A cold trap reduces the concentration of molecules with a partial pressure above their vapour pressure at the cold trap temperature [3].

- Catalytic oxidizers oxidise hydrocarbons in the presence of O_2 and a catalyst (in our case platinum on Al_2O_3) giving H_2O and CO_2 as end products [1]. The catalytic oxidizer operates at a temperature of about 400 °C.

- Scrubbers, normally in the form of powder or pellets, bind or react with the interfering compound.

- The Nafion$^®$ gas sample dryer removes H_2O vapour using a selective H_2O permeable co-polymer [7].

The two latter techniques will be described in more detail; in particular the effect of both techniques on the ethanol level in the sample flow.

2.8.1 CO_2 scrubbers

CO_2 absorbs very weakly in the CO ($\Delta v=1$) laser wavelength region; the strongest absorption is about 1000 times weaker than that of many other trace gases [3]. However, biological samples release CO_2 in much higher quantities than other compounds (except H_2O). In addition, in crop storage experiments elevated CO_2 levels (up to 10%) are often used to reduce the respiration of the crop. CO_2 can be removed very efficiently using chemical scrubbers such as soda lime or KOH. When soda lime (calcium hydroxide) is put in contact with CO_2, a strong, exothermic reaction takes place in which CO_2 binds to the soda lime pellets (forming H_2O and calcium carbonate, i.e., limestone). A pH-sensitive color indicator (e.g., ethyl violet) changes color as CO_2 reacts with the soda lime pellets [6]. However, ethanol molecules adsorb at the soda lime pellets giving a lower ethanol level and slow time response (data not shown).

After hydration, the surface of KOH pellets (potassium hydroxide) is dissolved, giving K^+ and OH^-. In contrast to soda lime, KOH does not trap ethanol from a gas flow. However, at elevated CO_2 levels, KOH starts to bind ethanol and already at 0.5% CO_2 a strong decrease in ethanol concentration is observed. At high CO_2 levels virtually all ethanol is removed as can be seen in Figure 2.8 [2].
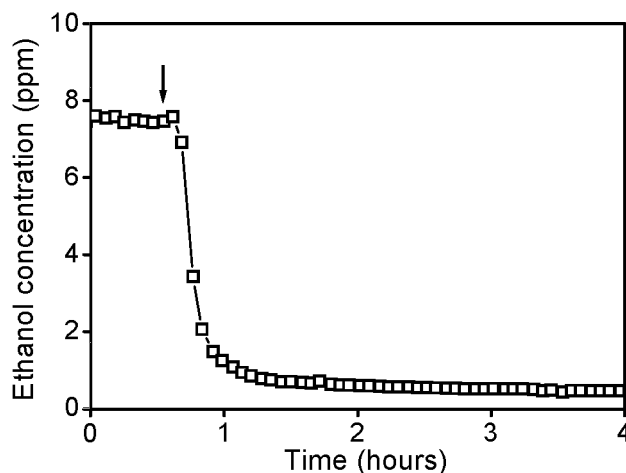
Figure 2.8: A gas flow containing ethanol is passed through a KOH scrubber. At the time indicated by the arrow, 3.8% CO_2 was added to the gas flow, leading to an instant reduction in ethanol level in the gas flow as part of the ethanol is trapped by KOH [2].

However, due to an improved determination of the ethanol and CO_2 absorption coefficients it became possible to use high CO_2 levels without affecting the calculated ethanol concentration (see Figure 2.9). Therefore, the CO laser-based spectrometer can also be used as a CO_2 detector with a large dynamic range (from the ppm level up to 10%).
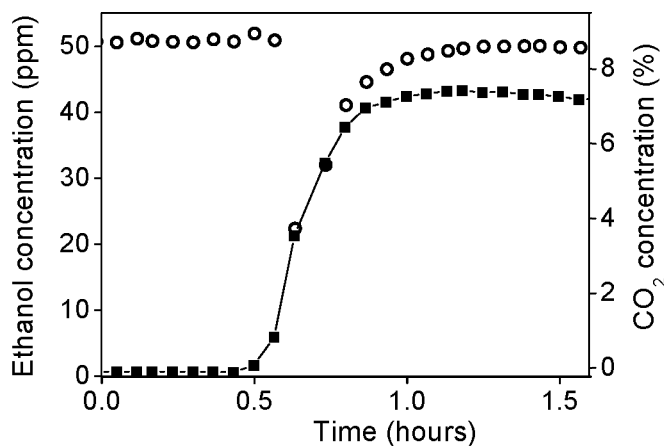
Figure 2.9: In a N_2 flow containing 50 ppm ethanol (○), addition of 7% CO_2 (■) (at t= 0.5 h) does not affect the calculated ethanol level. The resonance frequency of the PA cell is lowered by adding CO_2 since the velocity of sound in CO_2 (267 m/s) is lower than in N_2 (343 m/s). Therefore, the modulation frequency was adjusted to the newly calculated value (also at t= 0.5 h) giving a transient disturbance of the ethanol concentration.

2.8.2   H₂O vapour scrubbers

H₂O vapour can be efficiently removed using CaCl₂ or P₂O₅, the latter can reduce H₂O vapour to such low levels (a few ppm) that no cold trap is needed which is beneficial for long-term experiments. However, these H₂O vapour scrubbers trap ethanol partly (CaCl₂) or even totally (P₂O₅) as is shown in Figure 2.10.
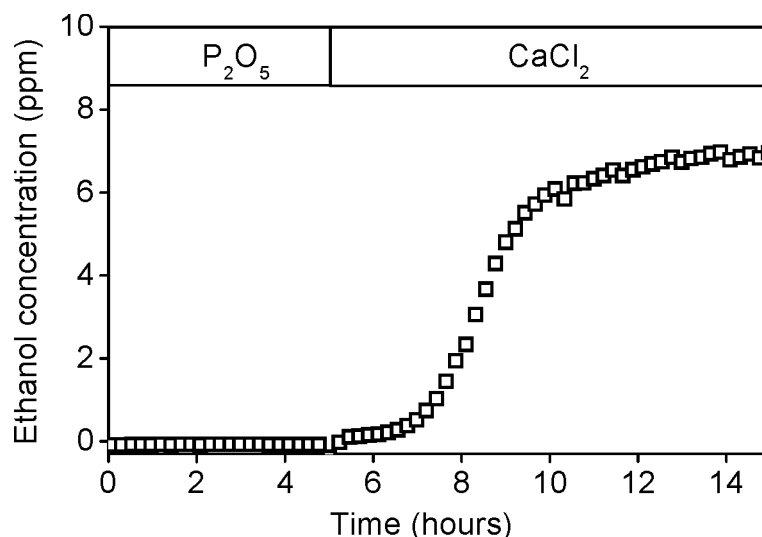
Figure 2.10: *At the start of the measurement a nitrogen flow containing 10 ppm ethanol is passed through a P₂O₅ scrubber. This scrubbers traps virtually all the ethanol from the gas flow. At t=5 h the P₂O₅ scrubber was replaced by a CaCl₂ scrubber, resulting in a slow time response and a partly removal of ethanol from the flow.*

2.8.3   C₂H₄ scrubbers

In commercial containers used for transport of C_2H_4 sensitive products, such as lettuce or celery, potassium permanganate pads are often installed to absorb the ethylene released by the crop [4]. Potassium permanganate oxidises alkenes to form glycols, i.e., ethylene is oxidised to ethylene glycol:

$$3C_2H_4 + 2KMnO_4 + 4H_2O \rightarrow 2MnO_2 + 2KOH + CH_2OHCH_2OH \qquad (2.2)$$
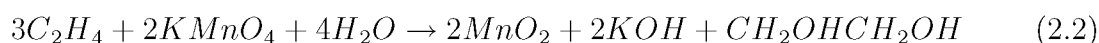
Also when ethane (C_2H_6) release from fruit is measured, the C_2H_4 level must normally be reduced since ethylene is released at a much higher rate than ethane (typically more than a hundred times) making C_2H_6 detection difficult due to spectral interference. C_2H_4 and C_2H_6 can not be separated using a cold trap, e.g., at -160 °C both gases still have vapour pressures above 100 Pa. Potassium permanganate removes C_2H_4 without affecting the level of C_2H_6. As a result, C_2H_6 measurements become more reliable.

Also when measuring nitric oxide (NO) release from fruit or plants with a CO $\Delta v=1$ laser, the C_2H_4 level should be reduced since the NO and C_2H_4 absorption bands overlap, and in addition, C_2H_4 is normally released at a much higher rate than NO. However, the polar NO molecule adsorbs very effectively on the potassium permanganate pellets, and in addition, a cold trap can not be used to separate the two compounds.

2.8.4   Nafion gas sample dryer

The Nafion$^\circledR$ gas sample dryer consists of two coaxial tubes: the sample flow is directed through the inner tube that is made of a H_2O permeable co-polymer Nafion$^\circledR$, while a dry gas flow is purged through the outer tube. H_2O is removed on basis of the humidity gradient between the in- and outside of the inner tube [7]. Most substances are retained quantitatively but some polar organic substances like ethanol are partly absorbed by the co-polymer. In subsequent measurements, the ethanol molecules can be released again, giving spurious results.

References

[1] K.C. Eastwell, P.K. Bassi, M.E. Spencer, Comparison and evaluation of methods for the removal of ethylene and other hydrocarbons from air for biological studies. Plant Physiol. **62** 723-726 (1978)

[2] M.O. Kelly, M.E. Saltveit, Effect of endogenously synthesized and exogenously applied ethanol on tomato fruit ripening. Plant Physiol. **88** 143-147 (1988)

[3] S.T. Persijn, R.H. Veltman, J. Oomens, F.J.M. Harren, D.H. Parker, CO laser absorption coefficients for gases of biological relevance: H_2O, CO_2, ethanol, acetaldehyde, and ethylene. Appl. Spectrosc. **54** 62-71 (2000)

[4] E.M. Welby, B. McGregor, 'Agricultural export transportation workbook.' Agriculture Handbook no. 700. Washington, DC, U.S.A. Department of Agriculture, pp 219 (1993)

[5] A.D. Wood, M. Camac, E.T. Gerry, Effects of 10.6-μ laser induced air chemistry on the atmospheric refractive index. Appl. Opt. **10** 1877-1884 (1971)

[6] http://www.nwdesigns.com/rebreathers/sofnolime.htm

[7] http://www.permapure.com/newweb/PRODUCTS.htm

2.9 Appendix: Absorption coefficients of water, CO_2, ethylene, acetaldehyde, and ethanol

Table 2.2: *Absorption coefficients (in $atm^{-1}cm^{-1}$) of water, CO_2, ethylene, acetaldehyde, and ethanol diluted in nitrogen. The standard deviation of the data (in parenthesis) is in the units of the last digit. A dash (-) indicates that no absorption coefficient could be determined due to, e.g., a weak absorption, high water interference, or low laser power. An asterisk (*) marks six laser lines that are used in the multicomponent analysis. Furthermore, absorption coefficients as calculated from the Hitran database are given for water and CO_2.*

laser line	frequency cm^{-1}	H_2O $atm^{-1}cm^{-1}$	H_2O Hitran	CO_2 $atm^{-1}cm^{-1}$	CO_2 Hitran	ethylene $atm^{-1}cm^{-1}$	acetaldehyde $atm^{-1}cm^{-1}$	ethanol $atm^{-1}cm^{-1}$
v31j10	1328.80481	$1.44\ (3){\cdot}10^{-2}$	$1.25{\cdot}10^{-3}$	-	-	-	3.7 (7)	$1.2\ (3){\cdot}10^{-1}$
v31j9	1331.87549	$1.11\ (6){\cdot}10^{-2}$	$1.33{\cdot}10^{-3}$	-	-	$1.6\ (1){\cdot}10^{-3}$	5 (2)	1.1 (4)
v31j8	1334.91235	$1.3\ (1){\cdot}10^{-2}$	$2.18{\cdot}10^{-3}$	-	-	-	5 (2)	1.2 (2)
v31j7	1337.91528	$1.82\ (2){\cdot}10^{-1}$	$1.76{\cdot}10^{-1}$	-	-	-	$1.0\ (2){\cdot}10^{1}$	1.4 (6)
v31j6	1340.88428	$8.7\ (5){\cdot}10^{-2}$	$4.52{\cdot}10^{-2}$	-	-	-	$7\ (2){\cdot}10^{-1}$	1.4 (2)
v30j12	1346.3717	$1.4\ (1){\cdot}10^{-2}$	$1.28{\cdot}10^{-3}$	-	-	-	-	2 (1)
v30j11	1349.54407	$5.1\ (7){\cdot}10^{-2}$	$4.56{\cdot}10^{-2}$	$4.8\ (9){\cdot}10^{-5}$	$2.48{\cdot}10^{-5}$	-	6 (3)	-
v30j10	1352.68286	$7.6\ (3){\cdot}10^{-3}$	$2.13{\cdot}10^{-3}$	$2.1\ (1){\cdot}10^{-4}$	$2.05{\cdot}10^{-4}$	$2.7\ (2){\cdot}10^{-3}$	6 (1)	1.5 (2)
v30j9	1355.78821	$1.23\ (9){\cdot}10^{-2}$	$4.87{\cdot}10^{-3}$	$5.9\ (1){\cdot}10^{-5}$	$4.35{\cdot}10^{-5}$	$3.6\ (2){\cdot}10^{-3}$	3.2 (6)	1.8 (4)
v30j8	1358.85974	$1.6\ (2){\cdot}10^{-2}$	$6.22{\cdot}10^{-3}$	$4.4\ (8){\cdot}10^{-5}$	$2.38{\cdot}10^{-5}$	$2.03\ (6){\cdot}10^{-3}$	4.3 (6)	2.5 (8)
v30j7	1361.89746	$4.4\ (2){\cdot}10^{-2}$	$2.71{\cdot}10^{-2}$	-	-	$3.2\ (2){\cdot}10^{-3}$	7 (2)	2.7 (9)
v30j6	1364.90112	$2.7\ (2){\cdot}10^{-2}$	$6.94{\cdot}10^{-3}$	-	-	-	-	3.2 (5)
v29j13	1366.98938	$4.0\ (6){\cdot}10^{-2}$	$4.29{\cdot}10^{-3}$	-	-	-	1.5 (3)	-
v29j11	1373.4364	$1.37\ (1){\cdot}10^{-1}$	$1.47{\cdot}10^{-1}$	-	-	-	6(1)	4 (1)
v29j10	1376.60999	$1.55\ (9){\cdot}10^{-2}$	$8.37{\cdot}10^{-3}$	$5.3\ (4){\cdot}10^{-5}$	$3.47{\cdot}10^{-5}$	$1.28\ (4){\cdot}10^{-2}$	4.6 (7)	6 (3)
v29j9	1379.74988	$4.43\ (7){\cdot}10^{-2}$	$4.88{\cdot}10^{-2}$	$8.9\ (9){\cdot}10^{-5}$	$4.21{\cdot}10^{-5}$	$3.5\ (6){\cdot}10^{-2}$	4.7 (6)	6 (1)

Table 2.2 continued

laser line	frequency cm^{-1}	H_2O $atm^{-1}cm^{-1}$	H_2O Hitran	CO_2 $atm^{-1}cm^{-1}$	CO_2 Hitran	ethylene $atm^{-1}cm^{-1}$	acetaldehyde $atm^{-1}cm^{-1}$	ethanol $atm^{-1}cm^{-1}$
v29j8	1382.8562	$1.17\ (8)\cdot10^{-2}$	$3.71\cdot10^{-3}$	$1.1\ (5)\cdot10^{-4}$	$8.35\cdot10^{-5}$	$1.542\ (8)\cdot10^{-1}$	4.2 (5)	6 (1)
v29j7	1385.92859	$3.6\ (2)\cdot10^{-2}$	$2.52\cdot10^{-2}$	$1.55\ (6)\cdot10^{-4}$	$1.37\cdot10^{-4}$	$1.1\ (4)\cdot10^{-1}$	3.9 (7)	5 (1)
v29j6	1388.96704	$2.7\ (1)\cdot10^{-2}$	$1.56\cdot10^{-2}$	-	-	-	5 (1)	4.2 (6)
v28j12	1394.14197	$2.6\ (1)\cdot10^{-1}$	$3.02\cdot10^{-1}$	-	-	-	-	10 (6)
v28j11	1397.38342	$4.6\ (1)\cdot10^{-2}$	$4.03\cdot10^{-2}$	$7.5\ (2)\cdot10^{-5}$	$6.59\cdot10^{-5}$	$2.7\ (3)\cdot10^{-1}$	2.8 (4)	5 (2)
v28j10	1400.59167	$3.00\ (6)\cdot10^{-2}$	$2.38\cdot10^{-2}$	$2.8\ (2)\cdot10^{-5}$	$1.02\cdot10^{-5}$	$2.24\ (1)\cdot10^{-1}$	3.9 (4)	-
v28j9	1403.76636	$2.71\ (9)\cdot10^{-2}$	$1.76\cdot10^{-2}$	$2.4\ (1)\cdot10^{-5}$	$5.13\cdot10^{-6}$	$4.5\ (2)\cdot10^{-1}$	4.7 (7)	7 (2)
v28j8*	1406.90735	$1.4\ (6)\cdot10^{-2}$	$7.76\cdot10^{-3}$	$2.61\ (6)\cdot10^{-5}$	$9.66\cdot10^{-6}$	$5.8\ (3)\cdot10^{-1}$	4.7 (4)	7 (2)
v28j7	1410.01453	$1.12\ (2)\cdot10^{-1}$	$1.58\cdot10^{-1}$	$3.6\ (3)\cdot10^{-5}$	$2.73\cdot10^{-6}$	$9.2\ (2)\cdot10^{-1}$	4.7 (5)	5 (1)
v28j6	1413.08777	$1.2\ (6)\cdot10^{-2}$	$5.66\cdot10^{-3}$	-	-	-	6 (1)	3.9 (8)
v27j13	1414.80469	$2.12\ (5)\cdot10^{-2}$	$1.82\cdot10^{-2}$	-	-	-	9 (2)	4 (2)
v28j5	1416.12695	$4.8\ (2)\cdot10^{-1}$	$5.24\cdot10^{-1}$	-	-	-	7 (2)	-
v27j12	1418.11401	$7.4\ (2)\cdot10^{-2}$	$7.66\cdot10^{-2}$	-	-	-	4.8 (8)	3 (2)
v27j11	1421.39026	$3.51\ (6)\cdot10^{-2}$	$2.85\cdot10^{-2}$	$1.2\ (1)\cdot10^{-5}$	$1.43\cdot10^{-7}$	$7.9\ (4)\cdot10^{-1}$	4.5 (5)	3.0 (8)
v27j10	1424.63318	$5.2\ (2)\cdot10^{-2}$	$4.71\cdot10^{-2}$	$1.1\ (2)\cdot10^{-5}$	-	1.33 (1)	3.8 (4)	2.5 (8)
v27j9	1427.84253	$2.08\ (5)\cdot10^{-2}$	$1.58\cdot10^{-2}$	$8\ (1)\cdot10^{-6}$	-	1.04 (6)	3.0 (3)	2.0 (6)
v27j8	1431.01831	$2.72\ (6)\cdot10^{-2}$	$2.54\cdot10^{-2}$	$9\ (1)\cdot10^{-6}$	-	$2.85\ (4)\cdot10^{-1}$	2.5 (2)	1.6 (4)
v27j7	1434.16028	$2.71\ (8)\cdot10^{-2}$	$2.25\cdot10^{-2}$	$8\ (2)\cdot10^{-6}$	-	$2.3\ (1)\cdot10^{-1}$	2.1 (2)	1.6 (4)
v27j6	1437.26843	$4.2\ (2)\cdot10^{-1}$	$4.37\cdot10^{-1}$	$4.7\ (8)\cdot10^{-5}$	-	$3.9\ (2)\cdot10^{-1}$	4.0 (6)	1.5 (6)
v27j5	1440.34241	$2.7\ (1)\cdot10^{-2}$	$1.07\cdot10^{-2}$	-	-	-	6 (2)	1.5 (1)
v26j12*	1442.15064	$1.32\ (4)\cdot10^{-2}$	$6.79\cdot10^{-3}$	$1.5\ (4)\cdot10^{-5}$	-	$3.5\ (3)\cdot10^{-1}$	3.3 (4)	1.96 (8)
v26j11*	1445.46155	$1.73\ (3)\cdot10^{-2}$	$1.15\cdot10^{-2}$	$1.2\ (2)\cdot10^{-5}$	-	1.92 (8)	3.0 (3)	1.8 (4)
v26j10	1448.73914	$5\ (2)\cdot10^{-2}$	$5.19\cdot10^{-2}$	$1.8\ (2)\cdot10^{-5}$	-	$4.4\ (1)\cdot10^{-1}$	2.8 (3)	1.8 (4)
v26j9	1451.98328	$3.9\ (2)\cdot10^{-1}$	$4.84\cdot10^{-1}$	$5.1\ (6)\cdot10^{-5}$	-	$7.5\ (4)\cdot10^{-1}$	2.1 (2)	1.7 (5)
v26j8	1455.19385	$6.2\ (3)\cdot10^{-1}$	$6.85\cdot10^{-1}$	$5.8\ (6)\cdot10^{-5}$	-	$3.3\ (1)\cdot10^{-1}$	1.9 (1)	1.6 (7)
v26j7	1458.37061	2.3 (4)	2.27	$1.6\ (1)\cdot10^{-4}$	-	1.09 (2)	1.8 (3)	1.3 (3)
v26j6	1461.51355	$3.3\ (1)\cdot10^{-2}$	$2.34\cdot10^{-2}$	-	-	$2\ (1)\cdot10^{-1}$	2.1 (3)	1.3 (4)
v25j13	1462.87659	$3.39\ (9)\cdot10^{-2}$	$2.81\cdot10^{-2}$	-	-	-	-	1.2 (4)
v25j12	1466.25549	$4.74\ (7)\cdot10^{-2}$	$4.56\cdot10^{-2}$	$1.1\ (4)\cdot10^{-5}$	-	$7.2\ (4)\cdot10^{-1}$	1.5 (2)	1.44 (8)
v25j11	1469.6012	$2.79\ (9)\cdot10^{-2}$	$2.56\cdot10^{-2}$	$1.07\ (3)\cdot10^{-5}$	-	$6.9\ (2)\cdot10^{-1}$	1.3 (1)	1.1 (2)

Table 2.2 continued

laser line	frequency cm^{-1}	H$_2$O atm^{-1}cm^{-1}	H$_2$O Hitran	CO$_2$ atm^{-1}cm^{-1}	CO$_2$ Hitran	ethylene atm^{-1}cm^{-1}	acetaldehyde atm^{-1}cm^{-1}	ethanol atm^{-1}cm^{-1}
v25j10	1472.91357	2.4 (8)$\cdot10^{-1}$	2.71$\cdot10^{-1}$	1.5 (3)$\cdot10^{-5}$	-	4.84 (3)$\cdot10^{-1}$	1.5 (1)	1.0 (5)
v25j9	1476.19251	2.2 (4)	2.37	9 (2)$\cdot10^{-5}$	-	1.17 (2)	1.7 (5)	-
v25j8	1479.43787	1.82 (6)$\cdot10^{-2}$	1.27$\cdot10^{-2}$	3.5 (5)$\cdot10^{-6}$	-	5.71 (4)$\cdot10^{-1}$	8 (9)$\cdot10^{-1}$	9 (5)$\cdot10^{-1}$
v25j7	1482.64941	2.04 (4)$\cdot10^{-2}$	1.59$\cdot10^{-2}$	5.2 (3)$\cdot10^{-6}$	-	5.7 (5)$\cdot10^{-1}$	8 (1)$\cdot10^{-1}$	1.0 (4)
v25j6	1485.82715	4.9 (1)$\cdot10^{-2}$	4.78$\cdot10^{-2}$	6.5 (8)$\cdot10^{-6}$	-	4.44 (8)$\cdot10^{-1}$	1.0 (2)$\cdot10^{-1}$	8 (3)$\cdot10^{-1}$
v24j12	1490.43225	2.54 (4)$\cdot10^{-1}$	2.93$\cdot10^{-1}$	-	-	3.0 (2)$\cdot10^{-1}$	7.1 (8)$\cdot10^{-1}$	-
v24j11*	1493.81274	3.09 (9)$\cdot10^{-2}$	2.96$\cdot10^{-2}$	-	-	2.792 (4)$\cdot10^{-1}$	7 (1)$\cdot10^{-1}$	6 (4)$\cdot10^{-1}$
v24j10	1497.15991	1.12 (4)$\cdot10^{-1}$	1.41$\cdot10^{-1}$	8 (1)$\cdot10^{-6}$	-	1.41 (4)$\cdot10^{-1}$	7.2 (6)$\cdot10^{-1}$	5 (1)$\cdot10^{-1}$
v24j9	1500.47376	8.8 (3)$\cdot10^{-2}$	9.13$\cdot10^{-2}$	8 (1)$\cdot10^{-6}$	-	6.9 (1)$\cdot10^{-2}$	6.6 (6)$\cdot10^{-1}$	5 (1)$\cdot10^{-1}$
v24j8	1503.75391	6.9 (2)$\cdot10^{-2}$	7.25$\cdot10^{-2}$	7 (2)$\cdot10^{-6}$	-	5 (4)$\cdot10^{-2}$	7.1 (8)$\cdot10^{-1}$	5 (2)$\cdot10^{-1}$
v23j13	1511.23547	6.6 (2)$\cdot10^{-2}$	6.99$\cdot10^{-2}$	-	-	-	6 (1)$\cdot10^{-1}$	4 (2)$\cdot10^{-1}$
v23j12	1514.68396	1.55 (3)$\cdot10^{-1}$	1.75$\cdot10^{-1}$	-	-	1.07 (3)$\cdot10^{-2}$	4.8 (4)$\cdot10^{-1}$	3.4 (8)$\cdot10^{-1}$
v23j11	1518.09937	1.63 (4)$\cdot10^{-1}$	2.07$\cdot10^{-1}$	-	-	-	6 (2)$\cdot10^{-1}$	-
v23j10	1521.48132	2.9 (8)	2.84	-	-	1 (1)$\cdot10^{-3}$	1.0(6)	-
v23j9	1524.82996	6.8 (2)$\cdot10^{-1}$	2$\cdot10^{-1}$	-	-	2.7 (7)$\cdot10^{-3}$	5 (1)$\cdot10^{-1}$	2 (1)$\cdot10^{-1}$
v23j8	1528.14502	1.43 (5)$\cdot10^{-1}$	1.39$\cdot10^{-1}$	-	-	1.8 (2)$\cdot10^{-3}$	4.5 (4)$\cdot10^{-1}$	1.4 (3)$\cdot10^{-1}$
v22j13	1535.52991	2.3 (1)$\cdot10^{-1}$	3.28$\cdot10^{-1}$	-	-	-	7 (2)$\cdot10^{-1}$	-
v22j11	1542.4635	8.6 (1)$\cdot10^{-1}$	1.05	-	-	-	4 (2)$\cdot10^{-1}$	-
v22j10	1545.88037	2.04 (7)$\cdot10^{-1}$	2.04$\cdot10^{-1}$	-	-	1.5 (4)$\cdot10^{-4}$	3.9 (4)$\cdot10^{-1}$	-
v22j9	1549.26379	1.42 (3)$\cdot10^{-1}$	-	-	-	-	4.8 (4)$\cdot10^{-1}$	-
v22j8	1552.61377	6.3 (2)$\cdot10^{-2}$	6.19$\cdot10^{-2}$	-	-	3.7 (1)$\cdot10^{-4}$	5 (6)$\cdot10^{-1}$	7 (2)$\cdot10^{-2}$
v22j7	1555.92993	1.35 (4)$\cdot10^{-1}$	1.65$\cdot10^{-1}$	-	-	5 (1)$\cdot10^{-4}$	4.7 (5)$\cdot10^{-1}$	-
v21j14	1556.35278	1.3 (4)$\cdot10^{-1}$	1.51$\cdot10^{-1}$	-	-	6 (1)$\cdot10^{-4}$	3.4 (3)$\cdot10^{-1}$	9 (7)$\cdot10^{-2}$
v22j6	1559.21228	6.4 (1)$\cdot10^{-1}$	7.89$\cdot10^{-1}$	-	-	-	5.7 (9)$\cdot10^{-1}$	-
v21j12	1563.42212	5.13 (9)$\cdot10^{-2}$	5.63$\cdot10^{-2}$	-	-	3.8 (4)$\cdot10^{-4}$	3.7 (5)$\cdot10^{-1}$	5 (1)$\cdot10^{-2}$
v21j11	1566.90723	3.52 (7)$\cdot10^{-2}$	3.4$\cdot10^{-2}$	-	-	2.2 (2)$\cdot10^{-4}$	3.5 (4)$\cdot10^{-1}$	7 (3)$\cdot10^{-2}$
v21j10	1570.35913	2.5 (4)$\cdot10^{-1}$	2.65$\cdot10^{-1}$	-	-	-	3.2 (3)$\cdot10^{-1}$	-
v21j9	1573.77747	5 (8)$\cdot10^{-2}$	4.95$\cdot10^{-2}$	-	-	1.4 (6)$\cdot10^{-3}$	2.9 (3)$\cdot10^{-1}$	6 (2)$\cdot10^{-2}$
v21j8	1577.16223	2.2 (4)$\cdot10^{-1}$	2.62$\cdot10^{-1}$	-	-	2.5 (3)$\cdot10^{-4}$	2.8 (3)$\cdot10^{-1}$	-

Table 2.2 continued

laser line	frequency cm^{-1}	H_2O $atm^{-1}cm^{-1}$	H_2O Hitran	CO_2 $atm^{-1}cm^{-1}$	CO_2 Hitran	ethylene $atm^{-1}cm^{-1}$	acetaldehyde $atm^{-1}cm^{-1}$	ethanol $atm^{-1}cm^{-1}$
v21j7	1580.51331	1.57 (4)·10^{-2}	1.58·10^{-2}	-	-	7.9 (6)·10^{-4}	2.7 (4)·10^{-1}	5 (2)·10^{-2}
v21j6	1583.83057	9.7 (3)·10^{-3}	7.73·10^{-3}	-	-	5.3 (2)·10^{-4}	2.7 (3)·10^{-1}	6 (1)·10^{-2}
v21j5	1587.11377	9.1 (2)·10^{-3}	6.13·10^{-3}	-	-	5.7 (3)·10^{-4}	3.2 (4)·10^{-1}	5 (2)·10^{-2}
v20j12	1587.91248	1.04 (2)·10^{-2}	4.77·10^{-3}	-	-	5.1 (7)·10^{-4}	2.7 (3)·10^{-1}	7 (4)·10^{-2}
v20j11	1591.4325	2.75 (5)·10^{-2}	2.19·10^{-2}	-	-	4.5 (3)·10^{-4}	2.8 (3)·10^{-1}	7 (3)·10^{-2}
v20j10	1594.91931	3.58 (9)·10^{-2}	3.16·10^{-2}	-	-	3.41 (4)·10^{-4}	2.8 (3)·10^{-1}	6 (4)·10^{-2}
v20j9	1598.37256	9.6 (3)·10^{-3}	4.57·10^{-3}	-	-	1.77 (9)·10^{-4}	2.4 (3)·10^{-1}	5 (2)·10^{-2}
v20j8	1601.79224	1.61 (3)·10^{-2}	1.29·10^{-2}	-	-	2.5 (1)·10^{-4}	2.5 (3)·10^{-1}	5 (2)·10^{-2}
v20j7	1605.17822	1.07 (4)·10^{-2}	6.7·10^{-3}	-	-	5.1 (2)·10^{-4}	2.4 (3)·10^{-1}	6 (3)·10^{-2}
v20j6	1608.5304	3.07 (5)·10^{-2}	1.8·10^{-2}	-	-	3.7 (1)·10^{-4}	2.9 (3)·10^{-1}	6 (3)·10^{-2}
v19j13	1608.89746	3.21 (9)·10^{-2}	3.49·10^{-2}	-	-	3.71 (4)·10^{-4}	2.5 (2)·10^{-1}	5 (2)·10^{-2}
v19j12	1612.4856	2.2 (4)·10^{-2}	1.69·10^{-2}	-	-	3.4 (2)·10^{-4}	2.6 (3)·10^{-1}	6 (2)·10^{-2}
v19j11*	1616.04053	3.99 (4)·10^{-1}	4.33·10^{-1}	-	-	2 (1)·10^{-4}	3.0 (7)·10^{-1}	-
v19j10	1619.56226	3.72 (6)·10^{-2}	3.75·10^{-2}	-	-	6.3 (1)·10^{-4}	2.5 (2)·10^{-1}	5 (2)·10^{-2}
v19j9	1623.05041	2.43 (4)·10^{-1}	2.86·10^{-1}	-	-	2.1 (1)·10^{-4}	2.0 (4)·10^{-1}	-
v19j8	1626.50513	3.44 (8)·10^{-2}	3.43·10^{-2}	-	-	3.2 (3)·10^{-4}	2.2 (2)·10^{-1}	4 (2)·10^{-2}
v19j7	1629.92603	2.35 (8)·10^{-2}	1.99·10^{-2}	-	-	3.2 (2)·10^{-4}	2.3 (2)·10^{-1}	6 (3)·10^{-2}
v18j14	1629.86328	2.4 (6)·10^{-2}	2.04·10^{-2}	-	-	3.3 (3)·10^{-4}	2.4 (1)·10^{-1}	6 (2)·10^{-2}
v18j13	1633.51941	6.1 (2)·10^{-2}	6.06·10^{-2}	-	-	1.8 (6)·10^{-4}	2.43 (8)·10^{-1}	-
v18j12	1637.14246	2.39 (4)·10^{-1}	2.46·10^{-1}	-	-	4 (2)·10^{-5}	2.4 (5)·10^{-1}	5 (2)·10^{-2}
v18j11	1640.7323	4.13 (8)·10^{-2}	3.75·10^{-2}	-	-	3.8 (3)·10^{-4}	2.22 (1)·10^{-1}	5 (2)·10^{-2}
v18j10	1644.28894	5.7 (1)·10^{-2}	6.17·10^{-2}	-	-	3.4 (3)·10^{-4}	1.92 (8)·10^{-1}	5 (3)·10^{-2}
v18j9	1647.81213	3.34 (4)·10^{-1}	3.68·10^{-1}	-	-	-	1.3 (7)·10^{-1}	-
v18j8	1651.30176	2.05 (4)·10^{-1}	2.33·10^{-1}	-	-	3 (1)·10^{-4}	1.6 (4)·10^{-1}	-
v18j7	1654.75757	1.18 (6)	1.08	-	-	-	4 (1)·10^{-1}	5 (2)·10^{-2}
v17j13	1658.22559	3.48 (5)·10^{-2}	2.88·10^{-2}	-	-	4.9 (2)·10^{-4}	2.36 (9)·10^{-1}	6 (4)·10^{-2}
v17j12	1661.88367	8.8 (2)·10^{-2}	9.3·10^{-2}	-	-	2.9 (5)·10^{-4}	2.2 (1)·10^{-1}	7 (4)·10^{-2}
v17j11	1665.50854	2.53 (6)·10^{-2}	2.5·10^{-2}	-	-	4.0 (3)·10^{-4}	2.28 (10)·10^{-1}	5 (2)·10^{-2}
v17j10	1669.1001	1.9 (4)	1.88	-	-	-	3.9 (10)·10^{-1}	5 (2)·10^{-2}

Table 2.2 continued

laser line	frequency cm^{-1}	H$_2$O atm^{-1}cm^{-1}	H$_2$O Hitran	CO$_2$ atm^{-1}cm^{-1}	CO$_2$ Hitran	ethylene atm^{-1}cm^{-1}	acetaldehyde atm^{-1}cm^{-1}	ethanol atm^{-1}cm^{-1}
v17j9	1672.65833	8.6 (3)·10^{-2}	7.69·10^{-2}	-	-	5.1 (9)·10^{-4}	3.08 (1)·10^{-1}	5 (4)·10^{-2}
v17j8	1676.18286	1.8 (5)·10^{-1}	1.57·10^{-1}	-	-	8 (2)·10^{-4}	4 (2)·10^{-1}	-
v17j7	1679.67371	2.5 (2)·10^{-1}	3.21·10^{-1}	-	-	1.24 (5)·10^{-3}	5.2 (4)·10^{-1}	7 (2)·10^{-2}
v16j12	1686.7096	8.8 (2)·10^{-2}	9.19·10^{-2}	-	-	7.4 (9)·10^{-4}	7.0 (6)·10^{-1}	5 (2)·10^{-2}
v16j11	1690.36951	2.18 (9)·10^{-1}	2.36·10^{-1}	-	-	1.1 (3)·10^{-3}	2.0 (4)·10^{-1}	-
v16j10	1693.99609	7.8 (2)·10^{-2}	8.33·10^{-2}	-	-	2.4 (1)·10^{-3}	1.08 (4)	5 (3)·10^{-2}
v16j9	1697.58923	9.01 (4)·10^{-1}	9.64·10^{-1}	-	-	-	1.2 (2)	5 (2)·10^{-2}
v16j8	1701.14868	1.9 (6)	1.88	-	-	-	1.5 (5)	5 (2)·10^{-2}
v15j14	1704.13123	5.17 (9)·10^{-1}	3.75·10^{-1}	-	-	3.32 (9)·10^{-3}	2.9 (2)	8 (7)·10^{-2}
v16j7	1704.67456	5.9 (2)·10^{-1}	6.99·10^{-1}	-	-	2.7 (1)·10^{-3}	2.6 (2)	6 (3)·10^{-2}
v15j13	1707.89221	3.5 (9)·10^{-2}	4.08·10^{-2}	-	-	1.83 (6)·10^{-3}	2.8 (2)	5 (2)·10^{-2}
v15j12	1711.62036	2.5 (4)·10^{-2}	2.41·10^{-2}	-	-	5.8 (2)·10^{-3}	3.6 (3)	6 (3)·10^{-2}
v15j11	1715.31519	1.28 (3)	1.29	-	-	4 (1)·10^{-3}	5.6 (3)	-
v15j10	1718.97681	7.1 (1)·10^{-1}	6.86·10^{-1}	-	-	1.9 (6)·10^{-3}	8.4 (3)	-
v15j9	1722.60498	3.63 (9)·10^{-2}	3.15·10^{-2}	-	-	1.14 (7)·10^{-2}	1.9 (6)·10^{1}	6 (2)·10^{-2}
v15j8	1726.19946	1.79 (4)·10^{-2}	1.46·10^{-2}	-	-	1.46 (5)·10^{-2}	1.3 (1)·10^{1}	8 (3)·10^{-2}
v14j14	1729.0564	3.45 (8)·10^{-1}	3.67·10^{-2}	-	-	4.6 (5)·10^{-3}	1.7 (1)·10^{1}	8 (7)·10^{-2}
v15j7	1729.76013	5.7 (2)·10^{-1}	7.55·10^{-1}	-	-	3.3 (2)·10^{-3}	1.63 (8)·10^{1}	6 (2)·10^{-2}
v14j13	1732.85254	9.1 (1)·10^{-1}	2.61·10^{-1}	-	-	1.11 (5)·10^{-2}	1.51 (5)·10^{1}	-
v15j6	1733.28711	1.17 (3)	4.54	-	-	1.16 (7)·10^{-2}	1.41 (5)·10^{1}	-
v14j12	1736.6156	4.42 (10)·10^{-2}	4.89·10^{-2}	-	-	9.6 (1)·10^{-3}	1.5 (1)·10^{1}	4 (2)·10^{-2}
v14j11	1740.34546	2.81 (5)·10^{-1}	2.75·10^{-1}	-	-	4.7 (2)·10^{-3}	1.56 (8)·10^{1}	5.1 (1)·10^{-2}
v14j10	1744.04211	9.1 (2)·10^{-2}	7.73·10^{-2}	-	-	5.3 (3)·10^{-3}	1.8 (1)·10^{1}	-
v14j9	1747.7052	5 (1)·10^{-1}	6.23·10^{-1}	-	-	4.0 (3)·10^{-3}	1.59 (7)·10^{1}	-
v14j8	1751.33472	3.28 (4)	3.08	-	-	-	1.12 (8)·10^{1}	-
v13j14	1754.93042	1.61 (3)·10^{-2}	1.55·10^{-2}	-	-	1.1 (1)·10^{-2}	2.0 (1)·10^{1}	8 (2)·10^{-2}
v14j7	1754.93042	1.78 (5)·10^{-2}	1.55·10^{-2}	-	-	9.2 (2)·10^{-3}	1.63 (8)·10^{1}	-
v13j13	1757.89685	5.8 (1)·10^{-2}	3.43·10^{-2}	-	-	6.3 (1)·10^{-3}	2.2 (1)·10^{1}	7 (3)·10^{-2}
v13j12	1761.69495	1.7 (2)	2.05	-	-	5 (2)·10^{-3}	2.29 (9)·10^{1}	-

Table 2.2 continued

laser line	frequency cm^{-1}	H_2O $atm^{-1}cm^{-1}$	H_2O Hitran	CO_2 $atm^{-1}cm^{-1}$	CO_2 Hitran	ethylene $atm^{-1}cm^{-1}$	acetaldehyde $atm^{-1}cm^{-1}$	ethanol $atm^{-1}cm^{-1}$
v13j11*	1765.45984	$2.19\ (6)\cdot10^{-2}$	$2.13\cdot10^{-2}$	-	-	$7.9\ (2)\cdot10^{-3}$	$2.1\ (1)\cdot10^{1}$	$8\ (1)\cdot10^{-2}$
v13j10	1769.19153	$4.3\ (1)\cdot10^{-2}$	$3.74\cdot10^{-2}$	-	-	$3.53\ (3)\cdot10^{-3}$	$1.51\ (9)\cdot10^{1}$	-
v13j9	1772.88965	$2.57\ (9)$	2.54	-	-	$4\ (3)\cdot10^{-3}$	$1.04\ (7)\cdot10^{1}$	-
v13j8	1776.55408	$2.3\ (5)\cdot10^{-2}$	$2.31\cdot10^{-2}$	-	-	$1.727\ (3)\cdot10^{-2}$	$7.3\ (4)$	$6\ (1)\cdot10^{-2}$
v12j14	1779.15833	$9\ (2)\cdot10^{-2}$	$2.59\cdot10^{-1}$	-	-	$6.18\ (2)\cdot10^{-3}$	$7.8\ (5)$	$9\ (4)\cdot10^{-2}$
v13j7	1780.18481	$6.6\ (2)\cdot10^{-2}$	$7.52\cdot10^{-2}$	-	-	$5.59\ (8)\cdot10^{-3}$	$6.1\ (3)$	-
v12j13	1783.02454	$1.93\ (5)\cdot10^{-2}$	$1.07\cdot10^{-2}$	-	-	$1.2\ (1)\cdot10^{-2}$	$5.3\ (3)$	$5.5\ (9)\cdot10^{-2}$
v12j12	1786.85767	$9.5\ (3)\cdot10^{-3}$	$8.6\cdot10^{-3}$	-	-	$1.51\ (4)\cdot10^{-2}$	$5.2\ (3)$	$6\ (1)\cdot10^{-2}$
v12j11	1790.65759	$4.0\ (1)\cdot10^{-1}$	$1.86\cdot10^{-1}$	-	-	$6.3\ (3)\cdot10^{-3}$	$4.9\ (3)$	-
v12j10	1794.42432	$3.23\ (8)\cdot10^{-2}$	$2.92\cdot10^{-2}$	-	-	$4.31\ (2)\cdot10^{-3}$	$4.0\ (3)$	$5\ (2)\cdot10^{-2}$
v12j9	1798.15747	$2.33\ (6)\cdot10^{-2}$	$2.41\cdot10^{-2}$	-	-	$2.92\ (1)\cdot10^{-3}$	$2.9\ (2)$	$5\ (3)\cdot10^{-2}$
v12j8	1801.85693	$3.94\ (9)\cdot10^{-2}$	$4.28\cdot10^{-2}$	-	-	$3.891\ (5)\cdot10^{-3}$	$2.1\ (1)$	$4\ (4)\cdot10^{-2}$
v11j14	1804.3335	$8.5\ (4)\cdot10^{-3}$	$6.45\cdot10^{-3}$	-	-	$2.82\ (3)\cdot10^{-3}$	$2.1\ (2)$	$4\ (2)\cdot10^{-2}$
v12j7	1805.52271	$1.09\ (3)\cdot10^{-2}$	$9.51\cdot10^{-3}$	-	-	$2.68\ (3)\cdot10^{-3}$	$1.6\ (1)$	$3.7\ (8)\cdot10^{-2}$
v11j13	1808.23474	$1.3\ (4)\cdot10^{-2}$	$1.38\cdot10^{-2}$	-	-	$3.87\ (8)\cdot10^{-3}$	$1.63\ (10)$	$4\ (2)\cdot10^{-2}$
v11j12	1812.10291	$6.4\ (1)\cdot10^{-2}$	$8.27\cdot10^{-2}$	-	-	$3.8\ (4)\cdot10^{-3}$	$1.37\ (8)$	-
v11j11	1815.93799	$5.2\ (2)\cdot10^{-3}$	$4.91\cdot10^{-3}$	-	-	$1.023\ (4)\cdot10^{-2}$	$1.34\ (8)$	$3.2\ (6)\cdot10^{-2}$
v11j10	1819.73962	$3.2\ (2)\cdot10^{-3}$	$2.73\cdot10^{-3}$	-	-	$1.11\ (2)\cdot10^{-2}$	$1.10\ (7)$	$2.9\ (3)\cdot10^{-2}$
v11j9	1823.50781	$1.33\ (4)\cdot10^{-2}$	$1.33\cdot10^{-2}$	-	-	$2.39\ (3)\cdot10^{-2}$	$1.01(6)$	$3\ (2)\cdot10^{-2}$
v11j8	1827.24231	$1.6\ (4)\cdot10^{-2}$	$1.58\cdot10^{-2}$	-	-	$3.09\ (5)\cdot10^{-2}$	$1.00(6)$	$3\ (2)\cdot10^{-2}$
v11j7	1830.94299	$6.6\ (2)\cdot10^{-2}$	$6.09\cdot10^{-2}$	-	-	$5.7\ (2)\cdot10^{-2}$	$9.6\ (5)\cdot10^{-1}$	$4\ (2)\cdot10^{-2}$
v10j13	1833.52637	$1.19\ (3)\cdot10^{-2}$	$9.44\cdot10^{-3}$	-	-	$7.41\ (9)\cdot10^{-2}$	$1.06(2)$	$3\ (2)\cdot10^{-2}$
v11j6	1834.60986	$1.61\ (8)\cdot10^{-2}$	$1.21\cdot10^{-2}$	-	-	$9.4\ (1)\cdot10^{-2}$	$1.04(6)$	$3.0\ (7)\cdot10^{-2}$
v10j12	1837.42969	$6.9\ (2)\cdot10^{-2}$	$8.86\cdot10^{-2}$	-	-	$1.77\ (4)\cdot10^{-1}$	$1.03(6)$	-
v10j11	1841.29968	$1.49\ (4)\cdot10^{-2}$	$9.95\cdot10^{-3}$	-	-	$2.37\ (9)\cdot10^{-1}$	$7.5\ (5)\cdot10^{-1}$	$2.6\ (4)\cdot10^{-2}$
v10j10	1845.13635	$9.9\ (2)\cdot10^{-2}$	$9.11\cdot10^{-2}$	$6.5\ (6)\cdot10^{-5}$	$5.98\cdot10^{-5}$	$9.38\ (7)\cdot10^{-2}$	$6.7\ (4)\cdot10^{-1}$	-
v10j9	1848.93958	$1.33\ (4)\cdot10^{-2}$	$1.27\cdot10^{-2}$	$3\ (2)\cdot10^{-6}$	$2.8\cdot10^{-6}$	$4.57\ (6)\cdot10^{-1}$	$5.7\ (3)\cdot10^{-1}$	$2.7\ (6)\cdot10^{-2}$
v10j8	1852.70911	$5.3\ (2)\cdot10^{-3}$	$3.69\cdot10^{-3}$	$9.11\ (1)\cdot10^{-5}$	$9.18\cdot10^{-5}$	$3.6\ (3)\cdot10^{-1}$	$4.7\ (3)\cdot10^{-1}$	$4\ (1)\cdot10^{-2}$
v10j7	1856.44482	$5.9\ (2)\cdot10^{-3}$	$3.48\cdot10^{-3}$	$1.3\ (1)\cdot10^{-5}$	$1.06\cdot10^{-5}$	$8.06\ (5)\cdot10^{-1}$	$4.6\ (3)\cdot10^{-1}$	$4\ (2)\cdot10^{-2}$

Table 2.2 continued

laser line	frequency cm^{-1}	H_2O $atm^{-1}cm^{-1}$	H_2O Hitran	CO_2 $atm^{-1}cm^{-1}$	CO_2 Hitran	ethylene $atm^{-1}cm^{-1}$	acetaldehyde $atm^{-1}cm^{-1}$	ethanol $atm^{-1}cm^{-1}$
v9j13	1858.89831	$1.02\ (3)\cdot10^{-2}$	$9.87\cdot10^{-3}$	$2.7\ (1)\cdot10^{-5}$	$2.59\cdot10^{-5}$	$3.3\ (5)\cdot10^{-1}$	$4.7\ (3)\cdot10^{-1}$	$5\ (3)\cdot10^{-2}$
v10j6	1860.14673	$5.6\ (2)\cdot10^{-3}$	$3.39\cdot10^{-3}$	$4.9\ (1)\cdot10^{-5}$	$1.17\cdot10^{-4}$	$6.21\ (2)\cdot10^{-1}$	$4.1\ (3)\cdot10^{-1}$	$4.5\ (6)\cdot10^{-2}$
v9j12	1862.83667	$4.6\ (2)\cdot10^{-3}$	$3.15\cdot10^{-3}$	$3.73\ (7)\cdot10^{-5}$	$1.5\cdot10^{-5}$	$2.45\ (2)\cdot10^{-1}$	$3.3\ (2)\cdot10^{-1}$	$4\ (3)\cdot10^{-2}$
v9j11	1866.7417	$5.7\ (2)\cdot10^{-2}$	$5.22\cdot10^{-2}$	$1.7\ (2)\cdot10^{-5}$	$1.19\cdot10^{-5}$	$5.21\ (3)\cdot10^{-1}$	$2.6\ (1)\cdot10^{-1}$	-
v9j10	1870.6134	$5.1\ (2)\cdot10^{-2}$	$5.2\cdot10^{-2}$	$2.8\ (3)\cdot10^{-5}$	$2.22\cdot10^{-5}$	$3.53\ (3)\cdot10^{-1}$	$1.8\ (1)\cdot10^{-1}$	$5\ (4)\cdot10^{-2}$
v9j9	1874.45166	$2.9\ (2)\cdot10^{-3}$	$1.93\cdot10^{-3}$	$5.04\ (3)\cdot10^{-5}$	$3.6\cdot10^{-5}$	$4.43\ (4)\cdot10^{-1}$	$1.6\ (1)\cdot10^{-1}$	$6\ (3)\cdot10^{-2}$
v9j8	1878.25623	$2.1\ (2)\cdot10^{-3}$	$1.12\cdot10^{-3}$	$5.45\ (2)\cdot10^{-5}$	$5.55\cdot10^{-5}$	$2.68\ (2)\cdot10^{-1}$	$1.4\ (1)\cdot10^{-1}$	$7\ (2)\cdot10^{-2}$
v9j7	1882.02698	$2.3\ (2)\cdot10^{-3}$	$1.21\cdot10^{-3}$	$3.93\ (3)\cdot10^{-5}$	$3.64\cdot10^{-5}$	$2.22\ (4)\cdot10^{-1}$	$1.39\ (9)\cdot10^{-1}$	$8\ (3)\cdot10^{-2}$
v9j6	1885.76379	$8.9\ (3)\cdot10^{-3}$	$5.14\cdot10^{-3}$	$7.22\ (4)\cdot10^{-5}$	$1.07\cdot10^{-4}$	$1.38\ (1)\cdot10^{-1}$	$1.2\ (1)\cdot10^{-1}$	$9\ (3)\cdot10^{-2}$
v8j12	1888.32251	$4.5\ (1)\cdot10^{-2}$	$1.13\cdot10^{-2}$	$4.7\ (4)\cdot10^{-5}$	$3.69\cdot10^{-5}$	$1.508\ (8)$	$1.12\ (5)\cdot10^{-1}$	$7\ (4)\cdot10^{-2}$
v8j11	1892.26257	$4.0\ (2)\cdot10^{-3}$	$3.59\cdot10^{-3}$	$9.6\ (2)\cdot10^{-5}$	$6.44\cdot10^{-5}$	$2.21\ (2)\cdot10^{-1}$	$9.4\ (5)\cdot10^{-2}$	$1.6\ (4)\cdot10^{-1}$
v8j10	1896.16943	$6.9\ (2)\cdot10^{-3}$	$6.11\cdot10^{-3}$	$2.71\ (2)\cdot10^{-3}$	$2.34\cdot10^{-3}$	$4.51\ (2)\cdot10^{-1}$	$7.5\ (5)\cdot10^{-2}$	$1.5\ (4)\cdot10^{-1}$
v8j9	1900.0426	$1.4\ (2)\cdot10^{-3}$	$8.52\cdot10^{-4}$	$1.91\ (1)\cdot10^{-4}$	$1.83\cdot10^{-4}$	$5.68\ (3)\cdot10^{-1}$	$6.5\ (5)\cdot10^{-2}$	$2.0\ (6)\cdot10^{-1}$
v8j8	1903.8822	$5.1\ (2)\cdot10^{-3}$	$3.77\cdot10^{-3}$	$4.45\ (1)\cdot10^{-4}$	$4.04\cdot10^{-4}$	$2.17\ (3)\cdot10^{-1}$	$8.0\ (6)\cdot10^{-2}$	$2.2\ (7)\cdot10^{-1}$
v8j7	1907.68799	$5.4\ (1)\cdot10^{-2}$	$4.59\cdot10^{-2}$	$6.87\ (2)\cdot10^{-4}$	$5.95\cdot10^{-4}$	$2.9\ (1)\cdot10^{-1}$	$6.8\ (1)\cdot10^{-2}$	$2.4\ (8)\cdot10^{-1}$
v8j6	1911.45984	$4.1\ (2)\cdot10^{-3}$	$3.48\cdot10^{-3}$	$4.19\ (6)\cdot10^{-4}$	$3.94\cdot10^{-4}$	$4.35\ (7)\cdot10^{-1}$	$9\ (1)\cdot10^{-2}$	$3.1\ (8)\cdot10^{-1}$
v7j12	1913.88586	$4.2\ (2)\cdot10^{-3}$	$3.56\cdot10^{-3}$	$1.81\ (2)\cdot10^{-3}$	$2.09\cdot10^{-3}$	$9.27\ (2)\cdot10^{-4}$	$7.6\ (7)\cdot10^{-2}$	$3\ (1)\cdot10^{-1}$
v8j5	1915.19763	$1.89\ (5)\cdot10^{-2}$	$1.76\cdot10^{-2}$	$1.191\ (4)\cdot10^{-3}$	$5.08\cdot10^{-4}$	$7.31\ (7)\cdot10^{-1}$	$7.1\ (4)\cdot10^{-2}$	$4\ (1)\cdot10^{-1}$
v7j11	1917.86096	$7.6\ (2)\cdot10^{-1}$	$5.37\cdot10^{-1}$	$1.261\ (5)\cdot10^{-3}$	$1.04\cdot10^{-3}$	$3.69\ (2)\cdot10^{-1}$	$2.1\ (5)\cdot10^{-1}$	$3.2\ (8)\cdot10^{-1}$
v7j10	1921.80286	$2.15\ (5)\cdot10^{-2}$	$1.74\cdot10^{-2}$	$1.33\ (9)\cdot10^{-3}$	$1.28\cdot10^{-3}$	$7.0\ (1)\cdot10^{-1}$	$7.6\ (3)\cdot10^{-2}$	$3\ (1)\cdot10^{-1}$
v7j9	1925.71106	$2.5\ (2)\cdot10^{-3}$	$1.93\cdot10^{-3}$	$1.37\ (1)\cdot10^{-4}$	$1.38\cdot10^{-4}$	$1.571\ (4)\cdot10^{-1}$	$7.6\ (8)\cdot10^{-2}$	$3.8\ (2)\cdot10^{-1}$
v7j8	1929.58569	$1.1\ (2)\cdot10^{-3}$	$6.72\cdot10^{-4}$	$1.291\ (3)\cdot10^{-4}$	$1.52\cdot10^{-4}$	$2.45\ (6)\cdot10^{-1}$	$7.8\ (5)\cdot10^{-2}$	$3(1)\cdot10^{-1}$
v7j7	1933.42651	$7.9\ (2)\cdot10^{-3}$	$7.98\cdot10^{-3}$	$4.42\ (9)\cdot10^{-3}$	$5\cdot10^{-3}$	$3.033\ (9)\cdot10^{-1}$	$8.2\ (7)\cdot10^{-2}$	$4\ (1)\cdot10^{-1}$
v7j6	1937.2334	$2.3\ (2)\cdot10^{-3}$	$2.27\cdot10^{-3}$	$1.2\ (3)\cdot10^{-4}$	$1.25\cdot10^{-4}$	$9.9\ (1)\cdot10^{-2}$	$9.5\ (8)\cdot10^{-2}$	$2.5\ (7)\cdot10^{-1}$
v6j12	1939.52515	$2\ (2)\cdot10^{-3}$	$1.6\cdot10^{-3}$	$3.15\ (4)\cdot10^{-4}$	$3.43\cdot10^{-4}$	$8.78\ (5)\cdot10^{-2}$	$9.5\ (9)\cdot10^{-2}$	$3\ (1)\cdot10^{-1}$
v6j11	1943.5354	$1.34\ (3)\cdot10^{-2}$	$1.21\cdot10^{-2}$	-	-	$6.1\ (6)\cdot10^{-2}$	$1.05\ (7)\cdot10^{-1}$	$3.0\ (9)\cdot10^{-1}$
v6j10	1947.51221	$2.2\ (2)\cdot10^{-3}$	$1.89\cdot10^{-3}$	$1.35\ (1)\cdot10^{-4}$	$1.13\cdot10^{-4}$	$3.93\ (9)\cdot10^{-2}$	$1.3\ (1)\cdot10^{-1}$	$3\ (1)\cdot10^{-1}$
v6j9	1951.45544	$8\ (2)\cdot10^{-4}$	$6.26\cdot10^{-4}$	$5.27\ (2)\cdot10^{-5}$	$4.1\cdot10^{-5}$	$2.46\ (2)\cdot10^{-2}$	$1.3\ (1)\cdot10^{-1}$	$2.3\ (8)\cdot10^{-1}$
v6j8	1955.36511	$7.9\ (2)\cdot10^{-3}$	$6.8\cdot10^{-3}$	$1.23\ (1)\cdot10^{-4}$	$1.27\cdot10^{-4}$	$1.134\ (5)\cdot10^{-2}$	$1.3\ (1)\cdot10^{-1}$	$1.9\ (6)\cdot10^{-1}$

Table 2.2 continued

laser line	frequency cm^{-1}	H_2O $atm^{-1}cm^{-1}$	H_2O Hitran	CO_2 $atm^{-1}cm^{-1}$	CO_2 Hitran	ethylene $atm^{-1}cm^{-1}$	acetaldehyde $atm^{-1}cm^{-1}$	ethanol $atm^{-1}cm^{-1}$
v6j7	1959.24097	9 (2)·10^{-4}	5.08·10^{-4}	4.05 (9)·10^{-5}	4.16·10^{-5}	7.52 (2)·10^{-3}	1.5 (2)·10^{-1}	1.4 (5)·10^{-1}
v6j6	1963.08276	1.5 (2)·10^{-3}	6.48·10^{-4}	3.3 (4)·10^{-5}	3.36·10^{-5}	1.601 (7)·10^{-2}	1.9 (2)·10^{-1}	1.3 (5)·10^{-1}
v5j12	1965.23877	2.8 (2)·10^{-3}	2.19·10^{-3}	6 (3)·10^{-4}	6.15·10^{-4}	1.27 (3)·10^{-2}	2.0 (2)·10^{-1}	1.3 (8)·10^{-1}
v6j5	1966.89063	1.7 (6)·10^{-2}	1.52·10^{-2}	-	-	1.19 (2)·10^{-2}	2.3 (4)·10^{-1}	1.2 (4)·10^{-1}
v5j11	1969.28394	2.0 (2)·10^{-3}	1.68·10^{-3}	-	-	1.444 (9)·10^{-2}	2.1 (2)·10^{-1}	1.4 (5)·10^{-1}
v5j10	1973.29578	4 (2)·10^{-4}	2.88·10^{-4}	7.59 (2)·10^{-5}	6.39·10^{-5}	1.904 (7)·10^{-2}	2.0 (2)·10^{-1}	1.1 (3)·10^{-1}
v5j9	1977.27417	3 (2)·10^{-4}	2.95·10^{-4}	9.53 (6)·10^{-6}	1.04·10^{-5}	1.39 (8)·10^{-2}	1.8 (2)·10^{-1}	9 (4)·10^{-2}
v5j8	1981.21887	1.2 (2)·10^{-3}	4.7·10^{-4}	-	-	1.511 (6)·10^{-2}	1.8 (2)·10^{-1}	7 (3)·10^{-2}
v5j7	1985.12964	7.1 (9)·10^{-3}	4.11·10^{-4}	-	-	1.78 (2)·10^{-2}	-	-
v4j12	1991.02502	8.9 (4)·10^{-3}	5.69·10^{-3}	-	-	2.64 (3)·10^{-2}	2.3 (3)·10^{-1}	1.0 (4)·10^{-1}
v4j11	1995.10523	4 (1)·10^{-3}	8.16·10^{-4}	-	-	4.28 (7)·10^{-2}	2.3 (3)·10^{-1}	8.9 (7)·10^{-2}

Chapter 3

A versatile photoacoustic spectrometer for sensitive trace gas analysis in the mid-infrared wavelength region (5.1-8.0 and 2.8-4.1 μm)

Abstract

A versatile CO laser-based photoacoustic spectrometer equipped with three photoacoustic cells placed inside the laser cavity is presented. The newly designed CO laser can operate both in the Δv=1 (5.1-8.0 μm) and Δv=2 mode (2.8-4.1 μm) at about 400 laser lines. Due to the wide emission range of the source many molecules of biological and atmospherical interest including methane, nitric oxide, and ethane can be detected with sensitivities typical at a (sub)ppb level. Due to the spectrometers fast time response (8 seconds at a flow rate of 10 l/h) rapidly changing gas emissions (such as in insect respiration) can be studied in detail. A variety of applications is given, showing the wide applicability of this spectrometer.

S.T. Persijn, E. Santosa, F.J.M. Harren
Life Science Trace Gas Exchange Facility, University of Nijmegen, the Netherlands

3.1   Introduction

For more than three decades laser based photoacoustics (PA) has proven to be one of the most sensitive techniques for trace gas analysis. As early as 1968 Kerr and Atwood were able to detect absorptivities down to $1.2 \cdot 10^{-7} cm^{-1}$ using a cw CO_2 laser to illuminate a PA cell [24]. There has been much research ever since to further improve the PA spectrometer which follows schematically three lines: improvement of the light source, PA detection cell, and data analysis. Nowadays, the most appropriate infrared light sources for sensitive trace gas detection include powerful carbon monoxide (CO) and carbon dioxide (CO_2) gas lasers [47], and since recently, cw optical parametric oscillators [27], and quantum cascade lasers [37]. The performance of the PA detection cell was enhanced using buffer volumes to suppress window signals [4] and differential Helmholtz resonator to eliminate background noise [51]. By placing the detection cell inside the laser cavity [21] or by using a multi-pass configuration [36], a typically one order of magnitude higher light intensity (and PA signal) can be obtained. The wide availability of fast computers is the main cause for the progress in data analysis; this allows the use of novel data reduction techniques [45] and the application of non-linear algorithms to calculate the proper concentrations in case of kinetic cooling [35].

Since standard techniques for trace gas analysis like gas chromatography are also continuously improving high demands are set on the performance of the PA spectrometer. In order to be a serious competitor, the PA spectrometer must have some distinct advantage(s) such as low cost, fast time response, or high sensitivity. The CO laser based spectrometer described in this paper combines the latter two features: a fast time response (down to a few seconds) and high sensitivity at a (sub)ppb level. Furthermore, due to the unparalleled wide emission range of the operated light source (5.1-8.0 and 2.8-4.1 μm) a large number of trace gases can be detected in contrast to most other currently existing PA spectrometers. Recent technical developments are discussed and a number of practical examples are given, showing the wide applicability of this spectrometer.

3.2   Experimental arrangement

3.2.1   Background of CO lasing

For a better understanding of experiments some background of processes and conditions necessary for laser action in CO is given. In the laser plasma, CO is vibrationally excited either by collisional energy transfer from vibrationally excited N_2 molecules or directly via inelastic electron scattering. When a vibrationally excited CO molecule (v=1) collides with a CO molecule in a higher vibrational state (v=w) two processes are possible [47]:

$$CO(v = 1) + CO(v = w) \rightarrow CO(v = 0) + CO(v = w + 1) + \Delta E' \qquad (3.1)$$

$$CO(v = 1) + CO(v = w) \rightarrow CO(v = 2) + CO(v = w - 1) - \Delta E" \qquad (3.2)$$
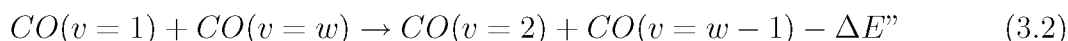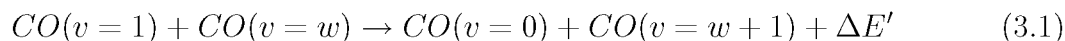
Due to the vibrational anharmonicity of CO's electronic ground state ($X^1\Sigma$) the spacing between vibrational levels decreases with v. Therefore pathways 3.1 and 3.2 are exothermic and endothermic, respectively. When the laser plasma is cooled down the endothermic

pathway will have a lower probability and the CO molecule can reach very high vibrational states through the exothermic pathway, a process known as VV or Treanor pumping [46]. Rotational thermalization occurs after almost every collision, and therefore the rotational temperature of each populated vibrational level is close to the translational temperature of the plasma. In contrast, the vibrational distribution is completely non-thermal and no vibrational population inversion occurs. In spite of this, lasing is possible on $\Delta v=1$ transitions when the higher vibrational state $(v+1,J-1)$ is more populated than the (v,J) state (partial inversion). Cooling down the gas mixture not only extends the emission range of the laser, but also shifts the emission to lines with lower J-values [3, 38]. In addition, laser action is possible on $\Delta v=2$ transitions, but in this mode the gain is 10-20 times lower as compared to the $\Delta v=1$ mode [48]. For this reason, single-line operation on $\Delta v=2$ laser transitions was only first observed in 1988 [17].

3.2.2 Experimental operating conditions
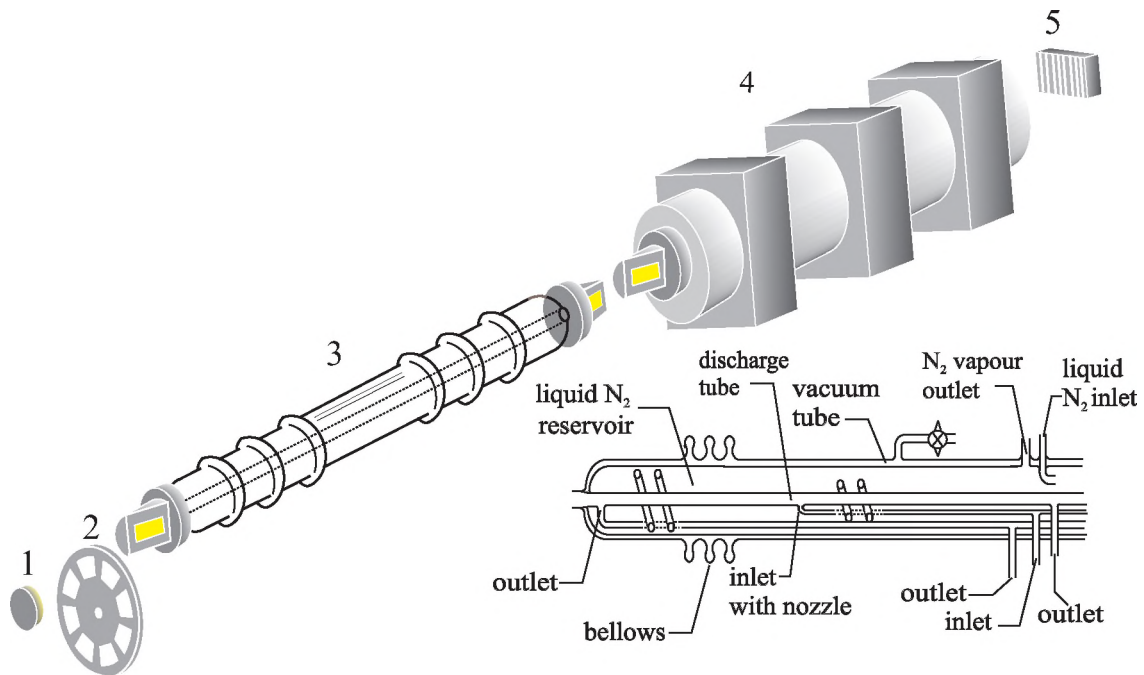
Figure 3.1: *Schematic view of the experimental set-up. 1) totally reflecting mirror with a radius of curvature of 4 m, 2) mechanical chopper operating around 1020 Hz, 3) CO laser tube, 4) triple PA cell, 5) grating. The inset shows more details of the CO laser tube that consists of a vacuum tube, liquid N_2 reservoir and discharge tube.*

The arrangement used in the experiments will be described briefly focusing thereby

in particular on some recent developments; for a more extensive description of the spectrometer the reader is refered to [5]. Figure 3.1 shows an overview of the experimental arrangement, and in detail, part of the newly designed CO laser tube. The laser tube consists of three concentric pyrex tubes, the outer tube (length 135 cm) which is evacuated acts as Dewar for the middle tube filled with liquid nitrogen. The liquid nitrogen cools down the inner discharge tube, containing a gas mixture of He, CO, N_2, and air. The mixture is admitted via two inlets and leaves the tube again via four outlets. This approach contrasts former designs that were characterised by a single in- and two outlets. In this tube with an inner diameter of 13.4 mm a discharge is maintained between two anodes (at a ground potential) at the end of the tube and two cathodes in the middle of the tube. A smaller diameter of discharge tube results in an increased laser power, however, very high demands are imposed on the straightness of the tube [2]. Following the approach of Grigor'yan, small rings were placed in the tube to make the gas flow more turbulent for an improved heat exchange between gas mixture and the wall of the discharge tube [16]. Hence a lower temperature of the gas mixture is anticipated and therefore a higher gain, i.e., higher laser power [38].
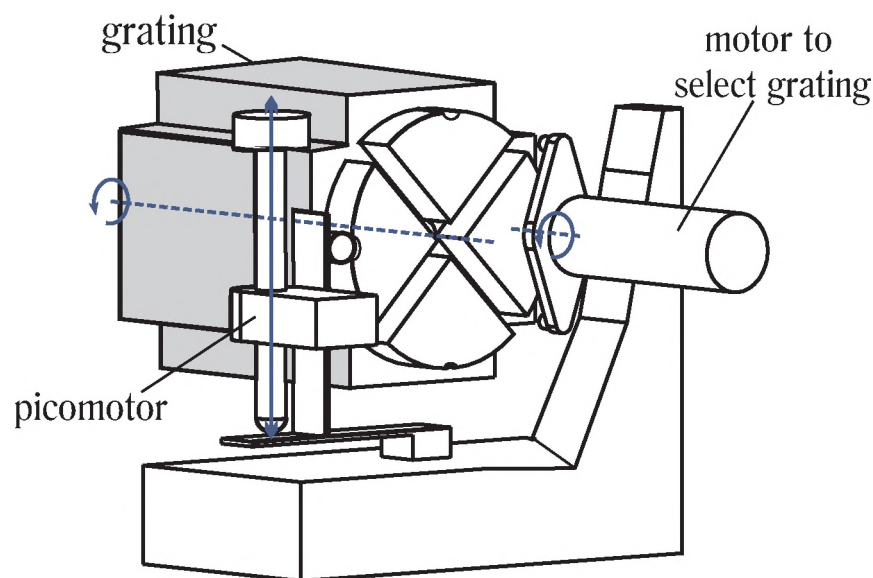
Figure 3.2: *The holder that accomodates up to four gratings for operation in the Δv=1 and Δv=2 mode. Switching between gratings is accomplished by a DC-motor using a so-called Geneva' drive mechanism for indexing, i.e., rotating the holder through a 90° angle. The vertical angle of the grating can be fine tuned using a picomotor. The horizontal angle for line selection is controlled by a stepper motor (not shown).*

New is also the operation of a grating holder which allows use of up to four different gratings (see Figure 3.2). Gratings in the holder are positioned for operation in the Δv=1 (230 lines/mm) and Δv=2 mode (450 lines/mm, blazed 2.8-4 μm, Zeiss, Germany). Switching between gratings is performed by a DC-motor (Maxon 15-series with a spur gear-

head GP16A) regulated by a control box. Fine tuning of the vertical angle of the grating is achieved by a pico-motor (New Focus Inc., USA). Both, DC-motor and pico-motor can be computer controlled. A pyro electric detector monitors the output power at zeroth-order. The ratio between out coupled power and intracavity laser power is determined by the grating characteristics. For operation in the $\Delta v = 1$ mode this ratio is strongly wavelength dependent; ranging between 0.2 and 0.002, i.e., two orders of magnitude (note for the grating operated in Chapter 2 this ratio changes less than one order of magnitude). The power coupled out via zeroth order varies even more and therefore the pyro-signal is fed to a computer controlled lock-in amplifier (5105 EG & G, Princeton Applied Research, USA) allowing also reliable power recording on laser lines that are either weak or show a low outcoupling at zeroth order.

The spectrometer is equipped with three resonant PA cells, hence the system is suitable for biological experiments that compare treated and control samples. By placing the PA cells inside the laser cavity a one order of magnitude increase in laser power and PA signal was obtained. The longitudinal resonance frequencies of three PA cells must be comparable within a few Hz, because the cells have a Q-factor of about 60 at a resonance frequency of 1020 Hz. In order to obtain the same resonance frequency in all PA cells, the resonator length of two PA cells was extended, while any remaining difference in resonance frequency is compensated by a small heater attached to the resonator (increasing the temperature of the resonator yields an increased gas temperature and hence a higher velocity of sound and resonance frequency).

Each of the two available wavelength regions has its own advantages. In the $\Delta v = 1$ mode (5.1-8.0 μm) the laser power is high (more than 30 Watt intracavity), and spectral interference between different kinds of molecules is rather low. For example, aldehydes (C=O stretch vibration at 1770 cm^{-1}) show their strongest absorption in a different wavelength region than alcohols (in plane OH-bending at 1400 cm^{-1}). The high level of H_2O vapour in combination with the strong absorption (ν_2 bending mode centred at 1595 cm^{-1}) causes severe spectral interference that become less only at the low-frequency side where a few molecules, such as methane (1306 cm^{-1}) and nitrous oxide (1285 cm^{-1}) show their strongest absorption. Figure 3.3 presents a typical recording of the laser power coupled out in zeroth-order. More than 200 laser lines are observed using a single alignment and gas mixture (typically, He:N_2:CO = 12:3:4 and a trace amount of air). Optimizing these conditions for a specific wavelength region will provide a large number of additional laser lines. In case vibrational bands overlap, laser action on two laser lines is possible [40] as the resolving power of the grating (230 lines/mm) is 1-2 cm^{-1} [15], close to the observed value of 1-3 cm^{-1}.

The two inserts in Figure 3.3 show the laser power on the v8 (v'=9 $\rightarrow$ v''=8) vibrational band as recorded with the newly designed CO laser tube, and a previous design. In the newly designed tube maximum output power is obtained at lower J-values than for the old design; on average J is 1 or 2 quanta lower on the different vibrational bands using the new laser tube under similar operation conditions. This indicates a lower rotational and translational temperature, i.e., lower temperature of the gas mixture, since rotational relaxation is very fast and rotational thermalization occurs after nearly each collision in
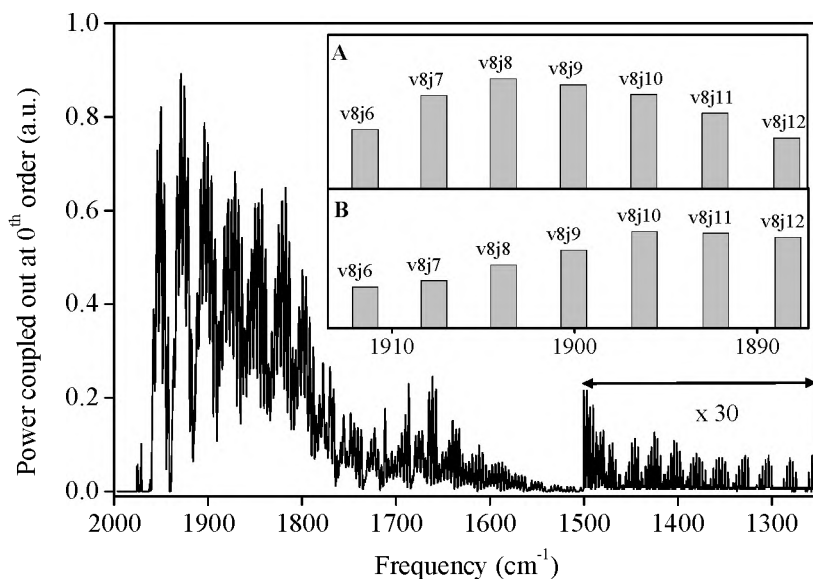
Figure 3.3: *Laser power coupled out in zeroth-order for the CO laser operating in the $\Delta v=1$ mode. Note that for frequencies below 1500 cm^{-1} the laser power is shown 30 times enlarged. The two insets depict the laser power on the v8 vibrational band as recorded with: A) the newly designed CO laser tube, B) a former design with single in- and double outlet and without rings, using similar operating conditions. For the newly designed tube the laser power shows a maximum at lower J-values than for the old design, e.g., for the v8 band the laser power is maximum at J=8 and J= 10, respectively.*

the discharge [2]. Note that the laser can also operate in a multi-line mode by replacing the grating with a mirror. Using a 90% reflecting mirror an output power >15 Watt was obtained, i.e., an intracavity laser power of approximately 300 Watt.

The main advantage of the $\Delta v=2$ mode (2.81-4.08 μm) is the low H_2O vapour absorption strength at these wavelengths. Although the laser power is a factor 10 lower than in the $\Delta v=1$ mode, the laser power still amounts up to a few watts intracavity on the strongest lines, which is higher than that of other available light sources in this wavelength region. A drawback of this wavelength band is the spectral overlap between different types of molecules, since molecules with C-H, N-H and O-H stretch vibrations all show absorptions in this region. A typical recording of the power coupled out in zeroth-order for a CO laser operating in the $\Delta v=2$ mode mode is presented in Figure 3.4.

Operating the CO laser in the $\Delta v=2$ mode requires low losses inside the laser cavity since in this mode the gain of the medium is relatively low. Three PA cells are placed inside the laser cavity, i.e., four additional ZnSe Brewster windows next to the pair of Brewster windows from the laser tube itself. Still, the number of laser lines and the laser power are similar to systems equipped with a single PA cell. For example, Martis et al. operated a single PA cell in their laser cavity, however, their system covered only the wavelength range between 2630 and 3570 cm^{-1} [32].
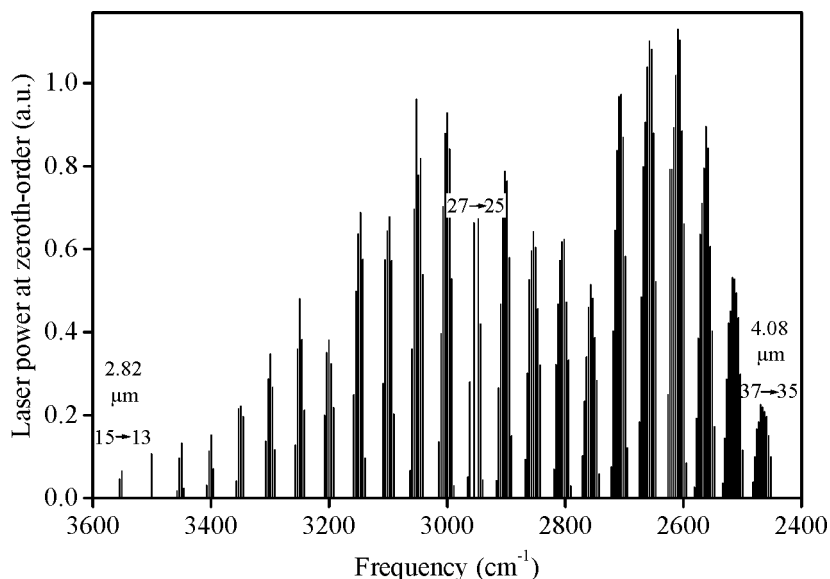
Figure 3.4: *Laser power coupled out in zeroth-order for the CO laser operating in the $\Delta v=2$ mode. Laser emission on vibrational laser bands from $v'=15 \to v''=13$-band till $v'=37 \to v''=35$-band is observed. The characteristic $v'=27 \to v''=25$-band is indicated which misses two laser lines due to self absorption on R-transitions.*

With this spectrometer sensitivities at ppb and sub-ppb level are attainable for many gases. When analyzing real gas mixtures there are a number of factors that affect detection limits:

- Acoustical noise originating from surroundings; noise from the flowing gas, in the case high flow rates are used as with for example insect respiration recordings; the intracavity placed chopper in combination with the laser cover (acts as acoustical waveguide).

- Interfering volatiles, often present at much higher concentrations than the trace gas of interest, can cause spectroscopic interference. In the $\Delta v=1$ mode the major interference is normally due to H_2O vapour, while in the $\Delta v=2$ mode methane and ethylene can give problems in case biological samples are studied.

- In the multicomponent analysis algorithm PA signals are measured sequentially on a set of selected laser lines, followed by calculation of the concentrations that are assumed to be constant within the measuring cycle. However, in reality this might not be the case as trace gas concentrations normally vary (due to for example a changing emission of the sample) giving an additional error in calculated concentrations. This problem is mainly overcome by first interpolating the PA signals on all laser lines and use these interpolated data to calculate (at one specific time) the concentrations of the different compounds. In most cases a simple linear interpolation yields already

a sufficient improvement in the calculated concentrations. Figure 3.5 presents an example in which the old and new calculation method are compared.
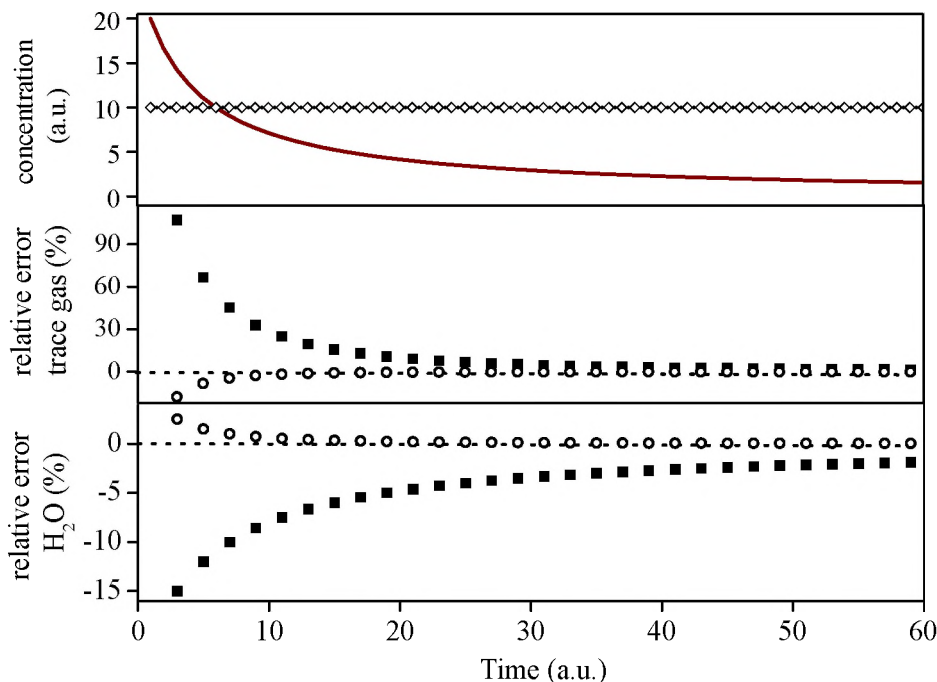
Figure 3.5: *The upper panel presents typical trace gas ($\Diamond$) and H_2O ($-$) vapour concentrations in an experiment. The H_2O vapour level decreases during the course of the experiment as the system becomes dry due to operation of the cold trap. The two lower panels present the relative errors in the concentrations using the new method with linear interpolating of the PA signals ($\circ$) and the old method ($\blacksquare$). The new approach yields much better results for both gases, especially when concentrations are changing rapidly.*

3.3 Operation in the $\Delta v=1$ mode

3.3.1 Detection of trace gases in the presence of O_2.

When studying biological samples, trace gases are normally buffered in a mixture of N_2-O_2. Oxygen as a homo-nuclear diatomic molecule has no dipole moment and therefore does not absorb infrared radiation. However, O_2 molecules, of which the ν_1 vibrational mode is centred at 1554 cm^{-1}, can be vibrationally excited via one of the two following mechanisms: First, for a CO laser operating around 1554 cm^{-1}, vibrationally excited trace gases can transfer their vibrational energy very efficiently to O_2. Secondly, during a collision between an O_2 and one trace molecule or two O_2 molecules a dipole moment is induced, a process known as collision-induced absorption. Because the induced dipole only exists for times on the order of the collisions, the spectra exhibit a large bandwidth [13].

The induced absorption strength of O_2 is relatively low, at atmospheric pressure maximum $4\cdot10^{-6}$ $atm^{-1}cm^{-1}$(calculated from [44]). However, due to the very high abundance of O_2, induced absorption can still be significant. The number of collisions required for a vibrationally excited O_2 molecule to relax to the ground state is $8.3\cdot10^7$ in pure O_2, while at STP $8\cdot10^9$ collisions per second take place [28]. Thus, relaxation of vibrationally excited O_2 to the ground state takes about 10 ms which is long compared to our modulation period of 0.9 ms. Due to its polar nature the normally very abundant H_2O molecule can promote vibrational relaxation [42, 52]. Other groups studying trace gases with a CO laser did not observe phase lags in the presence of O_2 since in their experiments the humidity in the gas sample was relatively high and hence relaxation is fast [3]. However, in our case a cold trap reduces the H_2O concentration to trace levels (<100 ppm) and the resulting slow relaxation results in the observed phase change.
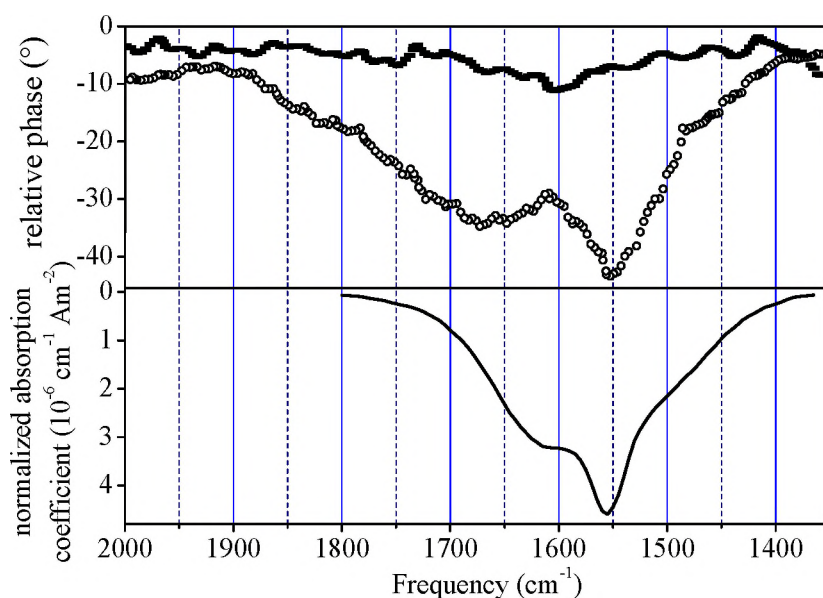
Figure 3.6: *The upper panel presents the phase angle for H_2O vapour and ethanol both at ppm level recorded in air (○) or nitrogen (■). Data are averages of five neigbouring laser lines. In nitrogen, the remaining structure in the phase angle is partly due to out-of-phase contributions of the background signal. The lower panel presents the O_2-air normalized absorption coefficients for collision-induced absorption as taken from [44]. The main mechanism responsible for the observed phase lag is probably vibrationally energy transfer from excited H_2O and trace gas molecules to the slowly relaxing O_2 molecules (see text). Note that a similar phase pattern is observed in absence of trace gas (i.e., only H_2O) or another trace gas.*

Figure 3.6 presents phase measurements in a mixture of water vapour and ethanol diluted in air and nitrogen. In addition, Figure 3.6 shows the collision-induced absorption strength as taken from the work of Thibault and co-workers [44]. The observed phase has a similar pattern as the collision-induced absorption strength, however with a long

tail at higher frequencies. If collision-induced absorption would be the main mechanism such a tail is not expected. If an O_2 molecule becomes vibrationally excited via energy transfer from another molecule, two different cases must be distinguished. First, molecules which are excited at frequencies above 1554 cm^{-1} probably loose some of their energy via rotational-translational energy transfer because in polyatomic molecules rotational-translational energy transfer is very rapid [28]. As a result, they have less internal energy, and are more close in resonance with O_2. Hence, vibrational energy transfer to O_2 is more likely to occur, resulting in the tail that has actually been observed. Second, a molecule which is excited at a frequency below 1554 cm^{-1} can loose some of its energy making vibrational energy transfer to O_2 less probable and hence no tail is expected on this low frequency side of the spectrum.
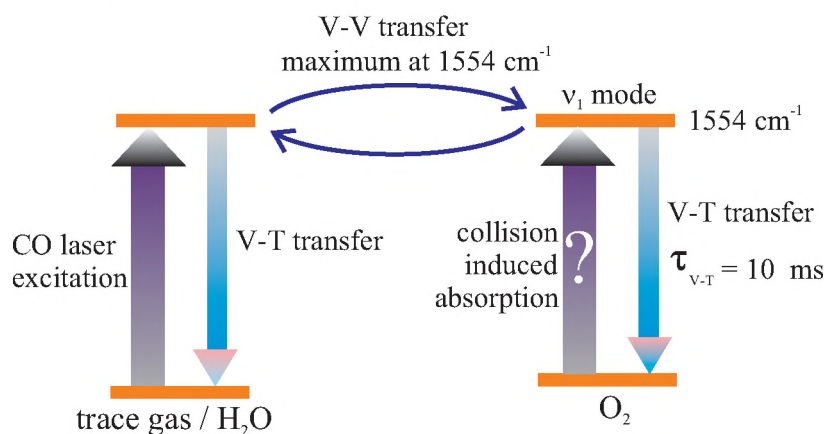
Figure 3.7: *Schematic overview of the excitation and energy transfer processes in the presence of O_2. O_2 molecules can become vibrationally excited via vibrational energy transfer from a vibrationally excited trace gas/H_2O or directly via collision-induced absorption. V-T transfer of H_2O and most trace gases takes place at a nano-second time scale, while for O_2 this process takes about 10 ms [28].*

Figure 3.7 presents a schematic overview of the excitation and energy transfer processes in an O_2 containing gas sample. The O_2 molecules can become vibrationally excited in case H_2O or trace gas molecules are excited around 1554 cm^{-1}. Especially at the low H_2O vapour levels (as in this study, typically below 100 ppm), O_2 molecules relax slowly (see [42] and references therein). In contrast, in a gas sample containing only N_2 no phase lag is expected over the entire wavelength region since the ν_1 mode of N_2 is centered at 2330 cm^{-1} making vibrational energy transfer to N_2 molecules unlikely due to the large energy gap (see Figure 3.6).

3.3.2 NO detection; slow vibrational-rotational relaxation and oxidation to NO_2

Nitric oxide (NO) has been known to have a crucial function in mammals as NO acts as a neuronal messenger molecule [7]. More recently it was found that NO also plays

an important role in plants and fruits, e.g., unripe fruits emit relatively large amounts of NO [29]. Nitric oxide is together with H_2O vapour the gas which has been studied most intensively with CO laser-based spectroscopic techniques, since a number of NO fundamental absorption lines coincide with the high power emission lines of the CO laser [14, 34, 31]. In the early seventies Patel was able to detect minute amounts of NO using a PA detector based on a complex spin-flip Raman CO laser [39]. Chemiluminescence can detect NO down to a concentration of 5 ppt which is much better than this spectrometer (1 ppb), however in contrast to chemiluminescence NO and NO_2 can be easily discriminated since their absorption spectra are different. Figure 3.8 shows the NO spectrum as was recorded using a certified gas mixture of NO buffered in nitrogen (10.2 ± 0.2 ppm, Air Liquide).
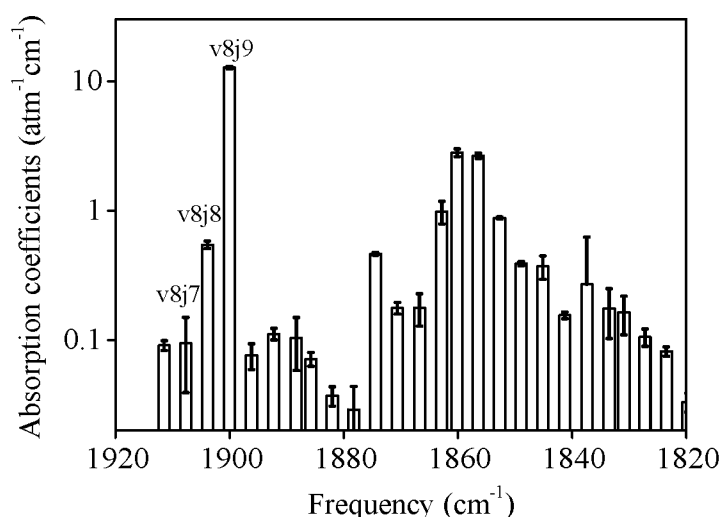
Figure 3.8: *Recorded NO absorption coefficients, the absolute value of the absorption coefficients has been scaled to Hitran database [22]. The error indicated is the standard deviation of the data. The relatively large standard deviation on some laser lines is due to H_2O vapour interference.*

Ideally, the vibrational energy of the NO molecule should be converted into translational energy within a time that is short compared to the modulation period of the light (in our case 0.9 ms). However, due to the high energy of NO's first vibrational state, vibrational-translational energy (V-T) transfer is slow, e.g., the V-T relaxation time of NO is 0.3 ms for low NO concentrations buffered in dry nitrogen [28, 3]. Rate constants for quenching of vibrationally excited NO by N_2, O_2, and H_2O are $3.3 \cdot 10^3$, $6.5 \cdot 10^5$, and $3.8 \cdot 10^7$ atm^{-1} cm^{-1}, respectively [3]. Therefore, addition of O_2 or the polar H_2O molecules drastically reduces the V-T relaxation time of NO. In a gas sample containing 10 ppm NO and about 35 ppm H_2O vapour buffered in N_2 phase shifts up to 68° were measured on laser lines showing strong NO absorption as compared to strong H_2O vapour absorption lines. By assuming that on these latter laser lines V-T relaxation is instantaneous (i.e., $\ll$ 0.3 ms) a phase shift of 56 ± 3 ° is found which is somewhat lower than the observed phase shift
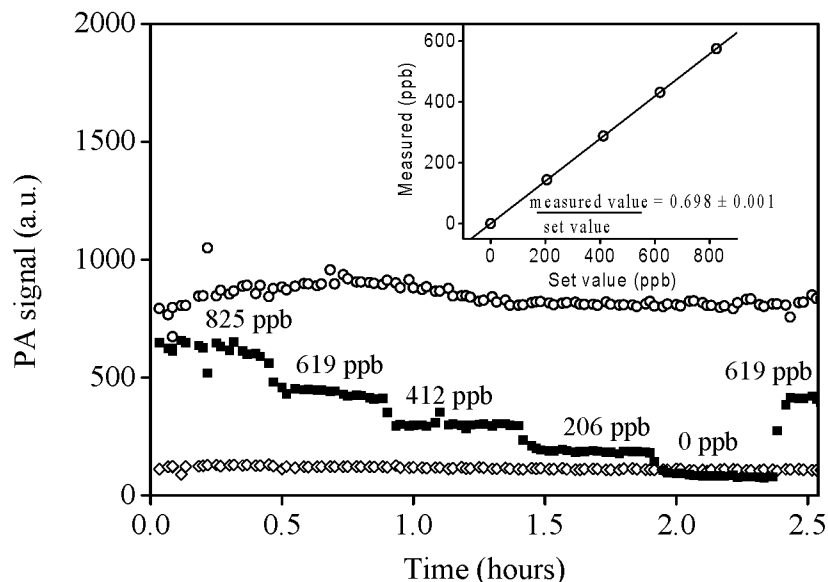
of $68 \pm 1°$ [3].

Figure 3.9: *NO recording in air on the set of 3 selected laser lines as indicated in Figure 3.8: v8j7 (○, very low NO, relatively strong H$_2$O absorption), v8j8 (◇, low absorption both by H$_2$O and NO), and v8j9 (■, strong NO and low H$_2$O absorption). The recorded value is only 70 % of the set value and therefore probably part of the NO is oxidised to NO$_2$.*

Figure 3.9 shows results of a measurement of NO buffered in air on three neighbouring CO laser lines; the system that was calibrated with NO buffered in pure nitrogen. To obtain a series of different concentrations a 10 ppm NO mixture was mixed dynamically with O$_2$ and N$_2$ using mass flow controllers. It is seen that only at the v8j9 the PA signal strongly changes as the NO concentration changes. All measured concentrations are systematically lower than the set values, probably due to partial oxidation of NO to NO$_2$. The time period between mixing and detection in the PA cell is on the order of a few minutes, much longer than the half-life time (T$_{1/2}$) of 5-12 s in air as stated by Snyder [43]. This discrepancy can be attributed to the absence of O$_3$ as T$_{1/2}$ of NO in O$_2$ is $\gg$ 1 year, however, T$_{1/2}$ of NO in air containing 15 ppb O$_3$ is only 100 s [11, 50].

3.4 Operation in the $\Delta v{=}2$ mode

3.4.1 Detection of C$_2$H$_6$; a marker for lipid peroxidation

In humans, animals, and plants many diseases seem to share a single cause, a class of molecules known as free radicals. These reactive molecules can start a chain of reactions known as lipid peroxidation which leads to cell membrane degradation [20]. Ethane (C$_2$H$_6$), one of the products of lipid peroxidation, can serve as a marker for membrane

degradation. However, most samples release ethane normally at trace levels [33]. Until recently, no sensitive C_2H_6 detectors were available and long accumulation periods were required in order to reach working range of the gas analyser (normally a gas chromatograph). When studying ripening fruits or plants, ethane detection using gas chromatography suffers from interference with the normally much more abundant ethylene (C_2H_4) that has a similar retention time as C_2H_6 [8, 33].
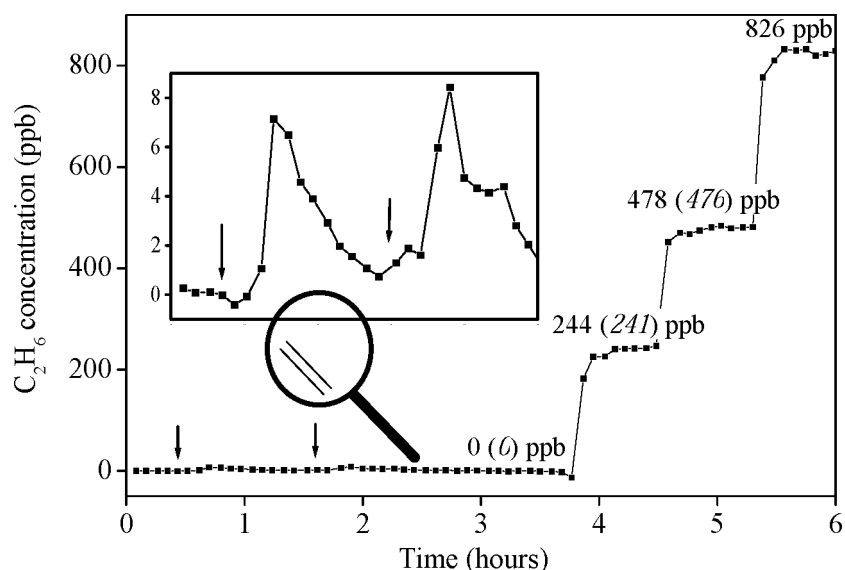

Figure 3.10: *Ethane recording using the CO laser operating in the $\Delta v=2$ mode. Ten ppm of C_2H_6 in N_2 was mixed dynamically with pure N_2 using electronic mass flow controllers (total flow rate 2 l/h). Set values and obtained values (the latter in parenthesis) are both given. At the times indicated by the arrows an injection of 1 ml N_2 with 10 ppm C_2H_6 was made, i.e., 10 nl C_2H_6. The inset shows these injections enlarged.*

Ethane can be detected much more sensitive using a CO laser based spectrometer operating around 3 μm [32, 41]. As a drawback, C_2H_4 and C_2H_6 show their strongest absorptions on the same laser lines and the use of a chemical C_2H_4 scrubber might be necessary to overcome this problem (see Chapter 2.8 and [32]). Figure 3.10 shows a recording of a series of C_2H_6 concentrations in nitrogen, for this purpose a certified gas mixture of 10 ppm C_2H_6 in nitrogen (purchased from Hoekloos) was mixed dynamically with pure N_2. In addition, small amounts of C_2H_6 were injected, showing high sensitivity of the system for C_2H_6 (detection limit is 0.5 ppb).

As a practical example of C_2H_6 detection, one has studied membrane damage in maize leaf induced externally by applying paraquat (methyl viologen) to the leaf. Paraquat is a well-known herbicide that interferes with the intracellular electron transfer systems of the weed [12]. As a result, super oxide (and possibly other radicals) accumulates, leading to destruction of lipid cell membranes in the leaves [10]. Figure 3.11 presents the results for a maize leaf that was treated in the dark with one mM paraquat (supplied by Gramaxone)
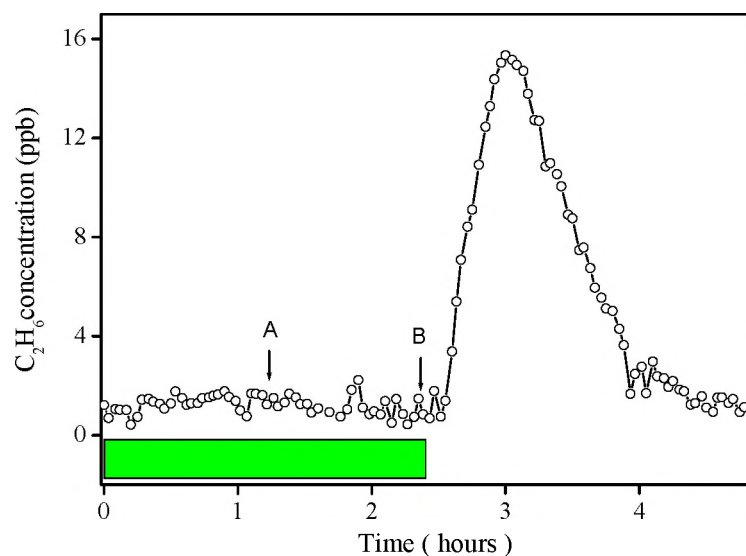
Figure 3.11: C_2H_6 emission by a paraquat treated maize leaf (fresh weight 2 gram). At the start of the measurement an empty cuvette was measured, showing the background level of C_2H_6 in the gas flow. At point A the maize leaf that had been treated with one mM paraquat in the dark for 1 h, was placed in the cuvette. The bar at the bottom indicates the dark period. From point B and further, the leaf was exposed to light (1000 μmol m^{-2} s^{-1}).

for 1 h. In the darkness the leaf releases no C_2H_6, but in the light an almost immediate response in C_2H_6 emission is observed. After exposing the leaf to light, electron transport takes place in the process of photosynthesis. Due to the paraquat, these electrons do not enter the photosystem, but lead to formation of free radicals causing membrane damage and C_2H_6 formation [10]. The high concentration of paraquat breaks down the photosynthetic system, and, eventually, kills the entire leaf as visually observed. Hence, a transient C_2H_6 burst is observed. To measure low and fastly changing C_2H_6 evolution by the leaf, one needs a fast and sensitive spectrometer as normal gaschromatographic analysis is not able to unravel this highly dynamical process.

3.4.2 Detection of methane; emission by cockroaches

Methane (CH_4) is another molecule that exhibits a strong absorption in the $\Delta v=2$ wavelength region. Its atmospheric concentration is at present only 1.7 ppmv, but on a permolecular basis CH_4 is 25 to 30 times more effective as greenhouse gas than CO_2 [25]. Hence, next to CO_2, CH_4 has the greatest influence on the global radiative balance and there exists a substantial interest in sources producing CH_4 [1].

Already in 1971 Kreuzer demonstrated detection of low CH_4 levels (10 ppb) was possible using a photoacoustic spectrometer based on a HeNe laser [26]. Later, Bijnen and co-

workers recorded CH_4 emission of insects using a CO laser operating in the $\Delta v=1$ mode [4], however this approach has several drawbacks, e.g., the laser power was relatively low on laser lines that show strong CH_4 absorption and, in addition, kinetic cooling occurs in gas samples containing O_2. Here, we recorded CH_4 by operating the CO laser in the $\Delta v=2$ wavelength region where many laser lines show a good degree of overlap with the CH_4 absorption lines. The sensitivity obtained in this work (1 ppb) is a factor of 10 better than that obtained in previous study [4]. Figure 3.12 shows measured and calculated (Hitran database) CH_4 absorption coefficients in a part of the $\Delta v=2$ wavelength region [22].
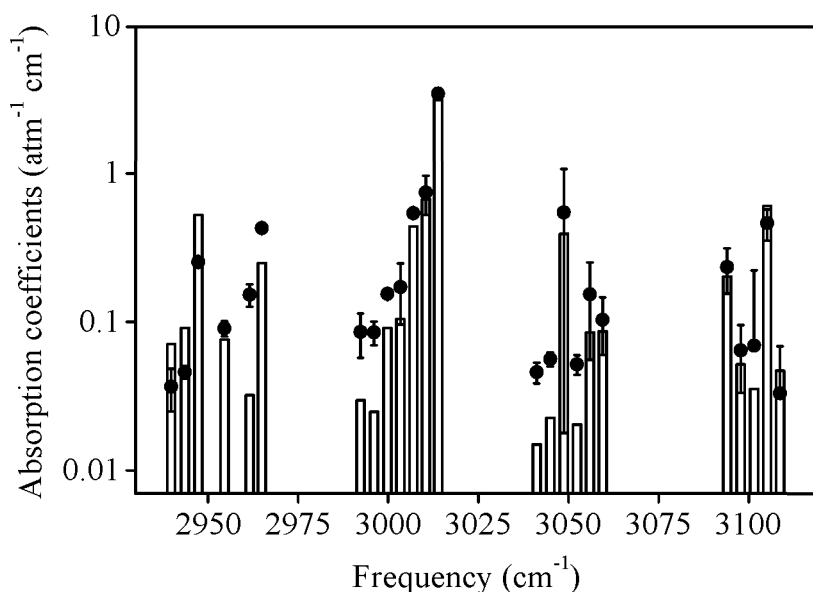
Figure 3.12: *CH_4 absorption coefficients as measured (•) and calculated (⊓) from Hitran database. The error indicated is the standard deviation of the data.*

Methanogens, a group of strictly anaerobic (i.e., without O_2) bacteria, produce CH_4 as an end product of their energy metabolism. Their habitat includes flooded soils, intestinal tract of humans and animals, large dental caries, and insects [23]. We studied breathing pattern of an American cockroach (*Periplaneta americana*) containing such bacteria by measuring the release of CO_2 and CH_4 [19]. Ten pairs of valves (spiracles) on the insects' body regulate the gas exchange between insect and atmosphere. When insects opens their spiracles O_2 can enter while CO_2 and CH_4 can leave the body. During the so-called flutter phase, spiracles are opened shortly and only a small amount of gas is exchanged with the atmosphere. In the burst phase spiracles remain open for a longer period leading to a relatively high emission of CO_2 [30]. Release of CH_4 was recorded using the photoacoustic spectrometer and CO_2 release monitored with an infrared gas analyzer (URAS 10E, Hartmann & Braun, Frankfurt am Main, Germany). Methane was recorded on a single laser line in order to obtain a good time response. Spectral interference due to CO_2 and H_2O released by the cockroach was negligible (as it was demonstrated by deliberately injecting these gases in the gas flow).
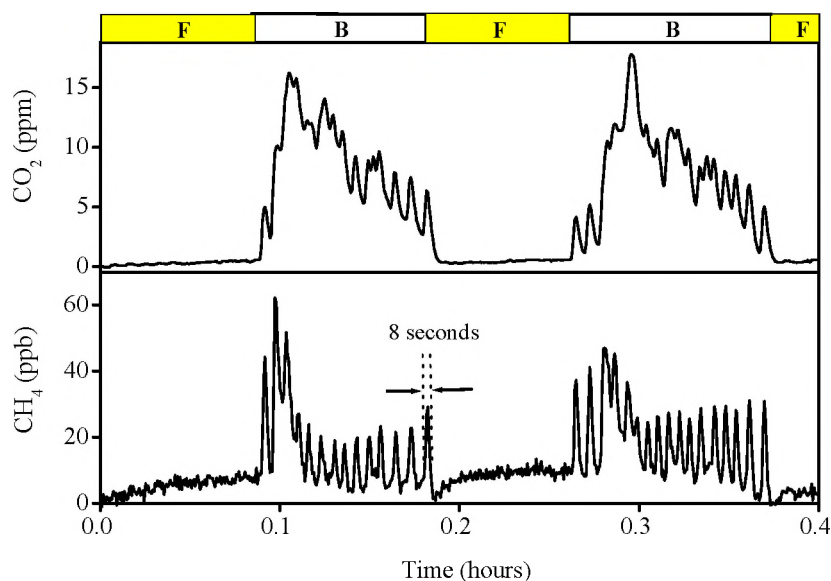
Figure 3.13: CH_4 and CO_2 release by a cockroach (Periplaneta americana, weight 1 g) kept at 22 °C, showing two characteristic respiration cycles. Over the insect an air flow of 20 l/h was passed. Subsequently the flow was split, 10 l/h to the PA cell and 10 l/h to the CO_2 analyzer. Two clearly different phases can be distinguished, i.e., fluttering (F) and burst (B). During the fluttering phase CO_2 emission is low, while CH_4 release initially rises rapidly but then becomes stable. During the burst period CO_2 emission is high and CH_4 release is initially also high but then decreases to lower levels.

Figure 3.13 shows two characteristic respiration cycles of the cockroach; each lasts about 20 minutes. The emission peaks of CH_4 and CO_2 coincide in time, however, the overall release patterns of CO_2 and CH_4 are dissimilar due to different physical properties of these gases and differences in refilling of the tracheal system [6]. The time response of both detectors was checked by injecting gas in the flow and determining the 1/e-decay time. Measured decay times are 6.3 ± 0.1 s for CO_2 and 3.56 ± 0.07 s for CH_4; this is in agreement with our observation; CO_2 emission peaks are broader than those of CH_4 (the latter are only 8 seconds wide).

Although that only few of the examined cockroaches emitted CH_4, and the fact that CH_4 emission of a single cockroach is low (<1 μmol g^{-1}h^{-1}), the total emission from all CH_4 releasing insects contributes significantly to the total CH_4 emission [19]. However, their precise contribution is still under debate [18].

3.5   Conclusions

A versatile photoacoustic spectrometer based on a newly designed CO laser was presented. The laser can operate both in $\Delta v=1$ and $\Delta v=2$ mode (5.1-8.0 and 2.8-4.1 μm) on almost 400 laser lines. The discharge tube has an additional inlet and an extra pair of outlets to

enhance gas refreshment in the tube. Furthermore, a number of rings placed within the discharge tube (to make the gas flow more turbulent) resulted in an improved cooling of the gas as evidenced by a shift of the laser output to lower J-values. Examples of NO, C_2H_6, and CH_4 detection with a sensitivity at a (sub)ppb level were discussed. Measurement of the respiration of a cockroach showed that the spectrometer is not only sensitive, but also has a good time response (8 seconds at a flow rate of 10 l/h).

3.6   Acknowledgements

References

[1] M.O. Andrea, P.J. Crutzen, Atmospheric Chemistry. In: 'Global Change' (ed. T.F. Malone and J.G. Roederer) Cambridge: ICSU Press/Cambridge University Press pp 75-113 (1985)

[2] E. Bachem, A. Dax, T. Fink, A. Weidenfeller, M. Schneider, W. Urban, Recent progress with the CO-overtone $\Delta v=2$ laser. Appl. Phys. B **57** 85-191 (1993)

[3] S. Bernegger, M.W. Sigrist, CO-Laser photoacoustic spectroscopy of gases and vapours for trace gas analysis, Infrared Phys. **30** 375-429 (1990)

[4] F.G.C. Bijnen, J. Reuss, F.J.M. Harren, Geometrical optimization of a longitudinal resonant photoacoustic cell for sensitive and fast trace gas detection. Rev. Sci. Instruments **67** 2914-2923 (1996).

[5] F.G.C. Bijnen, H. Zuckermann, F.J.M. Harren, J. Reuss, Multi-component trace gas analysis by three photoacoustic cells intracavity in a CO-laser; observation of anaerobic and post anaerobic emission of acetaldehyde and ethanol in cherry tomatoes. Appl. Opt. **37** 3345-3350 (1998)

[6] F.G.C. Bijnen, P. Kestler, J.H.P. Hackstein, F.J.M. Harren, J. Reuss, 'Sensitive photoacoustic in line recordings of H_2O, CH_4 and CO_2 release from insects', Chapter 8, PhD thesis F.G.C. Bijnen, University of Nijmegen (1995)

[7] D.S. Bredt, S.H. Snyder, A novel neuronal messenger. Neuron **8** 8-11 (1992)

[8] S.P. Burg, E.A. Burg, Ethylene evolution and sub-cellular particles, Nature **191** 967-969 (1961)

[9] S. Büscher, O. Schulz, A. Dax, H. Kath, W. Urban, Improvement of the performance of cw CO lasers by using externally ribbed wall cooled discharge tubes. Appl. Phys. B **64** 307-309 (1997)

[10] L.S. Chia, D.G. McRae, J.E. Thompson, Light-depenence of paraquat-initiated membrane deterioration in bean plants. Evidence for the involvement of superoxide. Physiol. Plant. **56** 492-499 (1982)

[11] J.E. Fergusson, Inorganic chemistry and the earth, chemical resources, their extraction, use and environmental impact. Pergamon Press, UK, 370-386 (1982)

[12] R. Ferrariiliou, A.T.P. Thi, P. Mazliak, J.V. Dasilva, Effects of membrane lipid-peroxidation on plant physiology. Annee Biol. **31** 1-23 (1992)

[13] L. Frommhold, Collision-induced absorption in gases. Cambridge University Press (1993)

[14] B.K. Garside, E.A. Ballik, M. Elsherbiny, J. Shewchun, Resonance absorption measurements of NO with a line-tunable CO laser: spectroscopic data for pollution monitoring. Appl. Opt. **16** 398-402 (1977)

[15] M.J. Grassi, 15 W high-efficiency liquid-N_2-cooled fast-axial-flow electric discharge CO laser operating single line. MSc thesis, The Ohio State University (1993)

[16] G.M. Grigor'yan, B.M. Dymshits, S.V. Izyumov, Verbesserung des Wirkungsgrades und der spezifischen Ausgangsenergie eines Elektroentladungs-CO-Lasers durch Intensivierung des Wärmeaustausches mit den Wänden. (translation from Russian by M. Müller) Sov. J. Quantum Electron, **17** 1385 (1987)

[17] M. Gromoll-Bohle, W. Bohle, W. Urban, Broadband CO laser emission on overtone transitions $\Delta v=2$. Opt. Commun. **69** 409-413 (1989)

[18] J.H.P. Hackstein, C.K. Stumm, Methane production in terrestrial arthropods. Proc. Natl. Acad. Sci. USA **91** 5441-5445 (1994)

[19] J.H.P. Hackstein, F.G.C. Bijnen, F.J.M. Harren, T.A. van Alen, J. Reuss, 'Methane emissions from cockroaches.' Chap. 7, PhD thesis F.G.C. Bijnen, University of Nijmegen, (1995)

[20] B. Halliwell, J.M.C. Gutteridge, Free radicals in biology and medicine. Oxford university press, Oxford (1989)

[21] F. Harren, J. Reuss, E.J. Woltering, D.D. Bicanic, Photoacoustic measurements of agriculturally interesting gases; detection of C_2H_4 below the ppb level, Appl. Spectrosc. **44** 1360-1368 (1990)

[22] Hitran Atmospheric Workstation for Windows, Ontar Corporation (1996)

[23] W.J. Jones, Diversity and physiology of methanogens. In: 'Microbial production and consumption of greenhouse gases: methane, nitrogen oxides, and halomethanes.' (ed. J.E. Rogers, W.B. Whitman), Washington D.C.: American Society for Microbiology pp 39-55 (1991)

[24] E.L. Kerr, J.G. Atwood, The laser illuminated absorptivity spectrophone: a method for measurement of weak absorptivity in gases at laser wavelengths. Appl. Opt. **7** 915-921 (1968)

[25] J.T. Kiehl, R.E. Dickinson, A study of the radiative effects of enhanced CO_2 and CH_4 on early Earth surface temperatures. J. Geophys. Res. **92** 2991-2998 (1987)

[26] L.B. Kreuzer, Ultralow gas concentration infrared absorption spectroscopy. J. Appl. Phys. **42** 2934-2943 (1971).

[27] F. Kühnemann, K. Schneider, A Hecker, A.A.E. Martis, W. Urban, S. Schiller, J. Mlynek, Photoacoustic trace-gas detection using a cw single-frequency parametric oscillator. Appl. Phys. B **66** 741-745 (1998)

[28] J.D. Lambert, 'Vibrational and rotational relaxation in gases.' Oxford: Clarendon

Press, (1977)

[29] Y.Y. Leshem, R.B.H. Wills, Harnessing senescence delaying gases nitric oxide and nitrous oxide: a novel approach to postharvest control of fresh horticultural produce, Biol. Plant. **41** 1-10 (1998)

[30] J.R.B. Lighton, Discontinuous gas exchange in insects. Ann. Rev. Entomol. **41** 309-324 (1996)

[31] U. List, W. Hermann, W. Urban, E.H. Fink, Spectral concidences between CO-laser and nitric oxide. A reinvestigation. Appl. Phys. **19** 427-429 (1979)

[32] A.A.E. Martis, S. Büscher, F. Kühnemann, W. Urban, Simultaneous ethane and ethylene detection using CO-overtone laser photoacoustic spectrometer -a new tool for stress/damage studies in plant physiology. Instrum. Sci. Techn. **26** 177-188 (1998)

[33] D.F. Meigh, Nature of the olefines produced by apples. Nature **184** 1072-1073 (1959)

[34] R.T. Menzies, M.S. Shumata, Remote measurements of ambient air pollutants with a bistatic laser system. Appl. Opt. **16** 2080-2084 (1976)

[35] M.A. Moeckli, C. Hilbes, M.W. Sigrist, Photoacoustic multicomponent gas analysis using a Levenberg-Marquardt fitting algorithm. Appl. Phys. B **67** 449-458 (1998)

[36] M. Nägele, M.W. Sigrist, Mobile laser spectrometer with novel resonant multipass photoacoustic cell for trace-gas sensing. Appl. Phys. B **6** 895-901 (2000)

[37] B.A. Paldus, T.G. Spence, R.N. Zare, J. Oomens, F.J.M. Harren, D.H. Parker, C. Gmachl, F. Cappasso, D.L. Sivco, J.N. Baillargeon, A.L. Hutchinson, A.Y. Cho, Photoacoustic spectroscopy using quantum-cascade lasers. Opt. Lett. **24** 178-180 (1999)

[38] C.K.N. Patel, Vibrational-rotational laser action in carbon monoxide. Phys. Rev. **141** 71-83 (1966)

[39] C.K.N. Patel, E.G. Burkhardt, C.A. Lambert, Spectroscopic measurements of stratospheric nitric oxide and water vapor. Science **184** 1173-1176 (1974).

[40] S.T. Persijn, R.H. Veltman, J. Oomens, F.J.M. Harren, D.H. Parker, Absolute absorption coefficients of the biologically interesting gases H_2O, CO_2, ethanol, acetaldehyde, and ethylene on CO laser frequencies. Appl. Spectrosc. **54** 62-71 (2000)

[41] E. Santosa, S. te Lintel Hekkert, F.J.M. Harren and D.H. Parker. The $\Delta V=2$ CO laser: photoacoustic trace gas detection. In: 'Photoacoustic and photothermal phenomena' (ed. F. Scudieri, M. Bertolotti), AIP Conference Proceedings 463 (Woodbury, New York) pp 612-614 (1998)

[42] H.K. Shin, Vibrational relaxation of water molecules near room temperature. J. Chem. Phys. **69** 1240-1245 (1978)

[43] S.H. Snyder, Nitric oxide: first in a new class of neurotransmitters. Science **257** 494-496 (1992)

[44] F. Thibault, R. Le Doucen, L. Rosenmann, J.M. Hartmann, C. Boulet, Infrared collision-induced absorption by O_2 near 6.4 μm for atmospheric applications: measurements and empirical modeling. Appl. Opt. **36** 563-567 (1997)

[45] S.B. Tilden, M.B. Denton, A comparison of data reduction techniques for line-excited optoacoustic analysis of mixtures. Appl. Spectrosc. **39** 1017-1022 (1985)

[46] C.E. Treanor, J.W. Rich, R.G. Rehm, Vibrational relaxation of anharmonic oscillators with the exchange-dominated collision. J. Chem. Phys. **48** 1789-1806 (1968)

[47] W. Urban, Infrared lasers for spectroscopy. In: 'Frontiers of laser spectroscopy of gases', A.C.P. Alves, J.M. Brown and M. Hollas, (Kluwer Academic Publishers, NATO-ASI Series) pp 9-42 (1988)

[48] W. Urban, Physics and spectroscopic applications of carbon-monoxide lasers, a review. Infrared Phys. **36** 465-473 (1995)

[49] R. Velusamy, M.M. Rao, Effect of phase lag between the interfering gases and pollutants in optoacoustic detection. Appl. Opt. **20** 3828-3829 (1981)

[50] Y. Wang, Production of nitrogen oxides in simulated lightning spark. PhD thesis

[51] V. Zeninari, V.A. Kapitanov, D. Courtois, Y.N. Ponomarev, Design and characteristics of a differential Helmholtz resonant photoacoustic cell for infrared gas detection. Infrared Phys. **40** 1-23 (1999)

[52] V.P. Zharov, V.S. Letokhov, 'Laser optoacoustic spectroscopy', Berlin Heidelberg: Springer Verlag (1986)

Chapter 4

On-line detection of trace gas emission by avocado under changing O_2 levels

Abstract

The dynamically fermentative behavior of avocado (*Persea america*, cv. Fuerte and Hass) was studied under anaerobic and low O_2 conditions. Time-evolution of CO_2 and fermentative metabolites (acetaldehyde and ethanol) were on-line monitored using a sensitive laser-based photoacoustic spectrometer. The emission of acetaldehyde and ethanol could be qualitatively described by a fermentation model. Switching from anaerobic to aerobic conditions yielded a high upsurge in acetaldehyde release (about 30-fold). Compared to other fruit this upsurge is unprecedented, probably due to the high ADH activity in avocado. The acetaldehyde formed after the switch to aerobic conditions, might, in part, explain the success of short anaerobic treatments in reducing ethylene release and ACC oxidase activity. In addition, post-hypoxic addition of O_2 resulted in a burst in acetaldehyde emission. These measurements present new ways to gain insight about internal gas atmosphere of the fruit.

S.T. Persijn‘ F.J.M. Harren
Life Science Trace Gas Exchange Facility, University of Nijmegen, Toernooiveld 1, 6525 ED Nijmegen, the Netherlands

4.1 Introduction

Respiration control is a prerequisite for slowing down ripening and senescence of fruits during storage. It is for this purpose that levels of 1-10% O_2 and up to 10% CO_2 are frequently applied during the storage period [3]. These alterations of gas compostion are commonly known as controlled atmosphere (CA). In addition, CA conditions inhibit ethylene production, a gaseous hormone which, even when present in minute concentrations, can promote senescence and reduce the shelf-life of crops [30]. The optimal storage temperature depends heavily on the fruit's origin; fruit from the temperate zone can be stored in some cases even below 0 °C, while (sub)tropical fruits are sensitive to chilling injury and therefore require higher temperatures [5]. A trend in storage of some commidities is to reduce the O_2 level even more in order to suppress the crops' respiration further [16]. Interestingly, a positive side effect of a low O_2 atmosphere on some commodities is a reduction in chilling injury symptoms [28]. By lowering the level of O_2, aerobic respiration is gradually replaced by alcoholic fermentation [38]. In the latter process, pyruvate formed in the glycolysis is converted into acetaldehyde, which in turn is reduced to ethanol. A schematic view of the alcoholic fermentation pathway is shown in Figure 4.1.
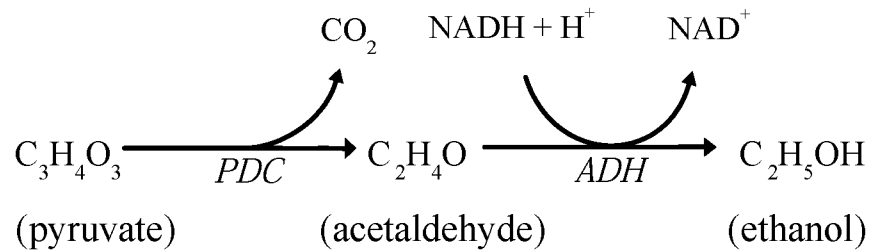
$$CO_2 \qquad NADH + H^+ \qquad NAD^+$$

$$C_3H_4O_3 \xrightarrow{\quad PDC \quad} C_2H_4O \xrightarrow{\quad ADH \quad} C_2H_5OH$$

(pyruvate) (acetaldehyde) (ethanol)

Figure 4.1: *Schematic overview of the alcoholic fermentation pathway. In the glycolysis glucose degrades to pyruvate yielding 2 ATP. Pyruvate is converted into acetaldehyde and CO_2, in a reaction catalyzed by pyruvate decarboxylase (PDC). The enzyme alcohol dehydrogenase (ADH) reduces acetaldehyde to ethanol. Alcoholic fermentation yields per glucose molecule only the 2 ATPs as generated in the glycolysis, which is very ineffective as compared to the 32 ATPs generated per glucose molecule in the normal respiratory pathway [33, 35].*

Short anaerobic periods delay ripening and ripening related processes in a variety of fruits (e.g. peach and avocado) [18, 29]. A similar response is obtained when acetaldehyde vapour is applied externally [18]. It is hypothesized that acetaldehyde delays fruit ripening by a biochemical alteration at the site of ethylene synthesis [24]. In particular, it was shown for avocado fruit that exogenously applied acetaldehyde inhibits ACC-oxidase activity (the enzyme active in the final step of ethylene biosynthesis) [29]. In part, the delay in ripening due to an anaerobic treatment is possibly caused by acetaldehyde formed after the anaerobic treatment, since returning the fruit from anaerobic to aerobic conditions yields a

transient burst in acetaldehyde due to oxidation of ethanol accumulated in the tissue [20]. Two pathways have been suggested to account for this burst: a NAD^+-dependent conversion of ethanol to acetaldehyde catalyzed by ADH and a hydrogen peroxide-dependent peroxidation controlled by catalase [20, 39].

When the O_2 level in a storage room is low, the crop will start to ferment [38, 21]. As such, acetaldehyde and ethanol can serve as markers for sub-optimal storage conditions; a timely observation is required in order to extend the storage period [31]. However, in the storage room the concentration of these (and other trace gases) is normally below the detection limit of conventional gas analyzers, and hence long accumulation periods are needed to obtain detectable concentrations. In addition, accumulation influences the level of other compounds thereby possibly altering the crops' metabolism [20]. Over the past years, laser-based photoacoustic trace gas detection proved to be a sensitive technique, allowing parallel detection of ethanol, acetaldehyde, and various other trace gases at, and below the part per billion level [39, 25]. An additional advantage of this method is the fast response making it suitable for on-line analysis.

Here, on-line measurements of trace gases (ethanol, acetaldehyde, CO_2, and ethylene) released by avocado (*Persea america*, family *Lauraceae* cv. Fuerte and Hass) using a CO laser-based photoacoustic spectrometer are presented. Avocado is an extraordinary fruit for a number of reasons: it possesses up to $3 \cdot 10^4$ stomata per fruit, the largest number of stomata reported for fleshy fruits [7], such a large number of stomata facilitate the gas exchange with the atmosphere. Avocados do not ripen while attached on the tree, the reason is not yet clear, but it is hypothesized that some tree factor inhibits ripening [1, 36]. Furthermore, avocado is one of the few fruits that contains high amounts of oil (up to 30 %) [32]. Trace gas release by avocados was studied under anaerobic, post-anaerobic, and post-hypoxic conditions. The kinetics of the acetaldehyde and ethanol emission was described by the mathematical model developed by Oomens et al. [22]. Our results are compared with data of other commodities and the possible impact of the results on fruit storage is discussed.

4.2 Material and methods

Avocado fruits (cv. Fuerte and Hass) were obtained from a local retailer. A single fruit was placed in a glass cuvette (volume 1 l) connected to a flow-through-system. The flow rate (2-5 l/h) was accurately controlled by mass flow controllers (Brooks, Veenendaal, The Netherlands). A three-level cold trap was operated to reduce the level of interfering compounds (mainly H_2O vapour) in the gas flow [25]. After passing the cold trap, the gas flow entered a photoacoustic cell placed inside the cavity of a line-tunable CO laser [6, 39]. To determine the trace gas concentrations in the gas flow, the photoacoustic signal was recorded on a set of selected laser lines. The number of lines depends on the number of compounds to be analysed (no. of laser lines $\geqslant$ no. of gases). The number of included laser lines determines the time resolution of the system; approximately one minute per laser line is required. In our case, the photoacoustic signal was recorded on six laser lines selected on basis of the following criteria: laser power, absorption strength, and spectral

interferences [25]. The concentration of acetaldehyde, ethanol, CO_2, ethylene, and H_2O vapour was calculated from the measured photoacoustic signals. An O_2 analyzer (Xendos 1800, Servomex, the Netherlands) monitored the O_2 level in experiments in which the O_2 level was gradually increased. All experiments were performed on single fruit to prevent averaging out of individual fruit responses; therefore results shown here do not represent the mean of many replicates, but show rather behaviour of a single piece of fruit. However, similar response patterns were observed in other analysed fruits, although absolute emission rates can vary considerably from fruit to fruit. All experiments were performed at room temperature.

4.3 Results

4.3.1 Avocado fruit under anaerobic conditions; modelling and comparison with other commodities.

Figure 4.2 shows release of ethanol, acetaldehyde, and CO_2 by an avocado under anaerobic conditions. During anaerobiosis, ethanol emission increases linearly with time, a linear fit of the data yields R = 0.998 (N=151, P<0.0001). The release of acetaldehyde, the precursor of ethanol, becomes stable after fruit was kept about 10 hours under anaerobic conditions.

The time-evolution of acetaldehyde and ethanol seems characteristic for a number of commodities kept under anaerobic conditions, including bell pepper [12, 21], salak (a tropical fruit, unpublished), and pear (see Figure 2.7). In addition, in Sturmer Pippin apples, ethanol content increased linearly for at least 60 days [11], while ethanol evolution increased linearly for Brussel sprouts and Jonagold apples for periods up to at least 15 and 50 days, respectively [31]. Oomens et al. described the observed emission pattern using a simple mathematical model [22]. It is assumed that emissions of acetaldehyde and ethanol is proportional to their internal concentrations and that emissions are low and therefore they do not alter internal levels. The following rate equations for acetaldehyde and ethanol evolution inside the fruit can be formulated:

$$\frac{d[AA]}{dt} = k_1[P] - k_2[AA] \tag{4.1}$$

$$\frac{d[EtOH]}{dt} = k_2[AA] \tag{4.2}$$

where [AA], [EtOH] and [P] are the concentrations in the fruit of acetaldehyde, ethanol, and pyruvate, respectively; k_1 and k_2 represent the PDC and ADH activities. Pyruvate is assumed to be non-limiting and constant. The rate equations 4.1 and 4.2 can be solved analytically for [AA] and [EtOH] using the boundary conditions [AA](0)=[EtOH](0)=0:

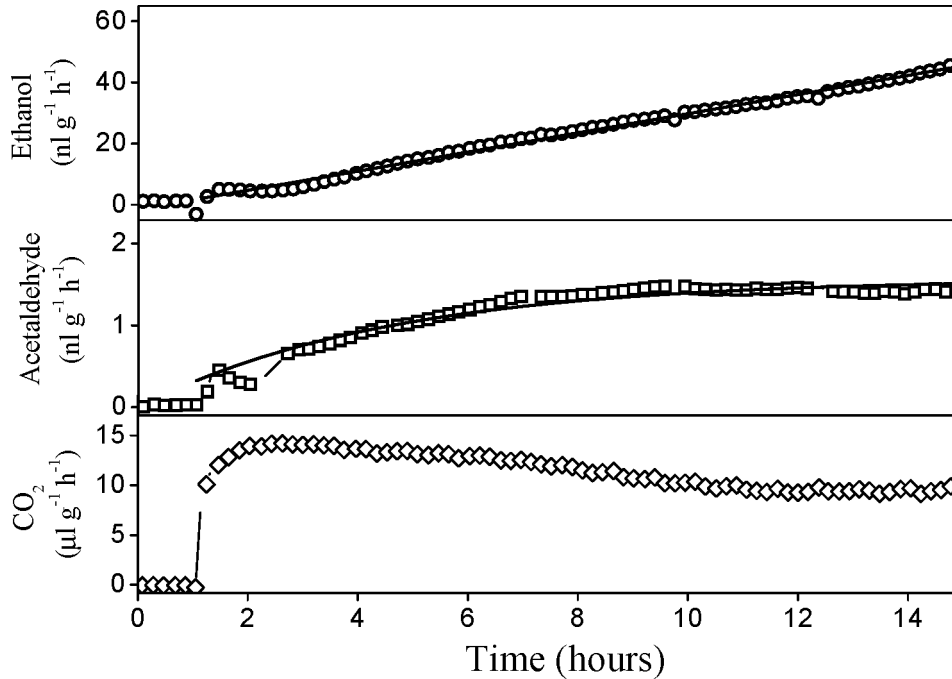$$[AA](t) = \frac{k_1[P]}{k_2} \cdot [1 - e^{-k_2 \cdot t}] \tag{4.3}$$

Figure 4.2: *Typical ethanol, acetaldehyde, and CO_2 release from avocado under anaerobic conditions. Note that only half the data points are shown for clarity. At $t=1$ h the avocado was placed in the cuvette under anaerobic conditions. The ethanol and acetaldehyde release are fitted (solid lines) using equations 4.3 and 4.4.*

$$[EtOH](t) = k_1[P] \cdot t + \frac{k_1[P]}{k_2} \cdot [e^{-k_2 \cdot t} - 1] \qquad (4.4)$$

Figure 4.2 shows a fit of the ethanol and acetaldehyde release using equations 4.3 and 4.4. While equations 4.3 and 4.4 describe the acetaldehyde and ethanol formation inside the tissue, our measurements are performed in the headspace of the cuvette. Therefore, each curve was fitted with its own parameters, although equations 4.3 and 4.4 contain in fact only two parameters, i.e., k_2 and $k_1[P]/k_2$.

4.3.2   Post-anaerobic and post-hypoxic effect in avocados; an unprecedentedly high upsurge in acetaldehyde.

Figure 4.3 presents the acetaldehyde and ethanol emission of another avocado fruit. Inserting the avocado in the cuvette is immediately followed by a short artificial peak in release of both, acetaldehyde and ethanol (see also Figure 4.2). This peak is due to spectral interference between ethanol and ethylene [25] and a change in resonance frequency because O_2 enters the flow system when opening the cuvette. Ethylene is released in relatively large amounts at the start of the measurement, since during that period O_2 is still available to the fruit. Under anaerobic conditions ethanol emission increases linearly with time (see
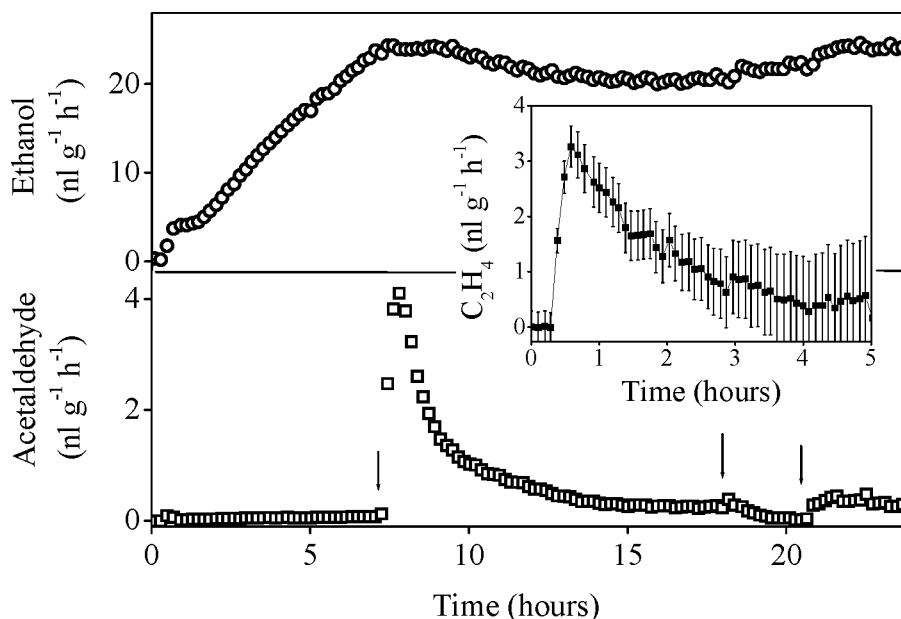
Figure 4.3: At $t = 0.3$ h, the avocado was placed in a cuvette under anaerobic conditions. At $t = 7.2$ h, as indicated by the left most arrow, 2.1 % O_2 was added to the gas flow giving an immediate and high upsurge in the acetaldehyde emission. At 18.2 h (middle arrow) anaerobic conditions were restored and at 20.6 h (right arrow) post-anaerobic conditions were repeated. An artificial peak occurs both in acetaldehyde and ethanol after the fruit was placed in the cuvette mainly due to C_2H_4 interference (see inset). After 4 h, C_2H_4 release decreases to insignificant levels. Note that the error in the C_2H_4 release increases as ethanol interference becomes larger.

also Figure 4.2). After adding 2.1% O_2 the ethanol release first stabilizes after which it decreases very slowly while release of CO_2 is almost not influenced (latter not shown). As only a very slow ethanol wash-out from the fruit is observed, some ethanol is probably still formed under these gas conditions [38, 21]. The acetaldehyde emission shows a completely different pattern; within minutes after adding O_2, a huge upsurge is observed. In the steepest part of the curve acetaldehyde emission triples within only 10 minutes. The actual emission by the fruit increases even faster, as the measured emission curve is broadened by the flow-system (mainly the cuvette). Table 4.1 presents some measured parameters of the post-anaerobic upsurge in acetaldehyde. The acetaldehyde emission increases 32-fold after switching to post-anaerobic conditions and shows a maximum in less than 1 h after adding O_2. Subsequently, emission of acetaldehyde decreases exponentially, fitting the emission with a single exponential decay yields a decay-time of 1.5 h ($R^2 = 0.97 \pm 0.02$), which is much faster than in case of ethanol.

Restoring again anaerobic conditions results in a fast decrease of acetaldehyde emission (fit exponential decay: $R^2 = 0.989$, decay time $= 0.70 \pm 0.05$ h). About 2.5 h after switching, virtually no acetaldehyde is released anymore. Zuckermann and co-workers hypothesized

Table 4.1: *Measured parameters of the post-anaerobic upsurge in acetaldehyde (AA) release. Data are average of four measurements plus standard deviation.*

$\dfrac{AA_{maximum}}{AA_{anaerobic}}$	32±15
period between adding O_2 and maximum AA release (h)	0.88±0.13 h
exponential decay time (h)	1.5±0.5 h
R^2 exponential fit	0.97±0.02

that the reduction in O_2 level arrests further formation of active O_2 species, and therefore H_2O_2 is no longer available for the conversion of ethanol to acetaldehyde [39]. Note that after restoring anaerobic conditions, some acetaldehyde is formed in the fermentation processes, but this amount seems insufficient to counteract the large drop due to the reduction in H_2O_2 level. After adding 2.1% O_2 again, a new, but smaller upsurge in acetaldehyde emission was observed.

As previously mentioned, short anaerobic treatments might extend fruits' shelf life, but the main interest in crop storage remains the application of low O_2 conditions to slow down ripening [8, 18]. Therefore, we studied the trace gas emission of avocado under such conditions; the post-anaerobic experiments were repeated starting with low O_2 levels instead of anaerobic conditions. Figure 4.4 shows the acetaldehyde release by avocados stored at low O_2 levels, after which the O_2 level was increased.
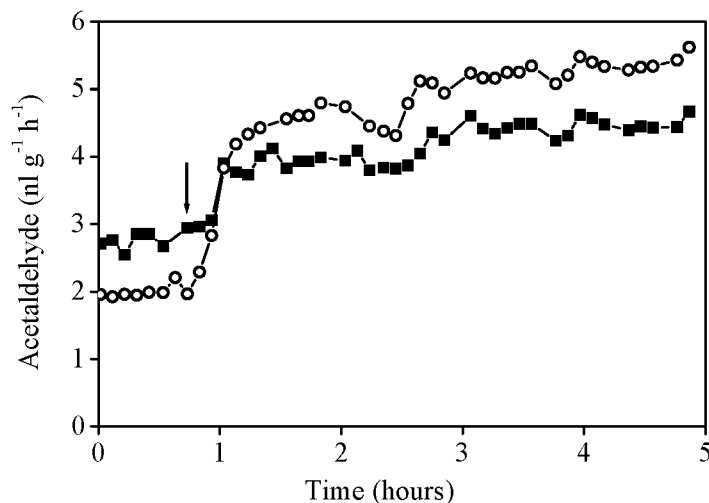

Figure 4.4: *Avocados were kept at 0.2 (○) and 0.6 % O_2 (■) for 16 hours, after which the O_2 level was increased to 1.2 % O_2. The results indicate that an upsurge in acetaldehyde, not only occurs when the fruit was initially kept under anaerobic conditions, but also after storage under low O_2 levels.*

Also in this case, an upsurge in acetaldehyde release is observed, similar to when starting with anaerobic conditions, however, shape and height of the upsurges are different (see Figure 4.3). In avocado fruit, a large radial O_2 gradient exists, in particular along skin and flesh and to a lesser extent along the seed [37]. This implies that although low O_2 concentration was externally applied, inner part of the tissue may be anaerobic. Hence, switching to higher O_2 levels might change part of the tissue from anaerobic to hypoxic conditions giving the expected upsurge in acetaldehyde. This is in agreement with our observation; starting from a low O_2 level (0.2%) results in a higher upsurge in acetaldehyde than starting at a somewhat higher O_2 level (0.6%), since at 0.2% O_2 more tissue will be anaerobic. The amount of acetaldehyde formed due to post-hypoxic addition of O_2 might therefore be indicative for the amount of anaerobic tissue. After storage under low O_2 levels, such acetaldehyde upsurge can possibly extend or shorten the crops' shelf-life, depending on the kind of crop [13, 4, 27, 29].

Figure 4.5 presents production rate of acetaldehyde from avocado under a stepwise increasing O_2 level. The acetaldehyde emission also shows a stepwise behaviour, but the stepsize diminishes at higher O_2 levels. As this stepsize is decreasing, probably less tissue is transferred each time from anaerobic to hypoxic conditions. The levels of CO_2 and ethanol are virtually not influenced by changes in O_2 level.
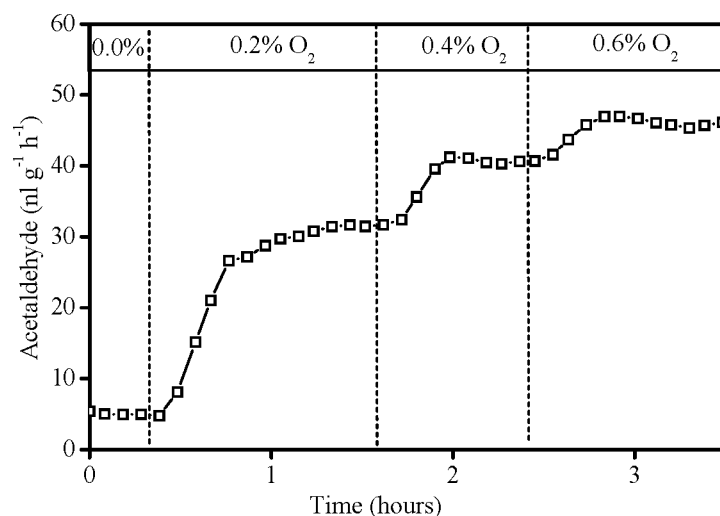

Figure 4.5: *Acetaldehyde release by avocado under a stepwise increasing O_2 level. The avocado was kept under anaerobic conditions for 15 hours before the measurement started. The O_2 level in the cuvette was increased in steps as marked by the dashed lines. The O_2 level in the cuvette stabilized within two minutes after adding extra O_2. Adding O_2 hardly influenced the ethanol and CO_2 release (data not shown).*

4.4   Discussion

Under anaerobic conditions, avocados released only small amounts of acetaldehyde (as compared to the amount of ethanol). Various other commodities, including certain apple [23] and pear (Figure 2.7) cultivars, release acetaldehyde and ethanol initially at similar rates upon exposing the fruit to anaerobic conditions. The observed burst in acetaldehyde during post-anaerobiosis was very high (32-fold increase) for avocado as compared to the upsurge found in other samples. For example, Zuckermann et al. observed a 3-fold increase in Red Bell pepper, Monk and co-workers found a 5-fold increase in *Glyceria maxima* rhizomes, while for Conference pears a 2-fold increase was observed (unpublished) [39, 20]. Both phenomena can probably be related to the high alcohol dehydrogenase activity in avocados, e.g., Ke and co-workers reported a 40 to 80-fold higher ADH activity (see Figure 4.1) for avocado as compared to pear fruit [14].

As opposed to Red Bell pepper, the post-anaerobic upsurge in acetaldehyde could not be prevented by slowly restoring the O_2 level. These contrasting results are possibly due to the different structure of both fruits: in the pepper the O_2 level in the tissue is almost equal to that of the surrounding atmosphere (e.g., in ambient air the internal O_2 level is 18% [21]), whereas large O_2 gradient exists in bulky avocado [37]. Due to such large gradient in avocado, each stepwise increase in the O_2 level is expected to bring a new inner layer of tissue from anaerobic to hypoxic conditions. Every O_2 addition will thus lead to a new post-anaerobic effect, giving each time a new burst in acetaldehyde emission. An upsurge in acetaldehyde was also observed when fruit was initially kept under low O_2 levels, instead of anaerobic conditions (see Figure 4.4). This result strengthens the assumption that, although O_2 was externally applied at a low level, part of the fruit tissue experiences anaerobiosis.

The acetaldehyde formed under anaerobic or after post-anaerobic/hypoxic conditions can influence the post harvest life of the fruit. As mentioned earlier, in a number of fruits the post harvest life can be extended. On the other hand, for some fruits (such as pear and grapes) a promotion of ripening was reported [13, 27]. Furthermore, acetaldehyde is a very reactive compound that is toxic to tissue and can cause post-anaerobic injury [24, 20]. In addition, certain compounds formed during the fermentation processes might lead to off-flavours or odours [10, 19].

Assuming that all CO_2 is generated in the alcoholic fermentation pathway (see Figure 4.1), the CO_2 production should equal the sum of acetaldehyde and ethanol production, albeit, our measurements indicate that, especially at the start of anaerobic period, CO_2 is released at a much higher rate. Equal CO_2 and ethanol releases are expected only after several months of anaerobiosis. For this calculation, CO_2 emission was assumed constant and ethanol release should continue to increase linearly (ethanol release of avocado increases linearly for at least 24 hours, while e.g., ethanol release by Jonagold apples increases linearly for anaerobic periods up to at least 50 days [31]). Also in other crops stored under anaerobic or low O_2 conditions, CO_2 is released at relatively higher rates than acetaldehyde and ethanol but in general not in such an extreme case as for avocado [17, 11]. Several possible explanations for the excess of CO_2 formation can be found in literature. For example, Bartley and co-workers showed that apples can metabolise ethanol

into ethyl acetate while Fidler suggested that CO_2 arises partly from malic acid oxidation [2, 10]. For an overview of reactions that generate CO_2 without the formation of ethanol and reactions in which ethanol is further metabolised the reader is refered to [23, 11]. Therefore, in avocado fruit such processes must play a dominant role.

The simple fermentation model gave an adequate, but qualitative, description of the ethanol and acetaldehyde release. In order to get an estimate for internal acetaldehyde and ethanol levels, the solubility K_H of these gases in the tissue must be known [15] (Henry's law constant $K_H = c_a/p_g$, c_a the concentration of the species in the liquid phase and p_g the partial pressure of that species in the gas phase [34]). To estimate this value, in pure H_2O of 24 °C, the K_H for acetaldehyde and ethanol are 15 and 200 M/atm, respectively. The ratio of ethanol to acetaldehyde inside the tissue should be 200/15 times higher than that measured by us in the headspace (note that avocado fruit has a high oil content and K_H values are therefore only an estimate). However, Peppelenbos et al. found using a gas exchange model, almost equal ratios for ethanol and acetaldehyde (377 and 267, respectively) in Cox Orange Pippin apples [23]. This result indicates that the ratio of 200/15, valid for steady-state conditions, might not apply here. Another complicating factor is that ethanol and acetaldehyde both continuously produced, diffuse out of the fruit, and are carried away from the headspace. In order to correct for this, the diffusion resistance of the fruit for ethanol and acetaldehyde has to be taken into account.

4.5   Acknowledgements

References

[1] I. Adato, S. Gazit, Postharvest response of avocado fruits of different maturity to delayed ethylene treatments. Plant Physiol. **53** 899-902 (1974)

[2] I.M. Bartley, P.G. Stoker, A.D.E. Martin, S.G.S. Hatfield, M. Knee, Synthesis of aroma compounds by apples supplied with alcohols and methyl esters of fatty acids. J. Sci. Food Agrc. **36** 567-574 (1985)

[3] R.M. Beaudry, The effect of O_2 and CO_2 partial pressure on selected phenomena affecting fruit and vegetable quality. Postharvest Biol. Technol. **15** 293-303 (1999)

[4] J.C. Beaulieu, G. Peiser, M.E. Salveit, Acetaldehyde is a causal agent responsible for ethanol induced ripening inhibition in tomato fruit. Plant Physiol. **133** 431-439 (1997)

[5] R. Ben Arie, S. Lurie, Prolongation of fruit life after harvest. In: 'Handbook of fruit set and development' S.P. Moneselise (ed), CRC Press, Inc, Boca Raton, Florida, 493-520

[6] F.G.C. Bijnen, J. Reuss, F.J.M. Harren, Geometrical optimization of a longitudinal resonant photoacoustic cell for sensitive and fast trace gas detection. Rev. Sci. Instruments **67** 2914-2923 (1996).

[7] M.M. Blanke, J.P. Bower, Surface features of the avocado fruit. Trop. Agric. (Trinidad) **67** 379-381 (1990)

[8] J.N. S. Dori, E. Lomaniec, E. Marinansky, E. Pesis, Effect of pre-storage treatments on mango fruit ripening. Ann. Appl. Biol. **125** 581-587 (1994)

[9] F.J.M. Harren, J. Reuss, E.J. Woltering, D.D. Bicanic, Photoacoustic measurements of agriculturally interesting gases; detection of C_2H_4 below the ppb level. Appl. Spectrosc. **44** 1360-1368 (1990)

[10] J.C. Fidler. A comparison of the aerobic and anaerobic respiration of apples. J. Exp. Bot. **2** 41-64 (1951)

[11] J.C. Fidler. The metabolism of acetaldehyde by plant tissues. J. Exp. Bot. **19** 41-51 (1968)

[12] Y. Imahori, M. Kota, H. Furukawa, Y. Ueda, K. Cachin, Ethanolic fermentation enzymes, their products and transcription of alcohol dehydrogenase from bell pepper fruit held under various low oxygen atmospheres. J. Japan. Soc. Hort. Sci. **69** 266-272 (2000)

[13] H.W. Janes, C. Frenkel, Promotion of softening processes in pear by acetaldehyde, independent of ethylene action. J. Amer Soc. Hort. Sci. **103** 397-400 (1978)

[14] D. Ke, E. Yahia, L. Hess, L. Zhou, A.A. Kader, Regulation of fermentative metabolism in avocado fruit under oxygen and carbon dioxide stresses. J. Amer. Soc. Hort. Sci. **120** 481-490 (1995)

[15] T.W. Kimmerer, R.C. MacDonald, Acetaldehyde and ethanol biosynthesis in leaves of plants. Plant. Physiol. **69** 840-847 (1987)

[16] O.L. Lau, C.L. Barden, S.M. Blankenship, P.M. Chen, E.A. Curry, J.R. DeEll, L. Lehman-Salada, E.J. Mitcham, R.K. Prange, C.B. Watkins, A North American cooperative survey of 'Starkrimson, Delicious' apple responses to 0.7% O_2 storage on superficial scald and other disorders. Postharvest Biol. Technol. **13** 19-26 (1998)

[17] J.A. Leshuk, M.E. Saltveit, Effect of rapid changes in oxygen concentration on the respiration of carrot roots. Physiol. Plant. **82** 559-568 (1991)

[18] S. Lurie, E. Pesis, Effect of acetaldehyde and anaerobiosis as postharvest treatments on the quality of peaches and nectarines. Postharvest Biol. Technol. **1** 317-326 (1992)

[19] J.P. Mattheis, D.A. Buchanan, J.K. Fellman, Change in apple fruit volatiles after storage in atmospheres inducing anaerobic metabolism. J. Agric. Food. Chem. **39** 1602-1605 (1991)

[20] L.S. Monk, R. Braendle, R.M.M. Crawford, Catalase activity and post-anoxic injury injury in monocotyledonous species. J. Exp. Bot. **38** 233-246 (1987)

[21] J. Oomens, H. Zuckermann, S.T. Persijn, D.H. Parker, F.J.M. Harren, CO-laser-based photoacoustic trace-gas detection: applications in postharvest physiology. Appl. Phys. B **67** 459-466 (1998)

[22] J. Oomens, S.T. Persijn, D.H. Parker, F.J.M. Harren, The onset of fermentation: real-time measurements and model calculation of ethanol and acetaldehyde emission. Acta Hort. (2000) accepted

[23] H.W. Peppelenbos, H. Zuckermann, S.A. Robat, Alcoholic fermentation of apple fruits at various oxygen concentrations model prediction and photoacoustic detection. In: 'CA '97 Vol. 2 Apples and Pears', E.J. Mitcham (ed.) 168-175 (1997)

[24] P. Perata, A. Alpi, Ethanol-induced injuries to carrot cell. The role of acetaldehyde.

Plant Physiol. **95** 748-752 (1991)

[25] S.T. Persijn, R.H. Veltman, J. Oomens, F.J.M. Harren, D.H. Parker, Absolute absorption coefficients of the biologically interesting gases H_2O, CO_2, ethanol, acetaldehyde and ethylene on CO laser frequencies. Appl. Spectrosc. **54** 62-71 (2000)

[26] E. Pesis, Y. Fuchs, G. Zauberman, Cellulase activity and fruit softening in avocado. Plant Physiol. **61** 416-419 (1978)

[27] E. Pesis, C. Frenkel, Acetaldehyde vapors influence postharvest quality of table grapes. HortScience **24** 315-317 (1989)

[28] E. Pesis, R. Marinansky, G. Zauberman, Y. Fuchs, Prestorage low-oxygen atmosphere treatment reduces chilling injury symptoms in 'Fuerte' avocado fruit. HortScience **29** 1042-1046 (1994)

[29] E. Pesis, D. Faiman, S. Dori, Postharvest effects of acetaldehyde vapour on ripening-related enzyme activity in avocado fruit. Postharvest Biol. Technol. **13** 245-253 (1998).

[30] M.S. Reid, Ethylene in postharvest technology. In: 'Postharvest technology of horticultural crops' A.A. Kader (ed.) University of California 2nd edn. pp 97-108 (1992)

[31] S.P. Schouten, Dynamic control of the oxygen content during CA storage of fruits and vegetables, CAPPT'95 Ostend, Belgium. 131-136 (1995)

[32] D.K. Salinkhe, D.B. Desai, Avocado. In: 'Postharvest biotechnology of fruits' CRC press Inc., Florida (1984)

[33] F.B. Salisbury, C.W. Ross, Plant Physiology, 4th edn. (Wadsworth, Belmont, CA) 272-273 (1992)

[34] R. Sander, Compilation of Henry's law constants for inorganic and organic species of potential importance in environmental chemistry (Version 3) http://www.mpch-mainz.mpg.de/~sander/res/henry.html (1999)

[35] M. Tadege, I. Dupuis, C. Kuhlemeier, Ethanol fermentation: new functions for an old pathway. Trends Plant Sci. **4** 320-325 (1999)

[36] P.O. Tingwa, R.E. Young, Studies on the inhibition of ripening in attached avocado (*Persea america* Mill.) fruits. J. Am. Soc. Hortic. Sci. **100** 447-449 (1975)

[37] M.L. Tucker, G.G. Laties, The dual role of oxygen in avocado fruit respiration: kinetic analysis and computer modeling of diffusion-affected respiratory oxygen isotherm. Plant Cell Environ. **8** 117-127 (1985)

[38] C.W. Yearsley, N.H. Banks, S. Ganesh, D.J. Cleland, Determination of lower oxygen limits for apple fruit., Postharvest Biol. Technol. **8** 95-109 (1996)

[39] H. Zuckermann, F.J.M. Harren, J. Reuss, D.H. Parker, Dynamics of acetaldehyde production during anoxia and post-anoxia in Red Bell pepper studied by photoacoustic techniques. Plant Physiol. **113** 925-932 (1997)

Chapter 5

Sensitive, on-line recordings of discontinuous water loss by Western Flower thrips (*Frankliniella occidentalis*) using a laser-based detector.

Abstract

On-line recordings of discontinuous H_2O loss by Western Flower thrips (*Frankliniella occidentalis*, average weight 50 μg) were performed operating a laser-based detector. The H_2O loss of a single thrips could be recorded with high sensitivity (practical detection limit 30 ppb). To our knowledge, these data represent on-line H_2O loss recordings of the smallest insects ever measured. We tested the effect of elevated CO_2 levels on the rate of H_2O loss. Elevated CO_2 levels are known to stimulate opening of the spiracles and hence exposure to high CO_2 levels in combination with an insecticide might be an effective tool to kill insects. Thrips could survive at 0% and 16% CO_2 for more than 10 hours while at 34% CO_2 this period was reduced to less than $2\frac{1}{2}$ hours. A surprising outcome of this research is that these small insects can survive such a long period under the low humidity (0% RH) of the applied gas flow.

S.T. Persijn[1], I. Wijkamp[2,†], J. Oomens[1,*], F.J.M. Harren[1]
[1] Life Science Trace Gas Exchange Facility, University of Nijmegen, Toernooiveld 1, 6525 ED Nijmegen, the Netherlands
[2]Research Station for Floriculture and Glasshouse Vegetables (PBG), Linnaeuslaan 2a, 1431 JV, Aalsmeer, the Netherlands.
[†]Current address: Rijk Zwaan Zaadteelt en Zaadhandel bv, Burgemeester Crezeelaan 40, 2678 ZG De Lier, the Netherlands
[*]Current address: FOM-Institute for Plasma Physics, Edisonbaan 14, Postbus 1207, 3430 BE Nieuwegein, the Netherlands

5.1 Introduction

Western Flower thrips (*Frankliniella occidentalis*) are small insects (1-2 mm, 50 μg) belonging to the order of Thysanoptera (Thripidae), the smallest winged insects [12]. *F. occidentalis* is widespread on greenhouse, agricultural and horticultural crops in North America and Europe [8, 19]. Since 1983, *F. occidentalis* is also a serious pest in Dutch greenhouses [14]. They have piercing-sucking mouth parts and feed by puncturing cells of plants, sucking out the cell contents thereby killing the plant tissue. Besides their pest status, thrips are also vectors of tosposviruses, a group of viruses which causes severe losses worldwide in important crops, as for example in tomatoes and chrysanthemums [20].

Controlled atmosphere (CA) storage using elevated CO_2 and/or reduced O_2 levels is frequently applied to retard ripening and extend the storage life of crops. As a positive side effect, CA storage conditions can be effective against pathogens and insect pests [4]. High CO_2 levels stimulate spiracle opening and hence, exposing insects to elevated CO_2 levels can lead to a desiccation of the insects. For example, H_2O loss in moth pupae has been shown to increase 6-fold after exposing the animals to 18 % CO_2 [3]. In addition, under elevated CO_2 and/or reduced O_2 levels the metabolic heat rate of insects decreases leading to energy shortage and mortality [22].

We tested the effect of elevated CO_2 levels on Western Flower thrips by monitoring H_2O loss from these insects. Currently, most research on gas exchange in insects is based on recordings of CO_2 released by insects; this is due to the wide availability of sensitive CO_2 analyzers (see for example [10]). Detection of H_2O vapour has proven to be a much more difficult task partly due to the high background level of H_2O vapour as compared to that of CO_2. Gravimetric methods used to detect H_2O vapour are very sensitive to movements of living insects and decapitation of insects is often necessary to overcome this problem [13]. In addition, recorded values must be corrected for the simultaneous, but not necessarily equal, mass changes of O_2 and CO_2 [9]. Measuring H_2O loss using radioactive isotopes has the advantage that it can be used in the presence of a high ambient H_2O concentration; however a drawback is its relatively poor time resolution [5]. Alternatively, H_2O vapour can be detected with a thin-film capacitor, a technique that has a good response time but insufficient sensitivity [17].

More recently, much more sensitive H_2O vapour detectors based on infrared absorption have been developed (see for example [21]). Here, we monitored H_2O loss from thrips using a photoacoustic detector based on an infrared laser. Photoacoustics is a sensitive technique for on-line monitoring of trace gases at high time resolution [6]. Recently, this detector has been applied to study CH_4 and H_2O vapour release by cockroaches and beetles with detection limits of 10 and 100 ppb, respectively [2]. These insects, with a weight of a few gram, release rather large quantities of H_2O vapour (typically a few hundred μmol/h). In contrast, thrips release only minute amounts of H_2O due to their small body size, imposing high demands on a detector and the content of H_2O vapour in the gas streaming over the insect. Hitherto, results shown here represent, to our knowledge, H_2O loss recordings of the smallest insects.

5.2 Material and Methods

Water vapour is on-line detected using a fast and sensitive photoacoustic technique [6]. The photoacoustic cell is placed inside the cavity of a liquid nitrogen-cooled carbon monoxide laser, the emission lines of which cover the infrared wavelength region between 5 and 7.9 μm. The use of this intense light source (up to 30 Watt inside the cavity), combined with the very strong absorption of H$_2$O vapour in this wavelength region, enables a sensitive detection of H$_2$O vapour. The detector is able to detect very small absorptions, but only on a relatively low background signal; typically the absorption signal should be larger than 1% of the background signal. In order to detect H$_2$O vapour release from such small insects requires the availability of a very dry gas flowing over the insect, this is achieved by placing a container with phosphorus pentoxide (P$_2$O$_5$) in the gas flow (see Figure 5.1). A more detailed description of the set-up can be found in [2]. The practical detection limit for H$_2$O vapour (30 ppb) is limited by the background level of water vapour (few ppm). This latter is due to residual H$_2$O after scrubbing and the desorption rate of H$_2$O vapour from tubings and the detection cell.
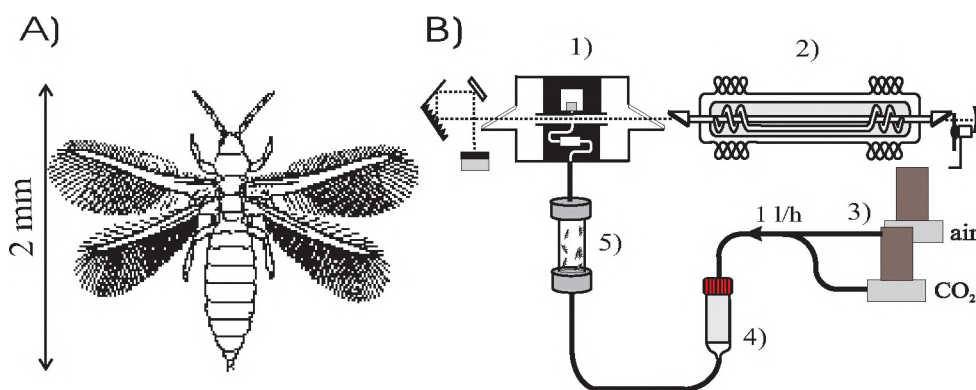
Figure 5.1: *A) Picture of F. occidentalis B) The experimental arrangement with 1) detection cell, 2) carbon monoxide laser, 3) mixing of air and CO$_2$ using mass flow controllers, 4) P$_2$O$_5$ scrubber, 5) insect cuvette. A gas mixture of air and CO$_2$ is scrubbed from H$_2$O vapour and passed through a small cuvette containing the insects. The outlet of the insect cuvette is connected to the detection cell.*

Prior to the experiments, thrips (*F. occidentalis*, see Figure 5.1A) were kept on chrysanthemums in a refrigerator (7 °C). Due to the low temperature the insects could be easily handled. Adult thrips (ranging from 1 to 26) with an average fresh weight of 50 μg per insect were put in a glass cuvette with a volume of 0.1 ml that was closed at both ends by a stainless steel mesh wire. A mixture of air and CO$_2$ (0-34 %) was prepared on-line by using electronic mass flow controllers (Brooks 5850, Veenendaal, the Netherlands). The gas flow at a total flow rate of 1 l/h was passed over the insect(s) (i.e., a flow velocity of 0.1 m/s in the insect cuvette) and subsequently entered the detection cell. In spite of the low flow rate used in the experiments, the detection cell still had a reasonably fast time

response due to small detection volume (26 ml). Initial, opening of the cuvette in order to insert insect(s) increases the level of H_2O vapour in the system. A very long washout curve is observed due to sticking of H_2O vapour to the cuvette, tubings, and detection cell. Experiments with an empty cuvette showed that it takes more than 5 hours before the H_2O vapour level in the detection cell becomes relatively constant.

The CO_2 release by the insect(s) was recorded by independent measurements using a commercial CO_2 infrared analyser (URAS 10E, Hartmann & Brown AG, Frankfurt am Main, Germany) at a flow rate of 0.5 or 1 l/h. CO_2 recordings were only performed in air free from CO_2. All experiments were performed at a room temperature.

5.3 Results
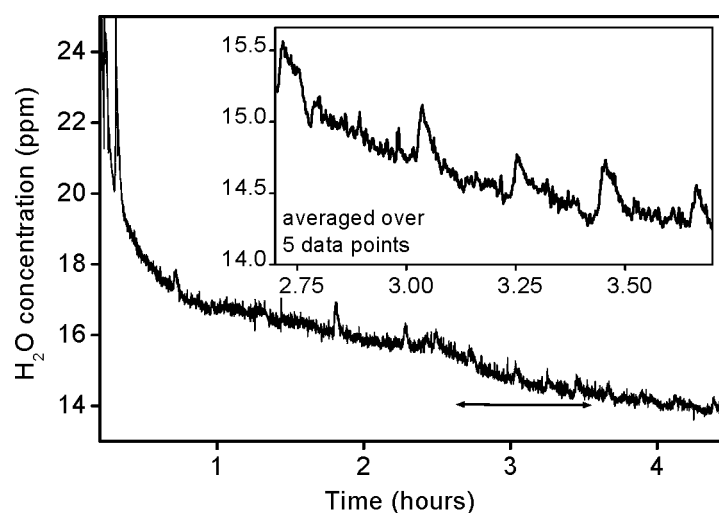
Figure 5.2: *Water emission of a single F. occidentalis in an air flow of 1 l/h. After placing the insect in the cuvette (t=0 h, data not shown) the H_2O level increases dramatically in the system. The long decay observed is due to a washout of H_2O sticking to the insect cuvette, tubings, and detection cell. The inset shows an average over 5 data points (15 seconds).*

Figure 5.2 shows release of H_2O vapour by a single *F. occidentalis*. At t=0 h the thrips was put in the cuvette (data not shown). The inset depicts an average over 15 seconds showing more pronounced the water emission peaks. After an initial period of irregularly occurring peaks, a more or less regular release pattern is observed with a periodicity of 4 h^{-1}. The H_2O loss is very small, typically below 1 nmol in each peak. No estimation of the cuticular H_2O vapour release could be made due to the washout of H_2O sticking to the insect cuvette, tubings, and detection cell.

Figure 5.3 shows water release of twenty-six *F. occidentalis* recorded at 1 l/h flow of air. The baseline H_2O vapour level is subtracted to show the H_2O loss peaks more clearly. At the start of the measurement many peaks are observed (see upper panel) indicating
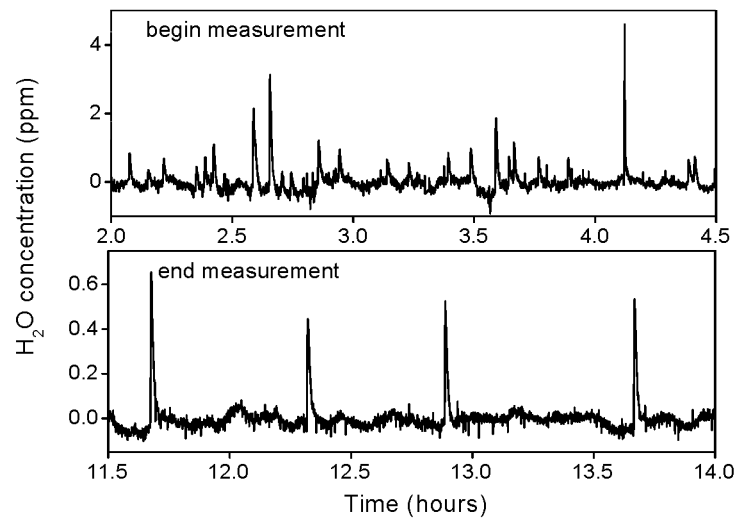
Figure 5.3: *Water emission by 26 thrips in an air flow of 1 l/h. The upper panel shows the H$_2$O loss 2 h after the thrips were put in the cuvette. The lower panel shows the H$_2$O loss of the same insects 9.5 h later. Note that the baseline H$_2$O level is subtracted.*

H$_2$O loss by many thrips. The frequency of the peaks decreases during the course of the measurement because a number of thrips died due to desiccation. The lower panel shows the H$_2$O vapour release 9.5 hours later than in the upper panel. A rather regular pattern is observed with only one peak appearing every 40 minutes, indicating that only a single thrips was still alive, as it was actually also observed during the measurement.
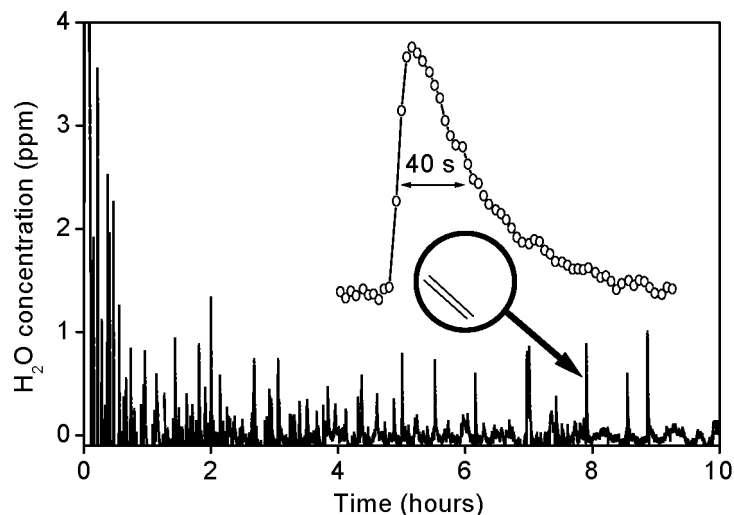
Figure 5.4: *Water emission by fourteen F. occidentalis in a 16% CO$_2$-84% air mixture (total flow rate is 1 l/h). At t=0 h the thrips were put in the cuvette. The baseline H$_2$O vapour level is subtracted for clarity. One of the release peaks is shown enlarged.*

The water emission by fourteen thrips in a 16% CO_2-84% air mixture is shown in Figure 5.4. Also here, the baseline H_2O vapour level is subtracted for clarity. The results under 16% CO_2 are very similar to those obtained with pure air. One of the peaks is shown enlarged. Unlike the fast rise ($\pm$ 10 s) there is a very slow decay with a time constant of 40 seconds; the latter is partly an instrumental effect since the polar H_2O molecule tends to stick to surfaces, and in particular to metals, i.e., the cell and mesh wire confining the insect.
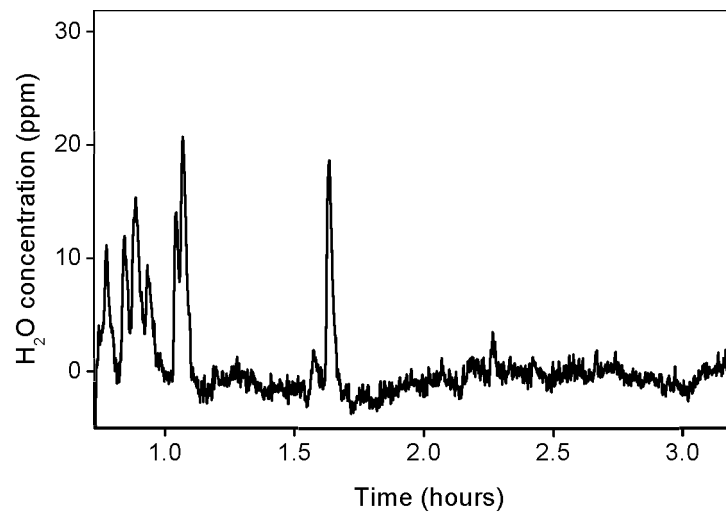
Figure 5.5: *Water emission by four thrips in a 34% CO_2-66% air mixture (total flow rate is 1 l/h). At t=0 h the thrips were put in the cuvette. The baseline H_2O vapour level is subtracted for clarity.*

The water emission by four thrips in a 34% CO_2-66% air mixture is shown in Figure 5.5. This result strongly deviates from the outcome of measurements performed under 0 and 16 % CO_2. In this case, H_2O release peaks are observed only during first $2\frac{1}{2}$ hours. Also in other experiments with a 34% CO_2-66% air mixture, peaks were only observed during the initial $2\frac{1}{2}$ hours. In addition, peaks observed due to H_2O release are much higher for thrips exposed to 34% CO_2.

No CO_2 peaks were observed in the experiments (performed under 0 % CO_2), this is possibly due to a lack of sensitivity of the URAS. In contrast, peaks due to H_2O vapour release were observed at all CO_2 levels (0, 16, and 34% CO_2) applied. At 0 and 16% CO_2, thrips could survive for more than 10 hours. In contrast, at 34% CO_2 the maximum survival time was less than $2\frac{1}{2}$ hour (survival time is defined as the time of the last peak in H_2O vapour release). Normally, measurements continued untill no peaks in H_2O emission were observed anymore. After the measurements insects were inspected to confirm that they were dead. Insects exposed to high CO_2 levels can be anaesthesized [7] and when returned to a normal atmosphere they can regain conciousness after as much as 1 hour. Possibly, some thrips might still be alive after the experiments although, what is more probable,

the insects were desiccated due the arid conditions under which these experiments were performed.

5.4 Discussion

To the best of our knowledge, *Drosophila melanogaster*, an insect with a weight of approximately 1 mg, was thus far the smallest insect for which water loss has been reported [21]. Here, we recorded H_2O emission from insects that weigh only 50 μg. Recording loss of H_2O vapour from even smaller insects, with corresponding smaller amounts of H_2O release, is difficult due to the relatively high background H_2O level in the gas flow and the detection cell.

The tracheal system of thrips is well developed and usually opens to the atmosphere by means of four pairs of spiracles making discontinuous H_2O loss via respiration possible and probably even necessary [9, 16]. However, care must be taken to interpret the observed discontinuous H_2O loss as discontinuous respiration; also activity can lead to a discontinuous release as it was shown in cockroaches (grooming led to single bouts) [9]. In addition, small insects like thrips are difficult to observe and therefore no good correlation between H_2O loss recordings and their behaviour can be made.

The CO_2 released by thrips could not be recorded with our URAS CO_2 analyzer, probably due to a relatively low detection limit of the analyzer (0.5 ppm). At present, novel light sources emitting in the strong CO_2 absorption regions at 2.7 and 4.3 μm are under development [18]. The laser-based detector used in this study is not very suitable to monitor CO_2 since none of the laser frequencies coincides with a strong CO_2 absorption. Using our experimental setup in combination with such newly developed light sources, however, will in the future also enable CO_2 recordings at a sub-ppb level. Using this approach, it is expected that, in addition to H_2O loss, the CO_2 emission by thrips can also be recorded as the unwanted CO_2 can be reduced to very low levels (sub ppm) using appropriate scrubbers. Hence, studying CO_2 release by small insects requires a less stable detector.

Thrips could survive more than 10 hours at 0 or 16% CO_2 while at 34% CO_2 this period was reduced to less than $2\frac{1}{2}$ hours. Already 75 years ago, Hazelhoff showed that elevated CO_2 levels stimulate spiracles to open leading thereby likely to an increased H_2O loss [7]. This was actually observed by Birchard who showed that exposing moth pupae to elevated CO_2 levels led to a dramatic increase in H_2O loss [3]. In confirmation, we observed that the amount of H_2O loss under 34% CO_2 is much higher than under 0% or 16% CO_2. Furthermore, elevated CO_2 and/or reduced O_2 levels lower the metabolic heat rate of many insects, which can lead to energy shortage [22]. Increasing the CO_2 level to 50% or higher can even lead to narcosis [7].

Under conditions of low relative humidity (RH) insects are more likely to desiccate as their H_2O emission increases, hence CA treatments can be more effective [1]. The H_2O loss can eventually lead to mortality as some critical level is reached [15]. Our measurements were performed at 0% RH and therefore results shown here may not apply to situations found in practice; for example in the flower bud, the RH is close to 100 %. The fact that these small insects with their thin cuticle (and therefore high cuticular H_2O loss) can

survive so long at 0 and 16% CO$_2$ is astonishing with respect to the 0% RH in the applied gas flow [9].

Due to its polar nature H$_2$O tends to stick to surfaces. In order to improve the time response the detection cell could be constructed from glass instead of brass and in addition, the stainless steel mesh wire confining the insect can be replaced by one made of teflon. Furthermore, the flow (1 l/h) used in these experiments could be increased. Although the average H$_2$O vapour concentration will be then lower the H$_2$O loss peaks will be narrower and in addition, the background H$_2$O level will decrease since the rate of desorption of H$_2$O vapour from the system is rather constant. For example, a five-fold increase of flow rate will lead to a less than five-fold reduction in the recorded peak value of H$_2$O vapour and at a lower H$_2$O background level giving a better insight into dynamics of emission.

5.5   Acknowledgements

References

[1] S.W. Bailey, H.J. Banks, A review of recent studies of the effects of controlled atmosphere on stored product pests. In: 'Controlled atmosphere storage of grain' (ed.) J. Shejbal (Elsevier, Amsterdam) 101-108 (1980)

[2] F.G.C. Bijnen, F.J.M. Harren, J.H.P. Hackstein, J. Reuss, Intracavity CO laser photoacoustic trace gas detection: Cyclic CH$_4$, H$_2$O and CO$_2$ emission by cockroaches and scarab beetles. Appl. Opt. **35** 5357-5368 (1996)

[3] G.F. Birchard, Diffusive water loss in *Automeris io* pupae: effect of hypobaria, CO$_2$ and mass, Comp. Biochem. Physiol. **99A** 537-540 (1991)

[4] A. Carpenter, M. Potter, In 'Quarantine treatments for pests of food plants' (Eds) J.L. Sharp, G.J.Hallman (Western Press, San Francisco, CA) 171-198, (1994).

[5] P.C. Croghan, J. Noble-Nesbitt, A.G. Appel, Measurement of water and carbon dioxide loss from insects using radioactive isotopes., J. Exp. Biol. **198** 227-233 (1995)

[6] F.J.M. Harren, J. Reuss, Photoacoustic spectroscopy. In: 'Encyclopedia of applied physics' Vol. 19 (ed.) G.L. Trigg (VCH, Weinheim) 413-435 (1997)

[7] E.H. Hazelhoff, Regeling der ademhaling bij insecten en spinnen., Thesis, University of Utrecht (1926)

[8] L. Hughes, E.A. Bazzaz, Effect of elevated CO$_2$ on interactions between the western flower thrips, *Frankliniella occidentalis* (Thysanoptera: Thripidae) and the common milkweed *Asclepias syiaca*. Oecologia **109** 286-290 (1997)

[9] P. Kestler, Respiration and respiratory water loss. In: 'Comparative Biochemisty and Physiology of Insects', (ed.) K.H. Hoffmann, 137-183 (1985)

[10] P. Kestler, Cyclic CO$_2$ release as a physiological stress indicator in insects. Comp. Biochem. Physiol. **100** 207-211 (1991)

[11] W.J. de Kogel, Host plant resistance to western flower thrips: variable plants and insects, Thesis, University of Amsterdam (1997)

[12] T.R. Lewis, Thrips, their biology, ecology and economic importance, Academic Press, London and New York (1973)

[13] J.R.B. Lighton, D.A. Garrigan, F.D. Duncan, R.A. Johnson, Spiracular control of respiratory water loss in female alates of the harvester ant *Ponomymex rugosus*. J. Exp. Biol. **179** 233-244 (1993)

[14] W.P. Mantel, M. van de Vrie, De Californische trips, *Frankliniella occidentalis*, een nieuwe schadelijke tripssoort in de tuinbouw onder glas in Nederland. Ent. Ber. **48** 140-144 (1988)

[15] S. Navarro, M. Calderon, Exposure of Ephestia cautella Walker pupae to carbon dioxide concentrations at different relative humidities: the effect of adult emergence and loss in weight. J. Stored Prod. Res. **10** 237-241 (1974)

[16] O.W. Richards, R.G. Davies, 'Imm's general textbook of entomology' 10th ed. Vol 2, Classification and biology, Chapman and Hall, 783-792 (1988)

[17] M.C. Quinlan, N.F. Hadley, New system for concurrent measurement of respiration and water loss in arthropods. J. Exp. Zool. **222** 255-263 (1982)

[18] K. Schneider, P. Kramper, S. Schiller, T. Mlynek, Toward an optical synthesizer: A single-frequency parametric oscillator using periodically poled LiNbO₃, Opt. Lett. **22** 1293-1295 (1997)

[19] J.L. Shipp, K. Wang, M.R. Binns, Economic injury levels for Western Flower Thrips (Thysanoptera: Thripidae) on greenhouse cucumber. J. Econ. Entomol. **93** 1732-1740 (2000)

[20] I. Wijkamp, F. Wetering, R. van de Goldbach, D. Peters, Transmission of tomato spotted wilt virus by Frankliniella occidentalis; median acquisition and inoculation period. Ann. Appl. Biol. **129** 303-313 (1997)

[21] A.E. Williams, M.R. Rose, T.J. Bradley, Using laboratory selection for desiccation resistance to examine the relationship between respiratory pattern and water loss in insects. J. Exp. Biol. **201** 2945-2952 (1998)

[22] S. Zhou, R.S. Criddle, E.J. Mitcham, Metabolic response of Platynota stultana pupae to controlled atmospheres and its relation to insect mortality response. J. Insect Physiol. **46** 1375-1385 (2000)

Chapter 6

The use of the inert tracer gas SF_6 as a tool to determine the tracheal volume and respirative behaviour of insects.

Abstract

The biological inert tracer gas SF_6 was used to study the respiration patterns of *Attacus atlas* pupae and adult American cockroaches (*Periplaneta americana*). From the released amount of SF_6 the tracheal volume of these insects could be determined. The calculated tracheal volume of the *Attacus atlas* pupae of (183 ± 56) $\mu l/g$ is in good agreement with values obtained by other techniques. In addition, the respiration pattern of the insect could be resolved in detail due to the fast time response of the laser based detector. The high sensitivity of the detector (5 parts per 10^{12}) opens new possibilities to study respiration behaviour even in the smallest insect species.

S.T. Persijn[1], Mitrayana[2], F.J.M. Harren[1]
[1] Life Science Trace Gas Exchange Facility, University of Nijmegen, Toernooiveld 1, 6525 ED Nijmegen, the Netherlands
[2]Gadjah Mada University, Sekip Utara III, Yogyakarta, Indonesia

6.1 Introduction

In terrestrial insects exchange of gases takes place through a system of internal gas filled tubes, the tracheal system, that connect to the atmosphere by valves known as spiracles. These latter can accurately control the exchange between the gas in the tracheal system and the outside air [5]. In contrast to vertebrates, the blood (haemolymph) has no important role in O$_2$ transport and storage; O$_2$ is directly carried to its site of utilisation by diffusion through the gas tubes [16]. More than 80 years ago, the functional characteristics of the tracheal system were already described by Krogh [7]. However, up to now, only a limited number of investigations have focussed on the total volume of this system. Techniques applied to determine the tracheal volume include vacuum extraction [18], mechanical compression [3] and stereological analysis [17]; each of these techniques is intrusive and, in addition, a stereological analysis is very time consuming.

Rauch and Hetz describe a number of non-intrusive techniques to determine the tracheal volume that are lacking such drawbacks [14, 6]. Another, elegant technique based on inert gas wash-out was developed by Bridges and co-workers [2] who placed pupae of the Giant silkworm moth *Hyalophora cecropia* in a vessel that was continuously flushed with a 20% O$_2$-80% N$_2$ mixture. At the onset of the constriction period the mixture was replaced by pure argon. The wash-out of N$_2$ during the subsequent burst was recorded with a mass spectrometer. The tracheal volume was derived from the amount of N$_2$ emerging from the animal. Measurements were repeated with N$_2$ replacing a 20% O$_2$-80% argon mixture to account for the inert gas solubility in the body fluids. In a similar, slightly simplified, approach we use biologically inert gas sulphur hexafluoride (SF$_6$), a gas that is widely used as tracer both in liquid and gas phase [15, 9]. SF$_6$ can be detected at extreme sensitivity level and high time resolution using a CO$_2$ laser based trace gas detector [4]. It is important to note that in contrast to Bridges et al., we also obtain the respiration pattern of the insect. The high sensitivity of the detector opens new ways to study the respiration in very small insects.

Release of SF$_6$ was monitored from *Attacus atlas* pupae and adult American cockroaches (*Periplaneta americana*) exposed to a SF$_6$ environment for several hours. SF$_6$ was detected by means of a laser based detector, while CO$_2$ was recorded using an infrared gas analyser. In addition, length changes of the abdomen of *Attacus atlas* were recorded with an infrared-reflection sensor in order to obtain a more complete picture of the insects' respiration.

6.2 Materials and methods

Insects were placed in a glass bottle (0.32 l) filled with air and SF$_6$ was injected in the bottle with a syringe to obtain a concentration of 0.63% SF$_6$. The insects were kept in the closed bottle for a period of 24 h (*Attacus atlas*) and 3 h (*Periplaneta americana*). The length of this period was chosen on a basis of the duration of the respiration cycle of the insect, which is typically 1.5 and 0.2 hours, respectively. As the insect is respiring O$_2$ is consumed and CO$_2$ is produced; keeping the insect too long in the closed bottle can influence the insects' respiration. For *Attacus atlas*, the O$_2$ level in the bottle decreases from 21.0 to 19.2%, while CO$_2$ concentration increases from 350 ppm to 1.3% at the end of the 24 h
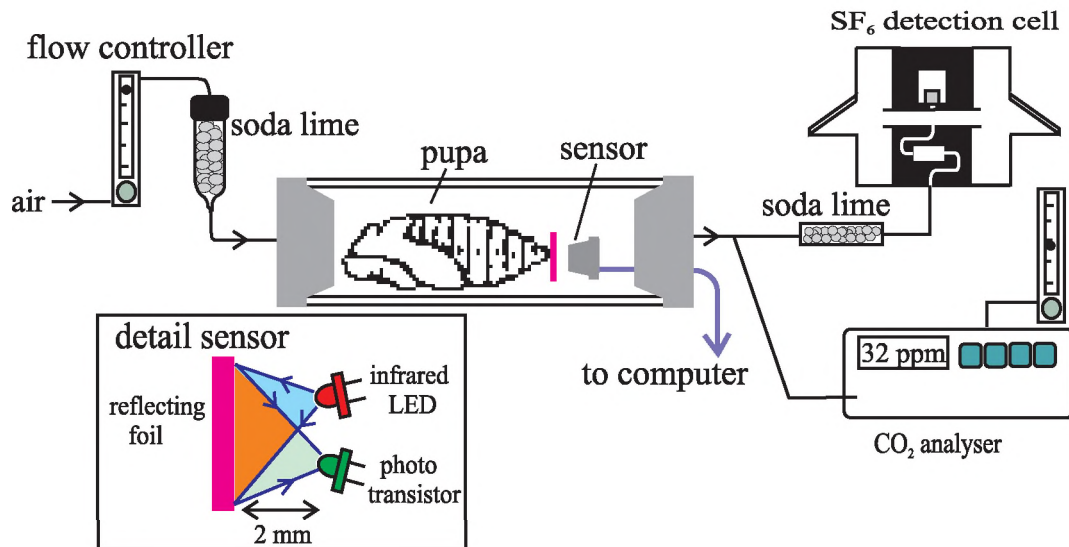
Figure 6.1: *Schematic overview of the experimental set-up. The insect is accomodated within a 23 ml sampling cuvette or in a 50 ml cuvette in a case when length changes were also recorded. A dry air flow (10 l/h) is scrubbed from CO_2 and passed over the insect. After the sampling cuvette the flow is split into two; 5 l/h to the CO_2 analyzer and 5 l/h to the PA detector. Before the SF$_6$ detector an additional CO_2 scrubber is placed since CO_2 interferes with the SF$_6$ recording. A single flow controller behinds the CO_2 analyzer can maintain these flow rates equal since the flow resistance of the PA cell is higher than of the CO_2 analyzer. Length changes were measured with an infrared-reflection sensor placed 2 mm from the insects' abdomen. A small reflecting foil was glued at the end of the abdomen to obtain a higher reflection signal.*

SF$_6$ loading period (assuming an average CO_2 release rate of 7.2 μmol/h and a respiration coefficient (RQ) of 0.7, i.e., for every molecule of O_2 consumed 0.7 molecule of CO_2 is produced). Note that the increase in CO_2 can be prevented by using a CO_2 scrubber. The chosen concentration of 0.63% SF$_6$ was a comprimise; a too high concentration would lead to an overload of the detector and reduce the O_2 level in the bottle, while a too low concentration would only give a clear view of the respiration pattern for a limited period. After the SF$_6$ loading procedure insects were transferred to the sampling cuvette and the measurement was started.

Figure 6.1 shows a schematic overview of the experimental set-up. Dry and CO_2 free air was flushed over the insects at a flow rate of 10 l/h using two flow controllers (Brooks, Veenendaal, the Netherlands). After passing the sampling cuvette the flow was split in two directions; 5 l/h was diverted to an infrared CO_2 analyzer (URAS 10E, Hartmann & Braun, Frankfurt am Main, Germany) and the rest to the laser based SF$_6$ detector.

To detect SF$_6$ we make use of the spectral overlap of the ν_3 stretching vibration of this molecule and emitted laser lines of the detector. The strongest absorption is that on the 10P16 laser line (947.74 cm^{-1}) where the SF$_6$ absorption coefficient is $6.5 \cdot 10^2$ atm^{-1} cm^{-1}

[11, 4]. A CO$_2$ laser based detector operating at this laser line can detect SF$_6$ concentrations down to 5 ppt (1 ppt = 1 part per 10^{12}) [4]. Both CO$_2$ analyzer and SF$_6$ detector were calibrated by injecting a series of known amounts of CO$_2$ and SF$_6$, respectively.

Length changes of *Attacus atlas* pupae could be monitored with a modified version of the infrared-reflection sensor developed by Hetz (see detail in Figure 6.1) [6]. A small reflecting foil was glued to the end of the abdomen. At 2 mm distance from the foil the sensor was placed. It consists of an infrared LED and a photo transistor that records the light reflected by the foil. The system was calibrated using a micrometer; length changes down to 0.5 μm could be resolved. The signal from the SF$_6$ detector, infrared-reflection sensor and CO$_2$ analyzer were fed into a computer and sampled at a second time scale. A fast Fourier transform filter was applied to the signal from the reflection sensor to remove high frequency components that were caused by electrical interference. All experiments were performed at room temperature (21 °C).

Experiments were performed on pupae from the moth *Attacus atlas* and on adult American cockroaches *Periplaneta americana*. In terms of the overall wing size the moth *Attacus atlas* (Saturniidae) is the largest moth in the world. The pupae under study are typically 4 cm long and have a weight of 5 g. The American cockroach *Periplaneta americana* (Blattidae) has spread throughout the world by commerce. Adult insects weigh about 1 g and are about 4 cm long.

6.3 Results
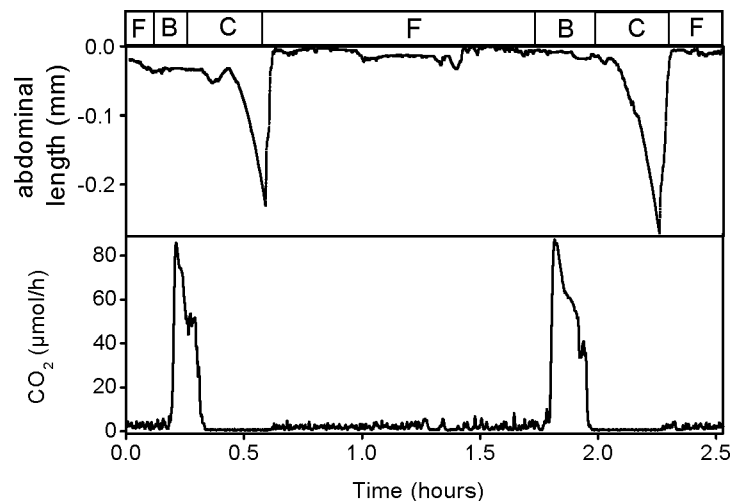
6.3.1 CO$_2$ emission and abdominal length

Figure 6.2: *CO$_2$ emisssion and relative abdomen length of Attacus atlas (length 41 mm, weight 4.49 g). The three phases of the respiration cycle; constriction (C), fluttering (F), and burst (B) can be distinguished in both plots. The length of the constriction period (0.288 ± 0.036 h, n=14) is 20 % of the total respiration cyclus (1.43 ± 0.30 h).*

Figure 6.2 shows a plot of the CO$_2$ emission and abdominal length obtained from an *Attacus atlas* pupa. From these data one observes that the pupa is respiring regularly with a period of 1.43 ± 0.30 h, an average CO$_2$ emission of 7.2 μmol/h and the constriction period lasts 17 minutes (n=14). Assuming a respiration coefficient (RQ) of 0.7, this implies that during the constriction period 50 μl CO$_2$ is produced while 70 μl O$_2$ is being consumed, hence a net decrease of 20 μl gas. In combination with the higher solubility of CO$_2$ (as compared to O$_2$) in haemolymph and tissue this results in an underpressure inside the insect during the constriction period [16, 19]. The length change associated with the underpressure depends on the elasticity of the abdomen, i.e., a higher stiffness corresponds to smaller length changes and a higher under pressure [6].
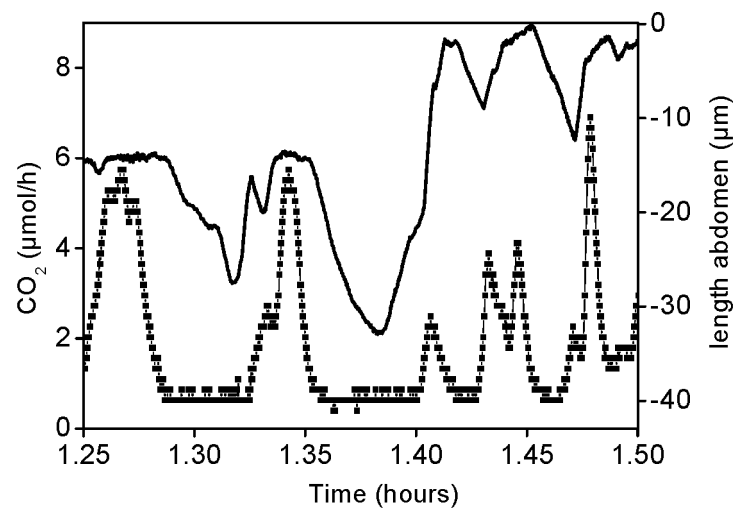

Figure 6.3: *CO$_2$ release (■) and relative abdominal length (-) in an expanded view of the flutter period in Figure 6.2. During short periods no CO$_2$ is released and the abdominal length decreases. Note that the recorded CO$_2$ emission shows less detail than the abdominal length data due to an averaging out by insect and measuring cuvette.*

Figure 6.3 presents an expanded view of the flutter period in Figure 6.2. The correlation between CO$_2$ emission and the abdomen length is similar to that observed during burst and constriction period; at the onset of a period of higher CO$_2$ release the length of the abdomen increases but in the subsequent period the length is rather constant; while if no CO$_2$ is released the length of the abdomen decreases. However, since such mini-constriction periods are very short (less than 3 minutes) the associated length changes are also small (less than 30 μm).

6.3.2 SF$_6$ washout from insects; insight in tracheal volume and respiration pattern

A good degree of correspondence between patterns of CO$_2$ and SF$_6$ release from *Attacus atlas* pupa is observed (see Figure 6.4).
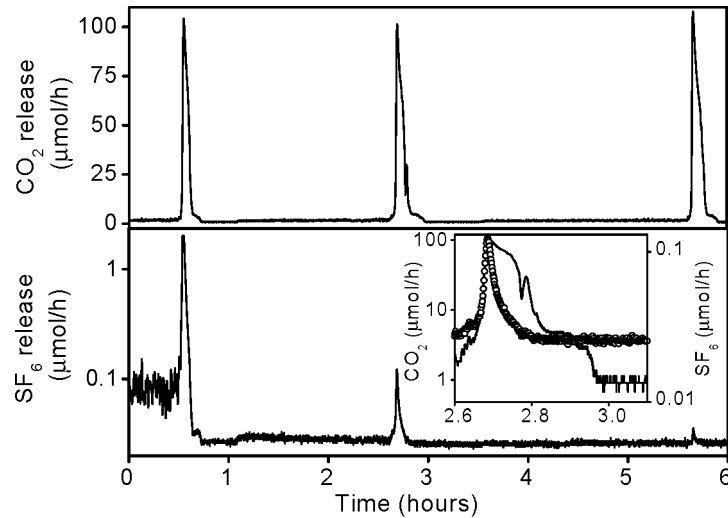
Figure 6.4: *CO$_2$ and SF$_6$ release of Attacus atlas (3.90 g) loaded with SF$_6$. After subtracting the background signal (mainly due to absorption of laser light by the windows of the SF$_6$ detection cell) from the SF$_6$ signal a total amount of 0.112 μmol SF$_6$ is released, yielding a tracheal volume of 112 μl/g. The inset depicts the burst around 2.7 hours enlarged, showing the different shapes of the SF$_6$ (○) and CO$_2$ (-) release curve.*

The contour of releases during the burst period is different (see inset); due to a decrease of the SF$_6$ concentration in the tracheal system the SF$_6$ release decreases fastly while in contrast, the CO$_2$ level in the tracheal system and hence the CO$_2$ release decrease more slowly as CO$_2$ dissolved in the haemolymph evaporates. The release of SF$_6$ is integrated to obtain the total amount of SF$_6$ released (0.112 μmol). From this, one calculates the tracheal volume of the insect to be 112 μl/g. Calculated volumes for various pupae range from 112 to 254 μl/g (n=3). Figure 6.5 presents the integrated SF$_6$ production from Figure 6.4.

During the first flutter period the integrated SF$_6$ release increases linearly with time. A linear fit of this period yields A = (-1.87±0.11)·10^{-4}μmol, B = (5.615±0.004)·10^{-2}μmol/h, (R=0.9995, n=1753, P<0.0001). Fluctuations around the linear fit are due to micro-constrictions and openings. Since the SF$_6$ release is constant and the internal SF$_6$ concentration decreases with time this implies that the average time the spiracles are open increases. During the first burst 66% of all released SF$_6$ is emitted.

Figure 6.6 presents the SF$_6$ release of another pupa. At t=0 h the insect was transferred from the bottle containing SF$_6$ to the measuring cuvette. The SF$_6$ released each respiration cycle decreases rapidly, but still up to 10 hours after loading the insect with SF$_6$, an elevated SF$_6$ emission is observed during burst periods. This indicates that SF$_6$ remains in the insect for a prolonged period. Some insight in the refreshment of the tracheal system can be gained from these data.

Figure 6.7 shows the CO$_2$ and SF$_6$ release of an adult *Periplaneta americana*. Note that the respiration cycle of *Periplaneta americana* lasts much shorter than that of *Attacus atlas*. Again a good agreement between values of CO$_2$ and SF$_6$ release is observed. The
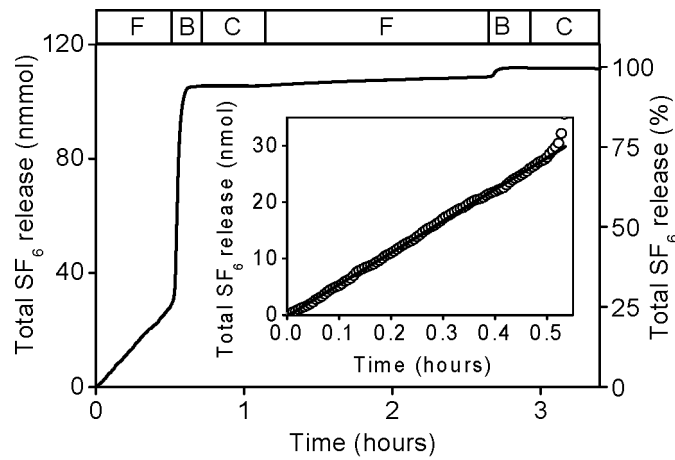
Figure 6.5: *Integrated SF$_6$ release from Figure 6.4. During the first flutter period SF$_6$ is released at a constant rate as the total amount of SF$_6$ released increases linearly with time (see inset). Note that only 10% of all data points are shown for clarity.*
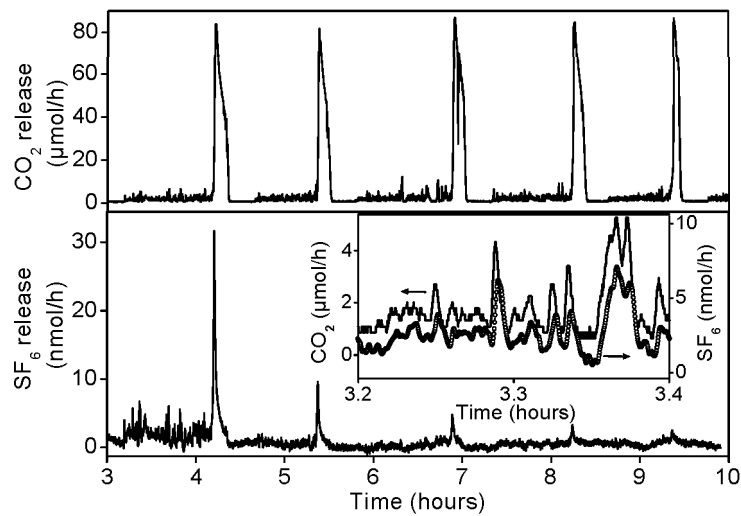

Figure 6.6: *CO$_2$ and SF$_6$ release by Attacus atlas which was loaded with SF$_6$ until t= 0 hours. The inset shows in detail part of the flutter period around 3.3 hours.*

amount of SF$_6$ released is lower than for *Attacus atlas* pupae due to a lower weight and tracheal volume.

6.4   Discussion

Calculated values of the tracheal volume of *Attacus atlas* pupae range from 112-254 μl/g (n=3). This range of values is similar as observed elsewhere using different techniques
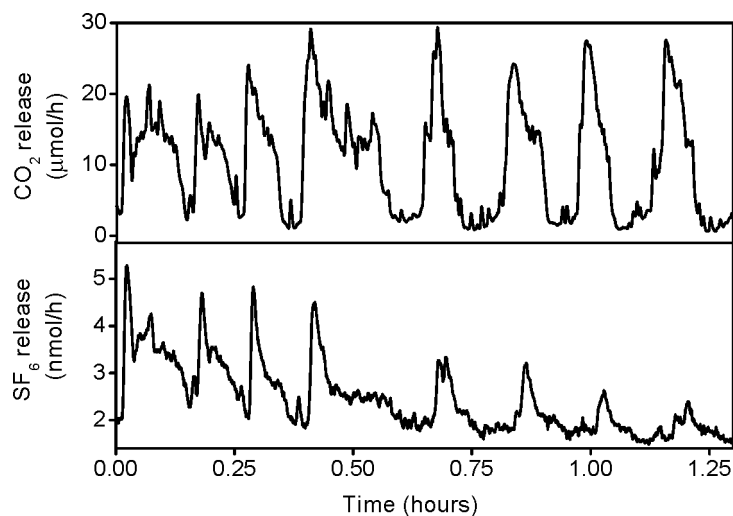
Figure 6.7: CO_2 and SF_6 release by *Periplaneta americana* (weight 0.832 g). This insect is breathing at a much higher frequency than *Attacus atlas*. The calculated tracheal volume is 28.2 $\mu l/g$. Note that the respiration pattern is not very regular as the insect is still stressed from being transferred.

[6]. As compared to other techniques like vacuum extraction, mechanical compression, and stereological analysis, the here presented method has the advantage that it is non-intrusive [18, 3, 17].

To calculate the tracheal volume of the insects it was assumed that all released SF_6 was stored in the tracheal system, however, a part of the SF_6 can also be stored in body fluids, tissues, cuticular lipids and the fat body of the insect. Fortunately, in most fluids and tissues the solubility of SF_6 is low (e.g. α_{SF6} in H_2O is $6.21 \cdot 10^{-3}$ ml ml^{-1} atm^{-1}, at 25 °C) [10]. An exception is formed by oil where the solubility is more than one order of magnitude higher [10]. To estimate the amount of SF_6 that is not stored in the tracheal system but in other part of the insects' body, a comparision can be made with the quantity of stored O_2. Snyder et al. assumed that the O_2 capacity of haemolymph and tissue was only 5% of the O_2 capacity of the tracheal system while Hetz found a value of about 20% [21, 6]. Oxygen has in general a higher solubility than SF_6, e.g., in pure H_2O the solubility of O_2 is about five times higher [10]. The error introduced will therefore be small by assuming that no SF_6 is stored in haemolymph and tissues although some SF_6 might be stored in the cuticular lipids and the fat body of the insect. Earlier, other inert gases (like argon) have been used to determine the tracheal volume; these have however a higher solubility and hence more gas is dissolved in the tissue and body fluids [2]. Bridges et al. used inert gases with high and low solubility to correct for the amount of inert gas dissolved in the tissue [2].

Secondly, both inserting the insect in the cuvette and SF_6 sticking to the cuticle may yield spurious signals. However, this transient disturbance is neglegible for *Attacus atlas* due to the long respiration cyclus (typically a few hours), and the low adsorption strength

of the non-polar SF$_6$ molecule to most materials (the amount of SF$_6$ sticking to the insects' cuticle can be found using a dead animal) [6]. Ideally, the insect should be transferred during the constriction period from loading to sampling cuvette, but transfer during the fluttering period introduces only a small error (<1%). Even for *Periplaneta americana* with its much shorter respiration cycle (typically 20 minutes) a relatively small error is introduced.

Recordings of the abdominal length in *Attacus atlas* are similar to the results from Hetz and Sláma [6, 20]. Sláma could convert the abdominal contractions to internal volume changes by placing the pupa under water and then calibrate his system [19]. As already noted by Hetz the abdominal length recordings are subject to various error sources, e.g., due to an abdominal movement the reflection foil can no longer be parrallel to the sensor giving a lower reflection signal [6].

The O$_2$ uptake, and hence the total gas exchange, in many organisms is proportional to their mass ($\dot{M}_{O2} \propto$ mass$^{0.75-0.8}$) [12]. Recording the respiration pattern of small insects requires therefore extremely sensitive gas detectors [1, 23]. Monitoring H$_2$O vapour release or O$_2$ uptake by small insects is especially problematic due to the high background concentration of these gases. The gas detector must therefore not only be very sensitive but also have a high accuracy. Using a micro-respirographic method allows one to monitor the O$_2$ uptake and CO$_2$ production of small insects but monitoring the release of various individual gases is difficult (the latter is in contrast to flow-through respirometry) [20]. Measuring the CO$_2$ release from small insects is relatively simple as the CO$_2$ concentration in the in flowing air to the insect can be efficiently reduced using a chemical scrubber (like KOH). The CO$_2$ resolution that can be obtained nowadays is stated to be 1 ppb making such currently available detectors sensitive enough to determine the respiration pattern of small insects like Drosophilla (weight typically 1 mg) [22]. However, no detailed information is obtained on the fluttering and constriction phase [23]. A possible solution to this problem is the use of more sensitive detectors and especially for CO$_2$ this seems feasible (CO$_2$ possesses a very strong infrared absorption around 2349 cm^{-1}). A sub ppb detection limit is anticipated when using a background free detection method like photoacoustics in combination with a suitable light source (e.g. OPO or quantum cascade laser [8, 13]).

Until such detectors are readily available the here presented SF$_6$ loading technique is a good alternative to study the respiration of very small insects. The SF$_6$ loading experiments show that, in addition to an estimate of the tracheal volume, the respiration pattern of the insect can be obtained; the latter information was not presented in the work of Bridges et al. [2]. If the insect is loaded with a higher SF$_6$ concentration (e.g. a 21% O$_2$-79% SF$_6$ mixture and using a reduced flow rate of 1 l/h, determination of respiration patterns for sub-μg insects appears feasible (assuming a tracheal volume of 100 μl/g, a typical value for many insects). Such performance is several orders of magnitude better than what obtainable by existing detectors.

6.4.1 Acknowledgements

References

[1] F.G.C. Bijnen, F.J.M. Harren, J.H.P. Hackstein, J. Reuss, Intracavity CO laser photoacoustic trace gas detection: cyclic CH$_4$, H$_2$O and CO$_2$ emission by cockroaches and scarab beetles. Appl. Opt. **35** 5357-5368 (1996)

[2] C.R. Bridges, P. Kestler, P. Scheid, Tracheal volume in the pupa of the saturniid moth Hyalophora cecropia determined with inert gases. Respir. Physiol. **40** 281- 291 (1980)

[3] J.B. Buck, M. Keister, Cyclic CO$_2$ release in diapausing pupae. II. Tracheal anatomy, volume and P$_{CO2}$; blood volume; interburst CO$_2$ release rate. J. Insect Physiol. **1** 327-340 (1958)

[4] T.T. Groot, G. Cotti, D.H. Parker, H.A.J. Meijer, F.J.M. Harren. Monitoring gas transport in rice using SF$_6$ as tracer gas detected by laser photoacoustics. In: 'Photoacoustic and Photothermal Phenomena', (ed. F. Scudieri and M. Bertolotti) AIP Conference Proceedings 463 (Woodbury, New York, 673-675 (1998)

[5] E.H. Hazelhoff, Regeling der ademhaling bij insecten en spinnen., Thesis, University of Utrecht (1926)

[6] S.K. Hetz. Untersuchungen zu Atmung, Kreislauf und Säure-Basenregulation an Puppen der tropischen Schmetterlingsgattungen Ornithoptera, Troides und Attacus, (Thesis Friedrich-Alexander Universitt, Erlangen-Nürnberg) (1994)

[7] A. Krogh, Studien über Tracheenrespiration: II Über Gasdiffusion in den Tracheen. Pflügers Arch. Gesamzte Physiol. Menschen Tiere **179** 95-112 (1920)

[8] F. Kühnemann, K. Schneider, A Hecker, A.A.E. Martis, W. Urban, S. Schiller S, J. Mlynek, Photoacoustic trace-gas detection using a cw single-frequency parametric oscillator, Appl. Phys. B **66** 741-745 (1998)

[9] B.K. Lamb, J.B. McManus, J.H Shorter, C.B. Kotb, B. Mosher, R.C. Harris, E. Allwine, D. Blaha, T. Howard, A. Guenther, R.A. Lott, R. Siverson, H. Westberg, P. Zimmerman, Development of atmospheric tracer methods to measure methane emissions from natural gas facilities and urban areas, Environ. Sci. Technol. **29** 1468-1479 (1995)

[10] T. Langø, T. Mørland, A.O. Brubakk, Diffusion coefficients for gases in biological fluids and tissues: a review, Undersea Hyperbar. M. **23** 247-272 (1996)

[11] R.S. McDowell, H.W. Galbraith, C.D. Cantrell, N.G. Nereson, E.D. Hinkley, The ν_3 Q branch of SF$_6$ at high resolution: Assignment of the levels pumped by P(16) of the CO$_2$ laser, J. Mol. Spectrosc. **68** 288-298 (1977)

[12] P.L. Miller, The American cockroach, (ed. W.J. Bell and K.G. Adiyodi) Chapman and Hall, London pp. 137-183 (1982)

[13] B.A. Paldus, T.G. Spence, R.N. Zare, J. Oomens, F.J.M. Harren, D.H. Parker, C. Gmachl, F. Cappasso, D.L. Sivco, J.N. Baillargeon, A.L. Hutchinson, A.Y. Cho, Photoacoustic spectroscopy using quantum-cascade lasers, Opt. Lett. **24** 178-180 (1999)

[14] P. Rauch, Vergleichende Messungen zur Bestimmung des Tracheenvolumens von verschiedenen Schmetterlingensstadien, Msc thesis, Erlangen, Germany (1993)

[15] G. Savidge, P. J. le B. Williams The PRIME 1996 cruise: an overview, Deep-Sea Res. Pt II **48** 687-704 (2001)

[16] K. Schmidt-Nielsen, Animal Physiology: Adaptation and environment., 2nd ed, Cambridge University Press, Cambridge (1981)

[17] A. Schmitz, S.F. Perry, Stereological determination of tracheal volume and diffusing capacity of the tracheal walls in the stick insect Carausius morosus (Phasmatodea, Lonchodidae), Physiol. Biochem. Zool. **72** 205-218 (1999)

[18] H.A. Schneiderman, C.M. Williams, An experimental analysis of the discontinuous respiration of the Cecropia silkworm. Biol. Bull. mar. biol. Lab., Woods Hole **112** 106-119 (1955)

[19] K. Sláma, A new look at insect respiration, Biol. Bull. **175** 289-300 (1988)

[20] K. Sláma, Active regulation of insect respiration, Ann. Entomol. Soc. Am. **92** 916-929 (1999)

[21] G.K. Snyder, B. Sheafor, D. Scholnick, C. Farrelly, Gas exchange in insect tracheal system, J. Theor. Biol. **172** 199-207 (1995)

[22] J.T. Vogt, A.G. Appel, Discontinuous gas exchange in the fire ant, *Solenopsos invicta* Buren: Caste differences and temperature effects. J. Insect Physiol. **46** 403-416 (2000)

[23] A.E. Williams, M.R. Rose, T.J. Bradley, Using laboratory selection for desiccation resistance to examine the relationship between respiratory pattern and water loss in insects., J. Exp. Biol. **201** 2945-2952 (1998)

Summary

In this thesis the photoacoustic technique has been applied to study trace gas emissions by fruit and insects. For this purpose a photoacoustic spectrometer was developed that can detect a wide range of trace gases at high sensitivity.

In chapter 1 the relevance of sensitive trace gas detection is discussed. A number of examples make clear that the range of applications is enormous, ranging from fruit storage to health care. Furthermore, an introduction to the photoacoustic technique is given.

In chapter 2 the experimental setup is described and absorption coefficients of some biological interesting trace gases were determined. H_2O and CO_2 absorption coefficients are compared with data from Hitran database and showed in general a rather good agreement. The obtained absorption coefficients are used in a multicomponent analysis of trace gas emission by Conference pears under anaerobic conditions. The use of a newly designed three-level cold trap reduced interference by H_2O vapour and other compounds. Due to an improved determination of absorption coefficients, less laser lines had to be included in the multi-component analysis giving a better time response as compared to previous studies.

Chapter 3 presents a novel photoacoustic detector, that is based on a newly designed CO laser. This laser can operate on about 400 laser lines in the $\Delta v{=}1$ and $\Delta v{=}2$ mode (5.1-8.0 and 2.8-4.1 μm, respectively) . The spectrometer is equipped with three intracavity photoacoustic cells, i.e., four additional Brewster windows. Although this introduces additional losses in the laser cavity, a proper operation in the $\Delta v{=}2$ mode with its low gain is still possible. Fast and simple switching between the two operation modes is achieved using a newly designed grating holder. A number of applications is given showing the versatility of this detector.

In chapter 4 trace gas emission by avocado fruit is studied during anaerobic and post-anaerobic conditions. Release of ethanol and acetaldehyde under anaerobic conditions followed a pattern that is similar to that of many other fruits. Returning the fruit to aerobic conditions yielded an unprecedentedly high upsurge in acetaldehyde. A similar response in acetaldehyde is observed when initial conditions are hypoxic instead of anaerobic.

Chapter 5 deals with H_2O loss recordings of tiny insects called thrips (50 μg), the smallest of all flying insects. Thrips are a serious pest in many countries all over the world. We were able to record the H_2O loss of a single individual. Interestingly, they could stand arid conditions for very prolonged periods. As a potential insecticide, we tested the effect of elevated CO_2 levels. Only very high CO_2 levels (34 %) showed a clear effect on the mortality of these insects.

Chapter 6 presents a novel SF_6 wash-out technique to estimate the tracheal volume of insects using a CO_2 laser based photoacoustic spectrometer. The tracheal volume was determined of pupae from the moth *Attacus atlas* and of the American cockroach *Periplaneta americana*. In addition, the respiration pattern of the insects was resolved in detail from both CO_2 and SF_6 release. The high sensitivity of the spectrometer for SF_6 detector (5 ppt) opens new ways to study respiration in even the smallest insect species.

Samenvatting

Fotoakoestische sporegas detectie aan fruit en insekten met behulp van mid-infrarood laserlicht

Al sinds de oudheid probeert de mens de houdbaarheid van bederfelijke produkten zoals fruit en groente te verbeteren. Veel van de traditionele bewaarmethoden zijn gebaseerd op een verandering van de gas atmosfeer rond het produkt. Een voorbeeld hiervan uit het oude China is het transport van fruit in gesloten potten waaraan verse bladeren en gras is toegevoegd. Hierdoor werd een atmosfeer gegenereerd met een lage O_2 en hoge CO_2 concentratie en rijpening van het fruit werd afgeremd. De ademhaling van insekten lijkt op het eerste gezicht maar weinig raakvlakken met fruitbewaring te hebben. Echter bij een nadere bestudering blijken er verassend veel overeenkomsten te zijn:

- Intern gas transport vindt in beide gevallen voornamelijk plaats via luchtkanalen.

- Kleppen vormen de overgang tussen luchtkanalen en atmosfeer; in geval van fruit worden deze kleppen stomata genoemd en bij insekten stigma. Het aantal kleppen verschilt wel behoorlijk, zo hebben kakkerlakken 20 kleppen (10 paar) terwijl een avocado er maar liefst 25.000 heeft.

- In zowel fruit als insekten kunnen zich anaërobe processen voordoen; in fruit bewaard onder lage O_2 condities leidt dit onder andere tot de vorming van ethanol (alcohol) en aceetaldehyde terwijl in de het darmstelsel van insekten er anaërobe condities heersen waar bacteriëen methaan, methanol en ethanol vormen.

Voor zowel insekten als fruit blijkt fotoakoestiek een uitstekende methode om de gasuitwisseling van het sample met de atmosfeer te onderzoeken. In dit proefschrift wordt de detectie van een groot aantal gassen beschreven: CO_2, CH_4, C_2H_4, C_2H_6, C_2H_5OH, C_2H_4O, H_2O, NO en SF_6. In de fotoakoestische detectoren zijn de krachtige CO-laser (5.1-8.0 en 2.8-4.1 μm) en CO_2-laser (9-11 μm) als lichtbron gebruikt. Het hoge vermogen van deze lichtbronnen in combinatie met de gebruikte golflengtes zorgen voor een uiterst gevoelige detectie van sporegassen, met typische detectie limieten van 1 ppb.

In hoofdstuk 2 zijn fotoakoestische spectra gemeten van een aantal biologisch zeer interessante gassen. De hieruit bepaalde absorptie coëfficiënten komen vrij goed overeen met literatuurwaarden. De absorptie coëfficiënten zijn gebruikt in een multi-component analyse van gasuitstoot van Conference peren onder anaërobe omstandigheden. De ethanol emissie van de vrucht blijkt linear te stijgen als functie van de tijd terwijl aceetaldehyde na ongeveer tien uur een plateau bereikt. Voor een betrouwbare bepaling van de sporegas concentraties is het belangrijk dat de concentratie van interferende gassen zoals water laag

is. Door middel van een koude val wordt de concentratie van interferende componenten verlaagd. Complementair hieraan zijn de vele soorten chemische scrubbers die doorgaans bedoeld zijn om één specifiek gas te verwijderen. Echter veel scrubbers blijken niet selectief en daarom is het gedrag van een aantal scrubbers bestudeerd, daarbij is voornamelijk gekeken naar het effect van de scrubbers op ethanol.

In hoofdstuk 3 wordt een fotoakoestische spectrometer gepresenteerd die is gebaseerd op een nieuw ontworpen CO-laser. Deze laser kan op ongeveer 400 laserlijnen werken in de $\Delta v=1$ en $\Delta v=2$ mode (5.1-8.0 en 2.8-4.1 μm, respektieveljk). Door het grote golflengte-bereik van deze laser kan een enorm aantal gassen met hoge gevoeligheid gedetecteerd worden. Een aantal toepassingen laat de grote veelzijdigheid van deze spectrometer zien.

In hoofdstuk 4 wordt de gas emissie van avocado's onder lage en veranderende zuurstof concentraties onderzocht. Het fermentatiegedrag van avocado's blijkt vergelijkbaar met dat van veel andere vruchten (onder andere peren, zie hoofdstuk 2). Avocado's produceren heel weinig aceetaldehyde, echter na omschakelen van anaërobe naar aërobe condities volgt er een snelle en ongekend hoge aceetaldehyde uitstoot. Als de vrucht wordt bewaard onder een lage zuurstofconcentratie waarna deze wordt verhoogd, blijkt een gelijksoortige verhoging in aceetaldehyde uitstoot op te treden. Hieruit kan inzicht worden gekregen in de interne zuurstofverdeling.

In hoofdstuk 5 wordt de wateruitstoot gemeten van trips, dit zijn heel kleine insekten. De kleinste insekten waar tot nu toe de wateruitstoot van is gemeten, is de fruitvlieg die 20 keer zwaarder is dan de 50 μg wegende trips. Het meten van de wateruitstoot piekjes, die typisch 1 nmol groot zijn, vereist extreem droge omstandigheden. Omdat trips voor de landbouw erg schadelijk zijn, worden ze bestreden en tevens geldt bij export van gewassen naar bepaalde landen dat trips aanwezig op de gewassen gedood dienen te worden. We hebben de invloed van hoge CO_2 concentraties onderzocht op de mortaliteit van trips, en verrassend genoeg hadden concentraties van 16% geen effect onder de aangebrachte omstandigheden (0% RV). Echter bij verhoging van de CO_2 concentratie tot 34% waren de insekten binnen 2.5 uur dood.

In hoofdstuk 6 wordt van *Attacus atlas* poppen en de Amerikaanse kakkerlak *Periplaneta americana* het volume van de tracheeën bepaald met behulp van een nieuwe SF$_6$ uitwas techniek. De gevonden tracheeën volumes blijken goed overeen te komen met waarden bepaald via andere technieken. Deze techniek biedt ook de mogelijkheid om de ademhaling van heel kleine insekten te bestuderen. Tevens zijn lengteveranderingen van *Attacus atlas* poppen gemeten met een infrarode reflektiesensor. Deze uiterst gevoelige sensor kan lengteveranderingen op sub-μm schaal meten. Indien het insekt de stigma gesloten houdt, en er dus geen gasuitstoot door de stigma is, wordt het insekt korter doordat zich een onderdruk in de tracheeën ontwikkelt.

Curriculum Vitae

Stefan Persijn was born on 4 June 1973 in Zevenaar. In the same city he graduated from grammar-school at the "Liemers College" in 1992, after which he started to study physics as an undergraduate at the University of Nijmegen. During his study he organised a study tour to England and was committee member of the student organisation for physics "Marie Curie". His practical training was performed in the same university at the Department of Molecular & Laser Physics and at ATO in Wageningen. He received his degree in physics in January 1997. In February of that year he started his Ph.D. research at the Department of Molecular & Laser Physics under supervision of Frans Harren. During his Ph.D. he worked for a short period on the ship "R.V. Pelagia", studying nitrogen fixation by cyanobacteria and he spent 5 weeks in Indonesia, at the Gadjah Mada University of Yogyakarta, where he installed a sealed-off CO_2 laser. Furthermore, he assisted at various physics and electronical practical. In May 2001 he started to work as a Post-doc at the University of Nijmegen.